# A Systematic Analysis of *Iron* and *iglr* Genes' Function in Axon Guidance within the Ventral Nerve Cord of *Caenorhabditis elegans*

**by**

**Nikolas Kokan**

B.Sc., University of British Columbia, 2016

Thesis Submitted in Partial Fulfillment of the
Requirements for the Degree of
Master of Science

in the
Department of Biological Sciences
Faculty of Science


SIMON FRASER UNIVERSITY
Summer 2021

## Declaration of Committee

| | |
|---|---|
| **Name:** | **Nikolas Kokan** |
| **Degree:** | **Master of Science (Biological Sciences)** |
| **Title:** | **A Systematic Analysis of *Iron* and *iglr* genes' Function in Axon Guidance within the Ventral Nerve Cord of *Caenorhabditis elegans*** |
| **Committee:** | **Chair:** **Carl Lowenberger**<br>Professor, Biological Sciences |
| | **Harald Hutter**<br>Supervisor<br>Professor, Biological Sciences |
| | **Nancy Hawkins**<br>Committee Member<br>Associate Professor, Molecular Biology and Biochemistry |
| | **Gordon Rintoul**<br>Committee Member<br>Associate Professor, Biological Sciences |
| | **Michael Silverman**<br>Examiner<br>Professor, Biological Sciences |

# Abstract

For the nervous system to develop properly, axons must connect neurons into networks by navigating to their target destinations. A large proportion of genes containing extracellular Leucine-Rich Repeats (eLRRs) function in neurodevelopment, including in axon guidance. The objective of this thesis is to identify novel eLRR genes in the *Caenorhabditis elegans*' *lron* and *iglr* gene families that function in axon guidance. Animals with mutations in these genes were observed with pan-neuronal and pioneer markers to identify mutations that induced axon guidance defects. Six mutants had significant axon guidance defects. In addition, *iglr-2* mutants were found to have fasciculation defects in the left ventral nerve cord. *lron-11* mutants had the most penetrant axon guidance defects. Therefore, *lron-11* animals were further characterized with several inter and motor neuron markers and further axon guidance defects were identified. This research suggests that *lron-11* and possibly other *lron*/*iglr* genes function as receptors in axon guidance.



**Keywords**: LRON; IGLR; *Caenorhabditis elegans*; Axon Guidance; Leucine-Rich Repeats; Neurodevelopment

*Dedicated to the friends, family, teammates and cats that have supported me throughout this endeavor*

# Acknowledgements

This research wouldn't have been possible (at least at this quality) without the help and support of the people in my life. Firstly, Dr. Harald Hutter has been an outstanding supervisor for me over the past few years. Without his advice, encouragement and mentorship I would not have developed into the researcher I am today. My skills and confidence as a scientist have vastly increased since I entered his lab. I will always be grateful that you gave me this wonderful opportunity Harald!

I would like to acknowledge Dr. Jie (Jessie) Pan, who suffered the majority of my questions during the past three years. Your patience and experience have been invaluable to me as I tried to solve problems with my experiments or find things in the lab! Furthermore, I would like to thank Rick Zapf who taught me several new techniques in my quest to stick two stubborn pieces of DNA together. I also want to thank Abigail Feresten for her help in the lab and for immediately making me feel welcome. I also want to mention Kiran Yaseen, who's diligence and hard work produced important contributions to this research that allowed me to complete this thesis on schedule.

My sage committee members Dr. Nancy Hawkins and Dr. Gordon Rintoul have given me fantastic advice that has shaped the course of my degree. They have helped me prioritize what research was most important and had great ideas for new experiments I should conduct, or how to solve expiremental problems.

I would also like to sincerely thank my parents for all the support and advice they have given me throughout this journey; especially once I finally convinced them I would be a terrible engineer.

Lastly, I would like to thank all the worms that gave their lives for this research and commemorate their sacrifice.

# Table of Contents

# List of Tables

# List of Figures

# List of Acronyms

| | |
|---|---|
| ACT | ACTin |
| AdipoR | Adiponectin Receptor |
| Amigo | Amphoterin-induced gene and open reading frame |
| AMPA | α-amino-3-hydroxy-5-methyl-4-isoxazolepropionic acid |
| AST | Astray |
| bp | Base pairs |
| *C. elegans* | *Caenorhabditis elegans* |
| CA | cornu Ammonis |
| Caps | Capricious |
| Cdc42 | Cell division control protein 42 homolog |
| CDH | CaDHerin |
| CFP | Cyan Fluorescent Protein |
| CFZ | *Caenorhabditis* FriZzled homolog |
| CLE | CoLlagen with Endostatin domain |
| CWN | *C. elegans* WNT family |
| DCC | deleted in colorectal cancer |
| DMA | Dendrite Morphology Abnormal |
| DNA | Deoxyribonucleic acid |
| DNC | Dorsal Nerve Cord |
| dNTP | deoxyribonucleotide triphosphate |
| DPY | DumPY |
| DSCAM | Down syndrome cell adhesion molecule |
| DsRed | Discosoma sp. Red |
| EFN | Eph(F)riN |
| EGL | EGg Laying defect |
| eLRR | extrcellular Leucine-Rich Repeat |
| EWM | Easiest Worm Media |
| FLP | FMRF-Like Peptide |
| FLRT | Fibronectin Leucine-Rich Transmembrane protein |

| | |
|---|---|
| FMI | FlaMIngo (cadherin plus 7TM domain) homolog |
| GABA | *gamma*-Aminobutyric acid |
| GAP | GTPase activating protein |
| GEF | Guanine nucleotide exchange factor |
| GFP | Green Fluorescent Protein |
| GLR-1 | GLutamate Receptor family (AMPA) |
| GPI | Glycosylphosphatidylinositol |
| GTPase | Guanosine triphosphatase |
| HMR | HaMmeRhead embryonic lethal |
| HPO | Hypersensitive to POre-forming toxin |
| HSE | Heparan Sulfate-glucuronic acid-5-Epimerase |
| HSPG | Heparan Sulfate ProteoGlycans |
| HST | Heparan SulphoTransferase |
| IG | ImmunoGlobulin |
| IgCAM | Immunoglobulin Cell surface Adhesion Molecules |
| IGLR | ImmunoGlobulin and LRR domains |
| ISLR | Immunoglobulin Super family containing Leucine-Rich Repeat |
| kb | Kilobase |
| KPC | Kex-2 Proprotein Convertase family |
| LAD | L1 CAM ADhesion molecule homolog |
| LIN | abnormal cell LINeage |
| Lingo | Leucine rich repeat and Immunoglobin-like domain-containing protein |
| LON | LONg |
| LRON | extracellular-Leucine Rich Repeat-Only |
| LRR | Leucine-Rich Repeat |
| LRRTM | LRR TransMembrane neuronal |
| LTP | Long-Term Potentiation |
| MIG | abnormal cell MIGration |
| MNR | MeNoRin |

| | |
|---|---|
| MOM | More Of MS |
| NGL | Netrin G ligands |
| NGR | NoGo Receptor |
| NID | NIDogen |
| ODR | ODoRant response abnormal |
| PAQR | Progestin and AdipoQ Receptor family |
| PCR | Polymerase Chain Reaction |
| PDZ | Domain present in PSD-95, Dlg, and ZO-1/2 |
| PLR | cell PoLaRity defective |
| PSD | PostSynaptic Density protein 95 |
| Rac | Ras-related C3 botulinum toxin substrate |
| RGEF | Rap Guanine nucleotide Exchange Factor homolog |
| Rho | Ras Homolog Family Member |
| RIG | neuRonal IGCAM |
| RNA | Ribonucleic acid |
| RNAi | RNA interference |
| Robo | Roundabout |
| RTK | Receptor Tyrosine Kinase |
| SALM | Synaptic adhesion-like molecules |
| SAX | Sensory Axon guidance |
| SDN | SynDecaN |
| Slitrk | Slit- and Trk-like |
| SLT | SLiT (*Drosophila*) homolog |
| SRA | Serpentine Receptor, class A (alpha) |
| TIAM | TIAM (mammalian Tumor Invasion And Metastasis factor) homolog |
| TPH | TryPtophan Hydroxylase |
| Trk | Tyrosine receptor kinase |
| UNC | uncoordinated |
| VAB | Variable ABnormal morphology |
| VNC | Ventral Nerve Cord |

| | |
|---|---|
| Wnt | Wingless |
| WRK | Wrapper/Rega-1/Klingon homolog |
| WVE | WAVE (actin cytoskeleton modulator) homolog |

# Chapter 1. Introduction

## 1.1. Development of Neural Circuits

The human brain is the most complex structure in the known universe. It contains approximately 100 billion neurons, which are supported by a comparable number of glial cells (Herculano-Houzel, 2009; Hilgetag and Barbas, 2009). Each neuron is connected to other neurons via thousands of synapses (Pakkenberg et al., 2003; Tang et al., 2001). The goal of neurodevelopmental research is to understand how this vast network is constructed.

We know that the nervous system originates during embryonic development when neural and glial precursor cells differentiate into neurons and glia respectively. These cells then migrate to regional positions in the fetal brain. Next, these neurons send out processes, called axons, that travel relatively great distances before synapsing with a specific type of neuron, in a specific region of the brain. Neurons communicate by sending electrical signals called action potentials along their axons to synapses at the tips of the axon. At the synapse these action potentials are converted to chemical signals that will directly interact with the dendrites of another neuron. The neural circuits created by these interconnected neurons will coordinate an organism's movement, interpret sensory information, and in some animals, they are capable of performing incredibly complicated cognitive tasks such as planning and goal driven decision making.

Axons properly connecting these neurons into coherent circuits is vital for the performance of these neural networks. How all of these axons navigate to each of their disparate destinations is only beginning to be uncovered. Scientists have discovered receptors on the axon's surface that bind external molecules to providing directional information to the axon. Some receptors bind diffusive molecular guidance cues, which can attract an axon along their concentration gradient or result in the axon being repelled from it. Axonal receptors can also bind guidance cues imbedded in adjacent surfaces. Binding these cues can enable an axon to extend along this surface or can prevent an axon from extending along a surface that would take it in the wrong direction. Some axon guidance receptors and their guidance cues have been discovered. However, we haven't identified many of the other proteins that interact with these receptors or

guidance cues to facilitate axon guidance. In the few axon guidance pathways that have been well characterized, elucidating the complex interactions between different proteins in these pathways has reshaped our understanding of how these axon guidance cues and receptors guide axons. Furthermore, due to the complexity and diversity of the axon guidance decisions required to create large neural networks, it is estimated that numerous axon guidance genes remain undiscovered (Chisholm et al., 2016).

### 1.1.1. Axon guidance

Neural circuits are often made up of neurons in different parts of the nervous system. To connect with these distant cells, neurons must send axons relatively large distances. At the extending edge of the axon is a growth cone, which must interpret the extracellular landscape to correctly navigate towards its target region. Growth cones possess finger-like projections called filopodia, with lamellipodia sheets between the filopodia (Figure 1.2). Growth cones use these projections to navigate through obstacles and identify the correct path toward their destination. The filopodia accomplish this by integrating signals from the different guidance cues in their environment, through receptors present in their cell membrane. These receptors become overrepresented on the side of the growth cone that faces an axon guidance cue, polarizing the growth cone (Bouzigues et al., 2007; Tojima et al., 2011).

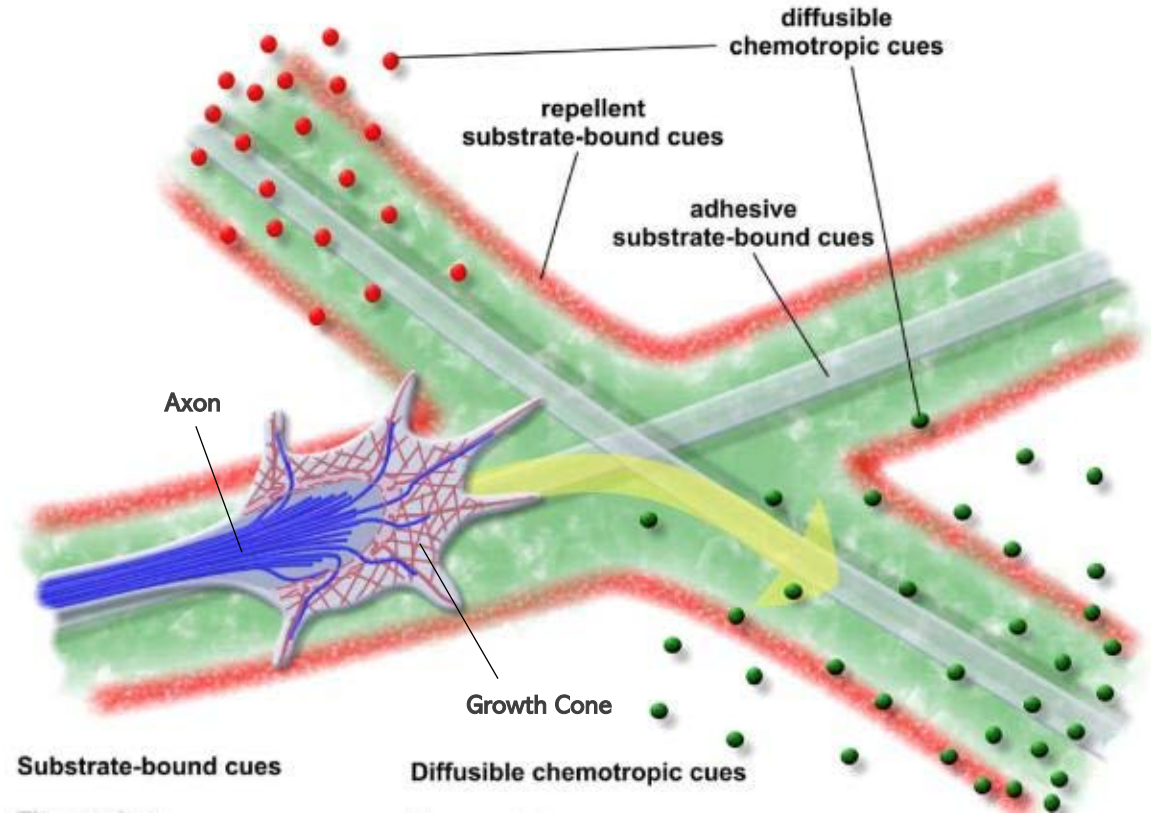


**Figure 1.1 Different types of axon guidance cues**
Axon guidance cues can be diffusible chemotropic cues, or substrate-bound adhesive cues. Cues can induce axon extension toward it or induce growth cone repulsion. (Modified from Lowery and Van Vactor, 2009).

Axon guidance cues can be chemotropic or adhesive (Figure 1.1). Secreted chemotropic cues form gradients which provide directional information to the growth cone. Adhesive cues present on adjacent cell surfaces provide guidance when the growth cone directly interacts with this surface. Attractive adhesive cues can also mechanically bind the growth cone to their surface. Guidance cues can also be bound in the extracellular matrix, which includes a fibrous network of collagen IV and laminin that supports cells and which axons extend along (Lowery and Van Vactor, 2009; Stoeckli, 2018).

Attractive cues induce the growth cone to turn toward them, while repulsive cues cause axons to be repelled away from them. However, the same guidance cue can be attractive to some growth cones, and repulsive to others, depending on the receptors present in the growth cones membrane. For example, netrins are secreted guidance cues that form a gradient capable of attracting or repelling growth cones (Hedgecock et

al., 1990; Hong et al., 1999; Kennedy et al., 1994; Wadsworth et al., 1996). This gradient can extend a considerable distance from the cells that originally secreted netrin. However, netrins can also become immobilized in the extracellular matrix, where they can act as a short range adhesion cue to growth cones extending along this substrate (Baker et al., 2006; Rajasekharan and Kennedy, 2009; Shekarabi et al., 2005). It is important to note that, over a growth cones journey it may change the receptors on its surface. This allows it to respond to different guidance cues at different times along its journey. This spatiotemporal regulation of receptors can allow growth cones to change directions when necessary to reach its destination. For more information, read this review (O'Donnell et al., 2009).

### 1.1.2. Growth cone dynamics

As described previously, growth cones contain filopodia projections with lamellipodia between them. Filopodia are composed of f-actin bundles which are constantly being polymerized at the distal end and depolymerized at the proximal end (Figure 1.2). When receptors respond to guidance cues, they induce changes in the rate of these two processes allowing for dynamic extension or retraction of filopodia (Figure 1.3; Bugyi and Carlier, 2010; Okabe and Hirokawa, 1991; Small, 1995; Suter and Forscher, 2000). Lamellipodia are composed of mesh-like networks of branched f-actin. Microtubules also extend into the filopodia, where they facilitate trafficking of cellular components and interact with actin (Figure 1.2; Cammarata et al., 2016). However, most microtubules end near the base of the growth cone, where they are contained by actin-arcs (Figure 1.2). When the growth cone moves in a direction, these arcs will reorient (Lee and Suter, 2008). This allows the microtubules to advance, consolidating the growth cones movements.

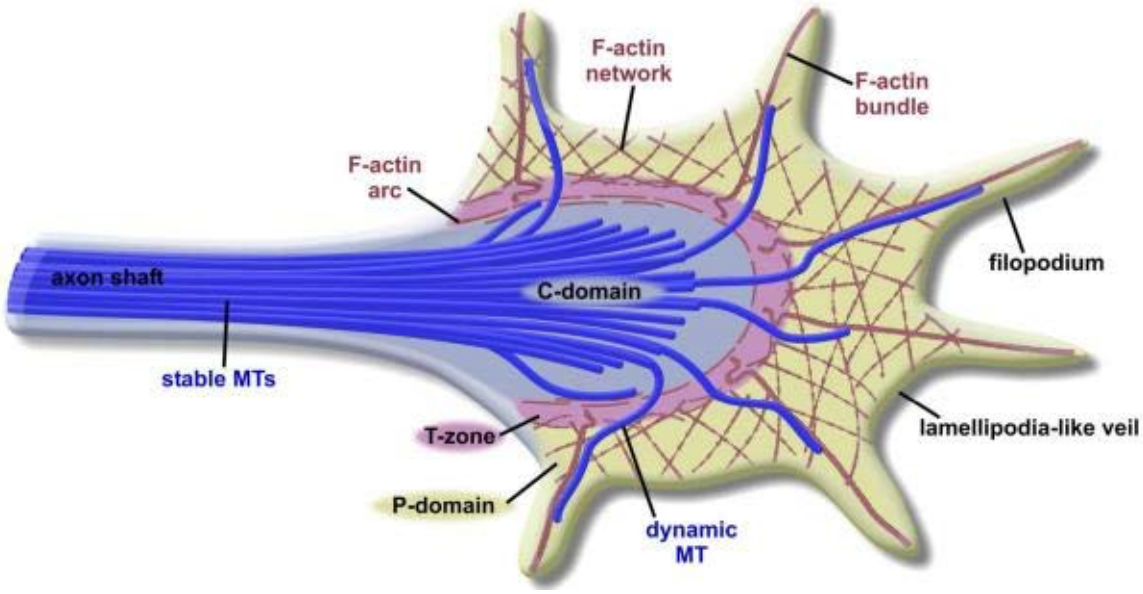


**Figure 1.2 Diagram of the growth cone cytoskeleton**
Filopodia consist of f-actin bundles and pioneer microtubules. Lamellipodia contain f-actin networks. Most microtubules remain at the base of the growth cone, where they are surrounded by f-actin arcs. (Lowery and Van Vactor, 2009).

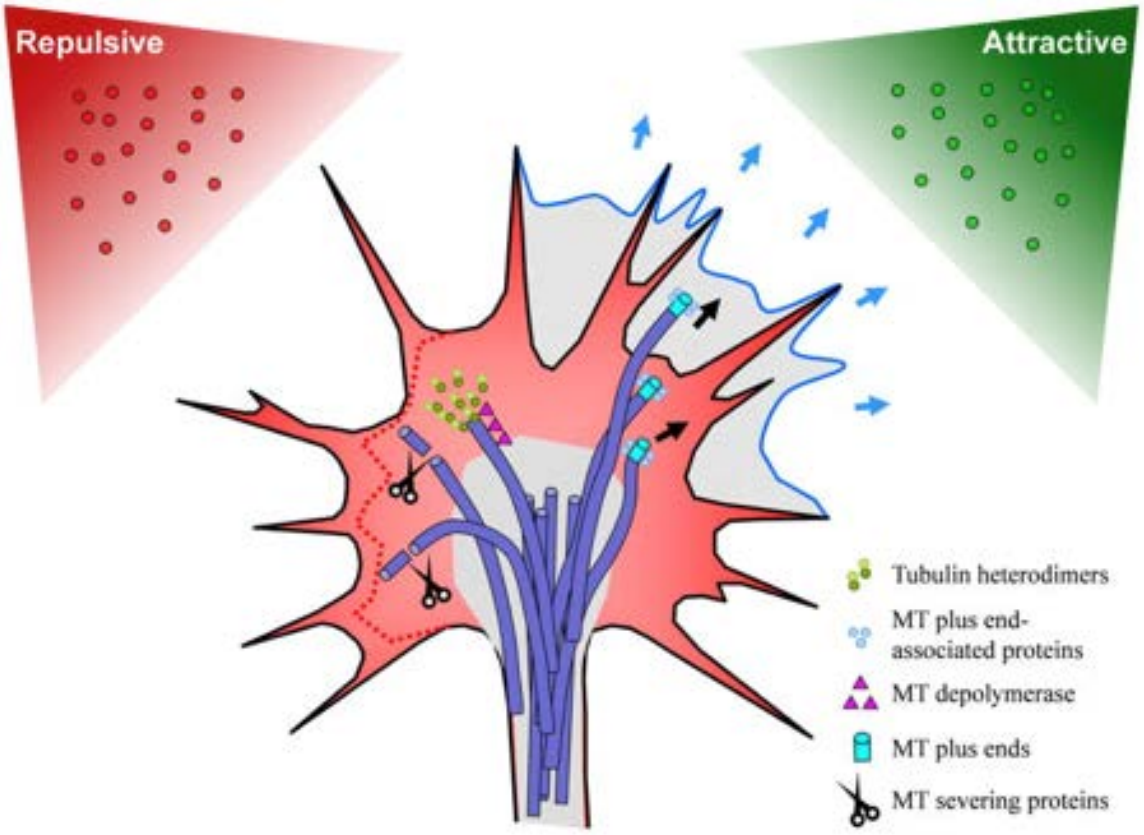


**Figure 1.3 Growth cone cytoskeleton remodeling in response to guidance cues**
In response to axon guidance cues, the cytoskeleton of the growth cone will dynamically remodel itself. F-actin bundles and pioneer microtubules will polymerize on the side of the growth cone facing an attractive cue. F-actin and microtubules will depolymerize or be actively severed in response to negative cues, or attractive cues on the other side of the growth cone. (Vitriol and Zheng, 2012).

Receptors on the surface of the growth cone interact with specific guidance cues. These receptors then convert this extracellular signal into an intracellular one. This intracellular signal will remodel the growth cone's cytoskeleton. If this signal is an attractive one, the cytoskeleton on that side of the growth cone will stabilize (Figure 1.3). Furthermore, the cytoskeleton on the far side of the growth cone will collapse (Figure 1.3). If the receptor's intracellular signal is repulsive, the local cytoskeleton will collapse (Figure 1.3). This remodeling is orchestrated by activating complex signaling pathways within the growth cone.

Adhesive cues can also influence the growth cone mechanically, when adhesive cues are bound by adhesion receptors on the growth cones surface. The adhesion receptors bridge the cell membrane to couple the extracellular substrate to the growth

cone's intracellular cytoskeleton. This coupling exerts a traction force on the f-actin bundles (Chan and Odde, 2008; Heidemann et al., 1990; Lowery and Van Vactor, 2009). In filopodia, the cell membrane has been forced outward, so there is a constant elastic force pushing the f-actin bundles inward, increasing their rate of depolymerization (Chan and Odde, 2008; Heidemann et al., 1990; Lowery and Van Vactor, 2009). This traction force resists the elastic force, slowing the rate of depolymerization at the base of the f-actin bundle. Therefore, f-actin polymerization now outpaces depolymerization, leading to the extension of the filopodia in the direction of the adhesive cue.

Rho-family GTPases such as Cdc42, Rac1 and RhoA, play a pivotal role in remodeling the actin cytoskeleton during axon guidance. Most axon guidance receptors signal through them to influence the cytoskeleton (Figure 1.4; Koh, 2006). While some receptors directly interact with Rho-family GTPases, many signal through guanine nucleotide exchange factors (GEFs) or GTPase activating proteins (GAPs) (Lowery and Van Vactor, 2009; Oinuma et al., 2004). GEFs activate GTPases, while GAPs inhibit them (Koh, 2006). Once mobilized, these GTPases will activate various downstream effectors, resulting in the spatially asymmetrical polymerization or depolymerization of f-actin.

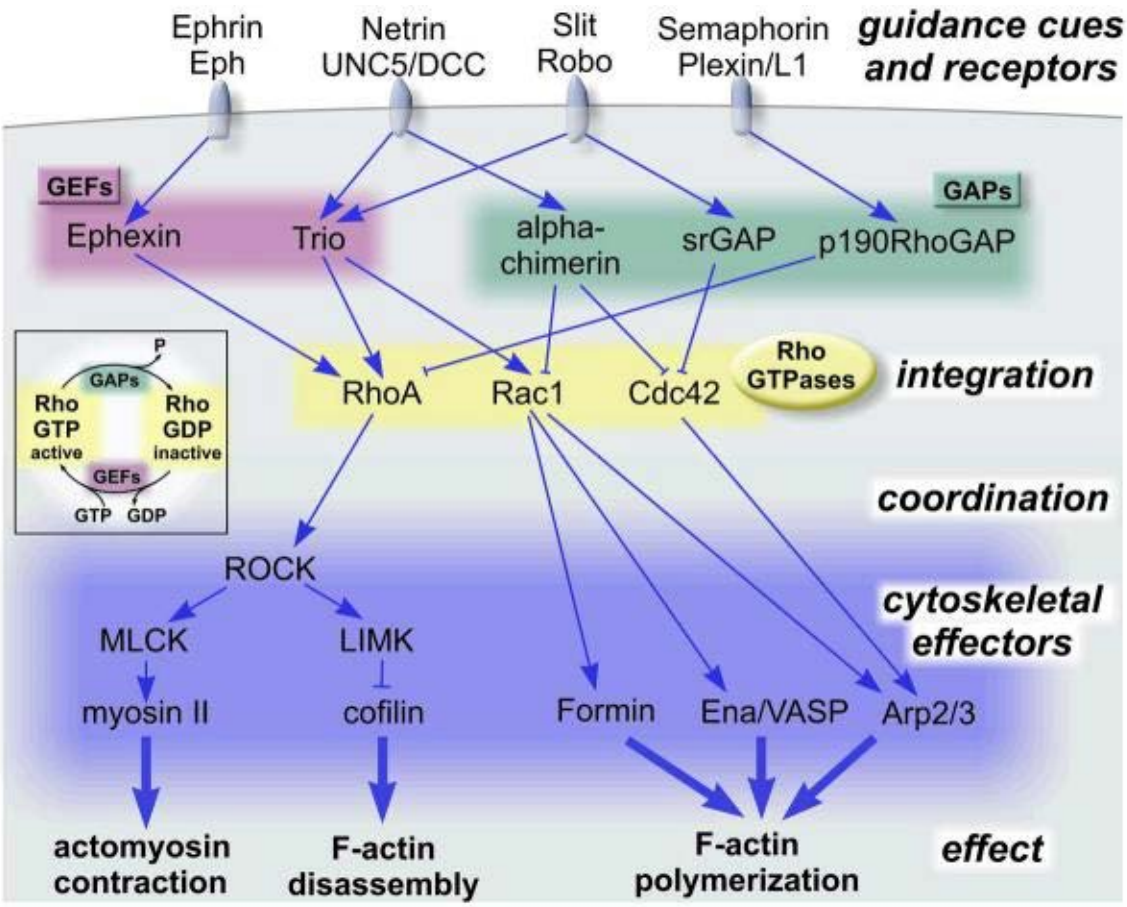


**Figure 1.4 Simplified depiction of intracellular signaling pathways that remodel the growth cones cytoskeleton during axon guidance**

When axon guidance cues bind their receptors on the growth cone's surface, this will elicit an intracellular signal that will remodel the cytoskeleton. Different receptors will activate different intracellular signaling pathways. (Lowery and Van Vactor, 2009).

## 1.2. *Caenorhabditis elegans* as a model organism for axon guidance

*C. elegans* are a species of round worm. They grow to approximately 1mm in length as adults. Due to their small size and fast generation time of three to four days, experiments on hundreds of worms can be prepared and executed quickly. The nervous system of *C. elegans* is also small, consisting of just 302 neurons, which form about 7000 synapses (White et al., 1986). These neurons have been grouped into 118 classes based on their connections, and their morphology (White et al., 1986). The entire connectome has been discovered through electron microscopy, and it is consistent between individuals (White et al., 1986). This allows for a detailed analysis of neural circuits, and errors in neurodevelopment can be more easily identified. *C.*

*elegans* are also transparent, so fluorescent labeling can be utilized to visualize subsets of neurons (Hutter, 2006). It is even possible to visualize some neurites as they grow (Bao and Murray, 2011; Fan et al., 2019).

### *1.2.1. C. elegans ventral nerve cord*

Most neuron cell bodies are part of ganglia in the head or in the tail of the worm. *C. elegans* largest neuropil is the nerve ring, which is located in the head. Two major longitudinal axon bundles traverse the length of the animal, the dorsal nerve cord (DNC), and the ventral nerve cord (VNC) (Figure 1.5). Of these, the VNC is the largest, and is located on the ventral side of the animal. It is the *C. elegans* equivalent of the spinal cord of vertebrates. Many axons enter the VNC running posteriorly from the head, in two parallel tracts. Most axons will enter the right tract, resulting in an asymmetrical VNC. In total, there are 50 axons in the right tract, and only 4 in the left tract. Since most synapses in *C. elegans* are made along the length of the axon (*en passant*) instead of at the end, the position of an axon within the VNC will determine its synaptic partners (Hall and Russell, 1991; White et al., 1986).

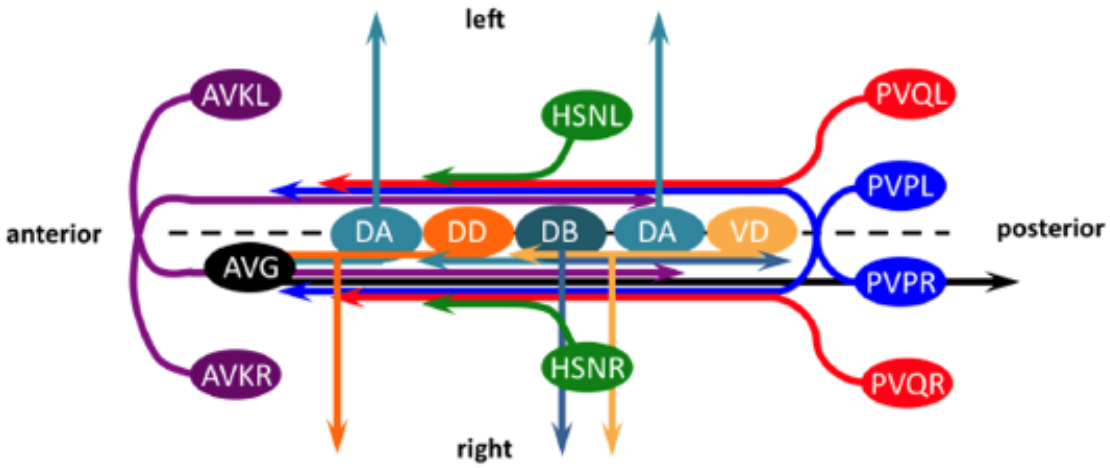


**Figure 1.5 Diagram of the C. elegans ventral nerve cord**
This diagram displays some of the neurons that send axons into the VNC. AVG pioneers the right axon tract, extending from just posterior of the nerve ring. PVPR pioneers the left VNC, extending from the tail. DA, DB, VD and DD motor neurons are located between the two tracts of the VNC. They send neurites into the right tract, and commissures dorsally. HSN neurons send their axons into the VNC near the vulva later in development and extends anteriorly. AVK neurons send their axons into the nerve ring, where they then enter the VNC and extend posteriorly. PVQL and PVQR enter the left and right VNC respectively from the tail. Command interneurons are not depicted here, they would be extending from the head posteriorly down the right axon tract. Reproduced with permission of Development (Steimel et al., 2010).

The VNC is pioneered by two neurons, AVG and PVPR (Durbin, 1987). AVG pioneers the right tract, and PVPR pioneers the left (Figure 1.5). These axons are important, because the later extending axons, termed follower axons, will typically utilize these pioneer axons to help guide them in the VNC. This includes the PVQL interneuron whose axon will closely follow the PVPR axon as it pioneers the left tract (Durbin, 1987). The pioneer growth cones must navigate to their destination without the benefit of an established tract, so they must rely on axon guidance cues in their extracellular environment to navigate. Therefore, these are important axons to observe in axon guidance research.

Other notable neurons in the VNC include the command interneurons. Their cell bodies are located in the head and their axons will enter the anterior VNC and travel posteriorly along the right tract. Another type of interneuron is the AVK neurons, whose axons must initially navigate anteriorly through the nerve ring before entering the VNC. AVKR's axon enters the left axon tract and AVKL's axon enters the right one. Interestingly, although AVKR extends along the left tract, it doesn't require the pioneer PVPR to navigate along the VNC. The HSN motor neurons migrate from the tail to just posterior of the vulva after embryogenesis. The HSN axons must make several important guidance decisions. First HSNL and HSNR must send their axons ventrally into the VNC, where they then should choose to extend anteriorly along the left and right tracts respectively.

Another important class of neuron in the VNC are the DA, DB, DD and VD motor neurons. These motor neurons cell bodies are located between the two axon tracts, spread out along the ventral midline of the VNC (Figure 1.5). The A- and B-type motor neurons DA and DB are cholinergic and the D-type motor neurons DD and VD are GABAergic. These motor neurons send their neurites into the right VNC and send their commissures dorsally to the DNC (Figure 1.6). Each motor neuron will send their commissure dorsally up the left side of the animal, or the right side in a consistent pattern.

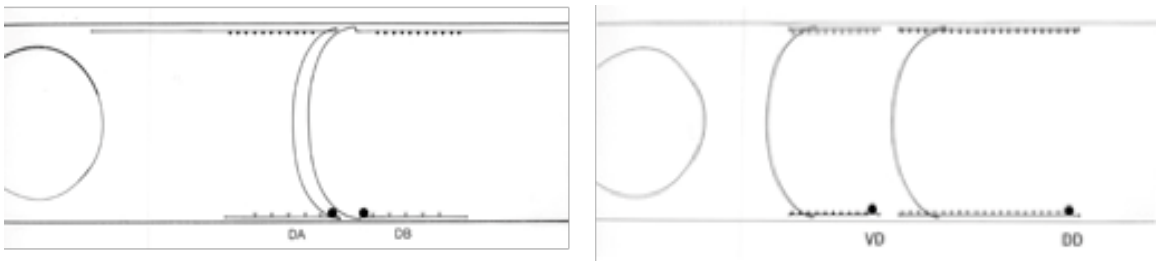


**Figure 1.6 Depiction of DA/DB and VD/DD motor neurons**
The DA/DB and DD/VD motor neurons all send commissures dorsally where they eventually enter the DNC. They also send neurites into the right VNC. The DA/DB motor neurons are excitatory whereas the DD/VD motor neurons are inhibitory. Neuromuscular junctions on axons are shown as black triangles. Dendritic synapses are shown as hollow triangles. (Edited from https://www.wormatlas.org/neurons/Individual%20Neurons/DDframeset.html).

## 1.3. Guidance cues and their receptors

In recent decades, researchers have discovered various genes functioning in axon guidance. These genes encode some of the guidance cues that provide spatial information to growth cones as they navigate through their environment. They also encode receptors that allow growth cones to respond to these extracellular cues. Without these receptors, growth cones would be blind to their surroundings and be unable to navigate to their target destination. However, mutations in these known guidance cues and receptors typically have partially penetrant axon guidance defects, implying there are parallel signaling pathways that haven't yet been discovered. Furthermore, the known axon guidance genes don't seem to fully account for all the guidance decisions axons make. Therefore, while this section covers most of the major known guidance cues and receptors, there are likely other important genes that have yet to be discovered.

### 1.3.1. UNC-6/netrin and its UNC-40/DCC and UNC-5 receptors

UNC-6/netrin was the first axon guidance cue to be discovered. It was named after the Sanskrit word Netr, which means 'guide'. This discovery was made in *C. elegans*, where researchers uncovered its involvement in dorsal-ventral axon navigation (Hedgecock et al., 1990). Its homolog netrin was later discovered in vertebrates (Kennedy et al., 1994). UNC-6/netrin is a highly conserved secreted protein with similarities to laminin, and it is thought to associate with the basement membrane (Hedgecock et al., 1990; Ishii et al., 1992).

In *C. elegans*, it is released by ventral cells to form a dorsal-ventral gradient (Wadsworth et al., 1996). It was originally proposed that growth cones expressing UNC-40/DCC were attracted to UNC-6, and growth cones expressing UNC-5 were repulsed (Hedgecock et al., 1990). It has since been discovered that UNC-40 also plays a role in repulsion from UNC-6, by forming a heterodimer with UNC-5 (Hong et al., 1999). This complex is important for long distance repulsion from UNC-6, where the concentration of UNC-6 is low (MacNeil et al., 2009). More recently, it has been revealed that UNC-5 is also involved in ventral axon navigation, toward high concentrations of UNC-6 (Levy-Strumpf and Culotti, 2014; Limerick et al., 2018). Furthermore, the UNC-6 gradient is used in *C. elegans* to guide some motor and interneurons along the ventral nerve cord, including the pioneer PVPR (Hutter, 2003). In *unc-6* mutants these axons will sometimes inappropriately cross the ventral midline into the parallel axon tract (Hutter, 2003).

Unlike *C. elegans*, *Drosophila melanogaster* and vertebrate genomes contain multiple netrins, however, netrin still plays a similar role during development in these organisms (Harris et al., 1996; Kennedy et al., 1994). In *Drosophila*, netrins are also expressed at the ventral midline, where it is an important cue for commissures navigating along the dorsoventral axis (Harris et al., 1996). In rats, it was found that the netrin secreting floor plate, the ventral-most part of the spinal cord, would attract commissures from the roof plate *in vitro* (Kennedy et al., 1994). Thus, it was posited that, like in *C. elegans*, the floor plate expressed netrins diffuse into a dorsal-ventral gradient that commissures then used to navigate. However, more recent *in vivo* studies utilizing genetic manipulation of mice demonstrated that Netrin-1 expression from cells along the commissure's path may be more important to guide the axons along the dorsoventral axis, where they act as an adhesive cue instead of a diffusive one (Dominici et al., 2017; Varadarajan et al., 2017).

### 1.3.2. SLT-1/Slit and SAX-3/Roundabout

Slit is a repulsive axon guidance cue that was discovered in *Drosophila* (Rothberg et al., 1990, 1988). In *Drosophila*, axons travel along parallel tracts in the ventral nerve cord, and cross between these tracts at specific points. The growth cones are prevented from crossing between tracts by the secreted repellent cue Slit which is released by glia cells in the midline (Kidd et al., 1999). Robo receptors expressed by

growth cones traveling along these axon tracts bind to Slit, resulting in repulsion from the midline. However, when an axon needs to cross the midline, this repulsion is no longer beneficial. Therefore, trafficking of the Robo receptors to the growth cone membrane is halted, which allows the growth cone to temporally ignore Slit's repulsion, and travel across the ventral midline (Keleman et al., 2005; Kidd et al., 1999).

In mice, there are three Slit paralogs, as well three Robos (Dickson and Gilestro, 2006). Similar to *Drosophila*, the Slit proteins repel commissures from the ventral midline through interactions with Robo receptors (Brose et al., 1999; Long et al., 2004). However, ROBO3's function has diverged, and it does not directly interact with Slit. Instead, one of its isoforms binds to Robo1 to promote Robo1's binding to Slit, the other isoform binds to Robo1 to inhibit this binding (Blockus and Chédotal, 2016; Z. Chen et al., 2008).

Slit's homolog in *C. elegans* is SLT-1 (Hao et al., 2001). SLT-1 is expressed by dorsal body wall muscles and promotes ventral navigation through long range repulsion, in parallel with UNC-6/UNC-40 ventral attraction (Hao et al., 2001). UNC-40 also interacts with SAX-3, *C. elegans*' Robo receptor, to mediate repulsion from SLT-1 (Yu et al., 2002). Unlike its homolog Slit, SLT-1 does not play a major role in preventing midline crossovers (Hao et al., 2001; Hutter, 2003). However, when *sax-3* is mutated animals exhibit penetrant ventral midline crossing events and nerve ring positioning defects that are not observed in *slt-1* mutants, suggesting it is involved in an SLT-1 independent axon guidance pathway (Hao et al., 2001; Hutter, 2003; Zallen et al., 1998).

SAX-3/Robo likely binds SLT-1/Slit through its Leucine-Rich Repeat (LRR) domain since mutations in SLT-1/Slit's LRR domain result in midline crossing defects (Battye et al., 2001; Hao et al., 2001). Furthermore, in *Drosophila* this phenotype could only be rescued by expression of a Slit protein with an intact LRR domain (Battye et al., 2001). Slit has also been shown to bind to Robo *in vitro*, but only if its LRR domain is present (Battye et al., 2001).

### 1.3.3. Ephrins

Ephrins act as anti-adhesion cell surface bound proteins in axon guidance. EphrinAs are glycosylphosphatidylinositol (GPI)-linked proteins, and EphrinBs are

transmembrane proteins; EphA and EphB receptors bind to the corresponding ephrinA and ephrinB families (Chilton, 2006). Both ephrins and their receptors can transduce signals, enabling bidirectional signaling when they interact (Arvanitis and Davy, 2008; Holland et al., 1996).

Crosstalk between ephrin signaling and netrin/Unc-5 signaling has been discovered in vertebrate motor axon navigation during limb development (Poliak et al., 2015). However, ephrin signalling's most well characterized role is to guide growth cones projecting from the retina to their correct position in the tectum's topographic map, which corresponds to the neuron cell bodies spatial position within the retina (Cang and Feldheim, 2013; Hindges et al., 2002; Lemke and Reber, 2005). ephrinAs are expressed in a repulsive gradient along the anterior-posterior axis of the tectum. ephrinA concentrations are high at the posterior of the tectum and low on the anterior side of the tectum. Similarly, ephrinBs are expressed in a gradient along the dorsoventral axis, with high expression on the dorsal side and low expression on the ventral side. However, this ephrinB gradient is attractive. Depending on a neuron's position in the retina, its growth cones will express different levels of the ephA and ephB receptors, which will allow it to navigate to a specific position in the tectum by interacting with these ephrin gradients. The more ephA receptors a growth cones expresses, the more strongly it will be repelled toward the anterior side of the tectum. The more ephB a growth cones expresses, the more it will be attracted toward the dorsal side of the tectum.

*C. elegans* have four GPI-anchored ephrins, VAB-2/EFN-1, EFN-2, EFN-3, and EFN-4, and one ephrin receptor VAB-1 (Chin-Sang et al., 1999; George et al., 1998; Wang et al., 1999). VAB-2, EFN-2, and EFN-3 act redundantly to prevent axons from inappropriately crossing the ventral midline of the VNC (Boulin et al., 2006). They signal through the VAB-1 receptor to promote growth cone collapse (Boulin et al., 2006). EFN-2, EFN-3, EFN-4, and VAB-1 signaling also plays a role in the proper termination of some axons (Mohamed and Chin-Sang, 2006). VAB-2, in parallel with SAX-3 and UNC-6, guides amphid axons ventrally (Grossman et al., 2013; Zallen et al., 1999). Interestingly, hypoxia induces axon guidance defects through the upregulation of VAB-1 expression (Pocock and Hobert, 2008). EFN-4 is the most divergent ephrin in *C. elegans* and signals non-canonically in the dorsal navigation of SDQ axons, and the

extension of AIY and D-type motor neurons (Chin-Sang et al., 2002; B. Dong et al., 2016; Schwieterman et al., 2016).

### 1.3.4. Wingless/Wnt and Frizzled receptors

In *Drosophila*, Wnt5 signals at the posterior commissure to repel some commissures anteriorly via a non-canonical Derailed receptor (Yoshikawa et al., 2003). However, this function is not directly conserved in vertebrates, where Wnt signaling instead has an attractive effect on commissural guidance in the spinal cord. Once commissures cross the floor plate, they are attracted rostrally by a Wnt gradient and repelled by Sonic hedgehog caudal expression (Bourikas et al., 2005; Lyuksyutova et al., 2003).

In *C. elegans*, there are five Wingless/Wnt genes, MOM-2, ELG-2-, LIN-44, CWN-1 and CWN-2, and four frizzled receptors, MOM-5, LIN-17, MIG-1 and CFZ-2 (Chisholm et al., 2016). These proteins have diverse functions in *C. elegans*, however their role in axon guidance is diminished in comparison to vertebrates (Sawa and Korswagen, 2013; Yam and Charron, 2013). In *C. elegans*, Wnts and their receptors impact the anterior-posterior outgrowth and navigation of several axons (Kennerdell et al., 2009; Maro et al., 2009; Pan et al., 2006; Song et al., 2010). Wnt signaling has also been implicated in determining the anterior-posterior polarity of several neurons (Hilliard and Bargmann, 2006; Prasad and Clark, 2006). Notably, the pioneer AVG exhibits polarity defects due to excessive Wnt signaling in *plr-1* mutants (Bhat et al., 2015; Moffat et al., 2014). *lin*-17/f*rizzled* mutants do display highly penetrant PVPR crossover defect, and defects in PVQL's ability to fasciculate to PVPR (Steimel et al., 2010).

### 1.3.5. Heparan sulfate and heparan sulfate proteoglycans

Heparan sulfate is a long polysaccharide chain that can attach to core proteins to form heparan sulfate proteoglycans (HSPGs). Enzymes modify its structure, and the differential modification of heparan sulfate in different parts of the developing organism, including modification of HSPGs, could act as a code that directs axon and cell navigation (Bülow and Hobert, 2004). In mice unable to synthesize heparan sulfate, the optic chiasm retinal axon and forebrain commissure defects observed were similar to Slit1/Slit2 double mutants and netrin-1 mutants defects respectively (Inatani et al., 2003).

Further work in mice revealed that without heparan sulfate, spinal commissures could not respond to netrin, suggesting that heparan sulfate is required for netrin signaling in these neurons (Matsumoto et al., 2007). Research in *Drosophila* confirmed that heparan sulfate functions in the Slit signaling pathway, through the HSPG Syndecan binding both Slit and Robo (Johnson et al., 2004; Steigemann et al., 2004). Syndecan may act as a coreceptor that modulates Slit signaling. Furthermore, severe disruption of heparan sulfate synthesis in zebrafish induces defects in retinal axons similar to the *ast*/*Robo2* mutant, indicating that heparan sulfate is required for Slit signaling in these axons (Lee et al., 2004).

In *C. elegans*, heparan sulfate has been implicated in axon guidance as well. The three heparan sulfate modifying enzymes and the HSPG SDN-1/Syndecan have been found to have nuanced roles in axon guidance (Rhiner et al., 2005). Mutations in SDN-1/Syndecan and the different modifying enzymes cause various inter and motor neurons axons to aberrantly cross the midline and result in motor neuron commissures defects (Bülow and Hobert, 2004; Rhiner et al., 2005). However, while sometimes these genes work together to guide an axon, the profile of axon guidance defects across different neurons in these mutants is unique. Like in other organisms, SDN-1/Syndecan was found to interact with SLT-1/Slit in the guidance of the AVM axon (Blanchette et al., 2015). The HSPG LON-2/glypican was also discovered to function in axon guidance (Blanchette et al., 2015; Bülow et al., 2008; Gysi et al., 2013). LON-2/glypican associates with UNC-40/DCC and was required for UNC-6/netrin signaling during AVM and inhibitory motor neuron neurite guidance (Blanchette et al., 2015; Gysi et al., 2013). However, this function did not require LON-2/glypican's heparan sulfate chain. Minor axon guidance defects have also been observed in the HSPGs UNC-52/Perlecan and CLE-1/collagen XVIII (Chisholm et al., 2016). Interestingly, while null mutations in vital heparan sulfate elongating enzymes are lethal, partial loss of function mutations in these enzyme that greatly reduce the amount of heparan sulfate in the embryo have highly penetrant axon guidance defects in many neurons, including PVQ, AVM, HSN, DD/VD and DA/DB motor neurons (Blanchette et al., 2017). This suggests that heparan sulfate might play a larger role in *C. elegans* axon guidance than was previously thought.

## 1.4. Adhesion receptors in axon guidance

### 1.4.1. Cadherins

Cadherins are a family of cell adhesion proteins that function in tissue formation and nervous system patterning during development (Gumbiner, 1996; Takeichi, 1995). Calcium binds to adjacent cadherins, resulting in the formation of a rigid rod structure and homophilic binding (Hill et al., 2001; S. D. Patel et al., 2003). Classical cadherins have a conserved intracellular domain that allows them to interact with catenins, which can link the receptor to the actin cytoskeleton (Pettitt, 2005; Ranscht, 1994; Stepniak et al., 2009). Classical cadherins also function as sensors that signal through catenins which participate in developmental signaling pathways such as the Wnt pathway (Clevers, 2006; Grigoryan et al., 2008; Stepniak et al., 2009). Classical cadherins have also been implicated in the outgrowth of retinal axons (Riehl et al., 1996). The *C. elegans* genome contains 12 cadherin genes, which encode 13 cadherin proteins, but only *hmr-1* is a classical cadherin (Cox et al., 2004; Hill et al., 2001). One of its splice variants, HMR-1B, plays a modest role in D-type motor neuron commissure guidance and AS motor neuron axon fasciculation, probably as a link between the growth cone and its substrate (Broadbent and Pettitt, 2002).

However, other *C. elegans* cadherins have been implicated in axon guidance, such as the Fat-like cadherin CDH-4. It contains the conserved 34 cadherin repeats characteristic of Fat cadherins and is expressed in most neurons (Tanoue and Takeichi, 2005). *cdh-4* mutations result in the disorganization of the VNC and DNC axon bundles, but axons that navigate individually were unaffected (Schmitz et al., 2008). This suggests CDH-4 may function in axon fasciculation. However, axon outgrowth polarity is affected in some interneurons and motor neurons in *cdh-4* mutants, suggesting it may also have a non-adhesive function (Schmitz et al., 2008). Another cadherin implicated in axon guidance is FMI-1 (Flamingo)/Starry night, which is a seven-pass transmembrane cadherin that functions in the planar cell polarity signaling pathway in *Drosophila* (Usui et al., 1999). In *C. elegans*, *fmi-1* mutations cause defects in synapse development and in axon guidance (Najarro et al., 2012; Steimel et al., 2010). D-type motor neurons send errant commissures into the left VNC and motor neurons often send commissures up the wrong side of the animal in *fmi-1* mutants (Steimel et al., 2010). *fmi-1* mutations also induce interneuron midline crossing defects in the VNC, including in the pioneer axon,

PVPR (Steimel et al., 2010). However, unlike in most other genes that are involved in PVPR guidance, *fmi-1* mutants also display pioneer/follower fasciculation defects between PVQL and the pioneer PVPR (Steimel et al., 2010).

### 1.4.2. IgCAMs

IgCAMs are a family of cell surface proteins consisting of immunoglobulin domains and sometimes containing additional fibronectin III repeats. They can mediate both homophilic and heterophilic adhesion (Cox et al., 2004). Furthermore, members of this family, which includes previously described UNC-40/DCC and SAX-3/Robo, act as receptors for secreted guidance cues (Dickson, 2002). In mice, IgCAMs have been shown to function in the development of its retinal axon pathways. Nr-CAM signals to reverse the semaphorin/plexin repulsion pathway to promote retinal axon adhesion (Kuwajima et al., 2012). DSCAM (Down syndrome cell adhesion molecule) also promotes the outgrowth and fasciculation of retinal axons (Bruce et al., 2017).

The *C. elegans* genome contains 17 IgCAMs, several of which function in axon guidance (Hutter et al., 2000; Teichmann and Chothia, 2000). Mutations in *lad-2*/*L1CAM* produce axon misdirection or extension defects in SMD, PLN, and SPQ neurons (X. Wang et al., 2008). LAD-2 has been shown to function as a non-canonical ephrin receptor, interacting with EFN-4 to mediate SPQ axon guidance (B. Dong et al., 2016). RIG-6/Connectin acts in the extension PLM and ALM axons and plays a minor role in D-type motor neuron axon guidance (Katidou et al., 2013). It also acts redundantly with RIG-1, RIG-3, and RIG-5 to prevent midline crossing of interneurons in the VNC (Schwarz et al., 2009). *wrk-1* mutants also display midline crossing defects in interneurons in the VNC, including in PVPR (Boulin et al., 2006; Schwarz et al., 2009). WRK-1 is capable of interacting with VAB-1 and VAB-2, and *wrk-1* mutants have similar midline crossing defects to *vab-1* worms (Boulin et al., 2006). Since WRK-1 is expressed by motor neurons along the ventral midline, it has been hypothesized that it repels VAB-1 expressing growth cones (Boulin et al., 2006).

## 1.5. The leucine-rich repeat motif

### 1.5.1. Leucine-rich repeat proteins

Although the Leucine-Rich Repeat (LRR) protein SLT-1/Slit is an important axon guidance cue, many other LRR proteins have not been well studied in the context of axon guidance. However, the LRR domain's ability to bind disparate proteins and the prevalence of the characterized LRR proteins in neurodevelopmental functions makes LRR proteins good candidates when looking for novel axon guidance genes (Bando et al., 2005; Dolan et al., 2007). The LRR motif is a common protein motif and is present throughout the three domains of life: eukaryotes, prokaryotes and archaea. It was first recognized in the leucine-rich α2-glycoprotein in 1985 (Bella et al., 2008; Takahashi et al., 1985). LRRs are 20-30 amino acids long and contain the following sequence: LxxLxLxxNxL; L is leucine, N is asparagine and x can be any amino acid (Kobe and Kajava, 2001). However, other hydrophobic amino acids can sometimes replace leucine and asparagine. A single LRR consists of a β sheet and a α helix. Multiple LRRs domains together form a larger, concave β sheet that facilitates protein-protein interactions (Kobe and Deisenhofer, 1994). However, the general structure of LRR proteins can vary greatly, allowing them to bind to diverse ligands (Figure 1.7). LRR's have also been shown to dimerize in some cases (Kajander et al., 2011; Scott et al., 2006, 2004).

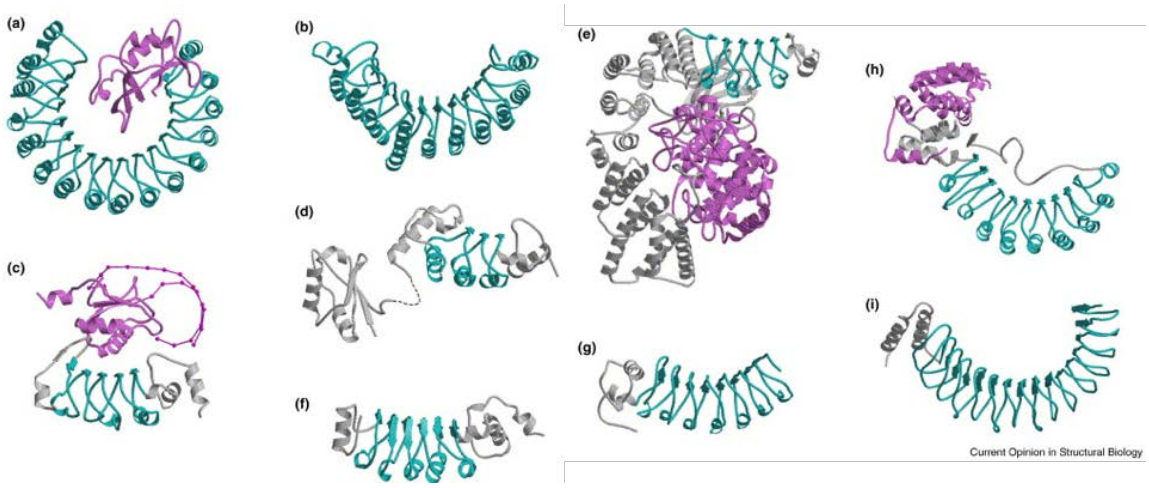


**Figure 1.7 Depiction of the structure of various LRR proteins**
LRR repeats together form a concave β sheet that is used for protein-protein interactions. The variance in shape of LRR proteins is displayed in this figure. The LRR domain is in blue, the flanking regions that are important for the LRR's function are in gray, and other domains are

depicted in pink. These proteins are **a)** RI (PDB code 2BNH), **b)** rna1p (PDB code 1YRG), **c)** U2A′–U2B″ (PDB code 1A9N), **d)** TAP (PDB code 1FO1), **e)** RabGGT (PDB code 1DCE), **f)** dynein LC1 (PDB code 1DS9), **g)** InlB (PDB code 1D0B), **h)** Skp2–Skp1 (PDB code 1FQV) and **i)** YopM (PDB code 1G9U). (Modified from Kobe and Kajava, 2001).

The majority of LRR proteins are involved in signal transduction pathways (Kobe and Deisenhofer, 1994). As a common protein type, LRR proteins are involved in many processes including adhesion, extracellular matrix formation, RNA processing, immune response, apoptosis, modulation of voltage gated channels, memory, and neural development (Bando et al., 2005; Bella et al., 2008; Ma et al., 2006; Peltola et al., 2011). Extracellular LRR (eLRR) proteins in particular have been discovered to function in many neural processes, including in synapse formation, synapse plasticity, dendrite/axon guidance, and fasciculation (Bando et al., 2005; Dolan et al., 2007).

The LRR TransMembrane neuronal (LRRTMs) proteins are a family of single-pass transmembrane proteins that contain only LRRs on their extracellular domain (Figure 1.8c, 1.8f; de Wit and Ghosh, 2014). This family is expressed on the postsynaptic membrane and is involved in excitatory synapse differentiation. The most well characterized member of this family, LRRTM2, functions in postsynaptic differentiation by recruiting synaptic proteins, such as the important scaffolding protein PSD-95 (via its PDZ binding motif), as well as glutamate receptor subunits (de Wit et al., 2009; Linhoff et al., 2009). LRRTM1 and LRRTM2 also promote presynaptic differentiation by transynaptically binding to the influential presynaptic organizer neurexin with their LRR domains (Ko et al., 2009; Yamagata et al., 2018). LRRTM4 induces presynaptic differentiation through a different mechanism, by binding glypicans, a heparan sulfate proteoglycan (de Wit et al., 2013).

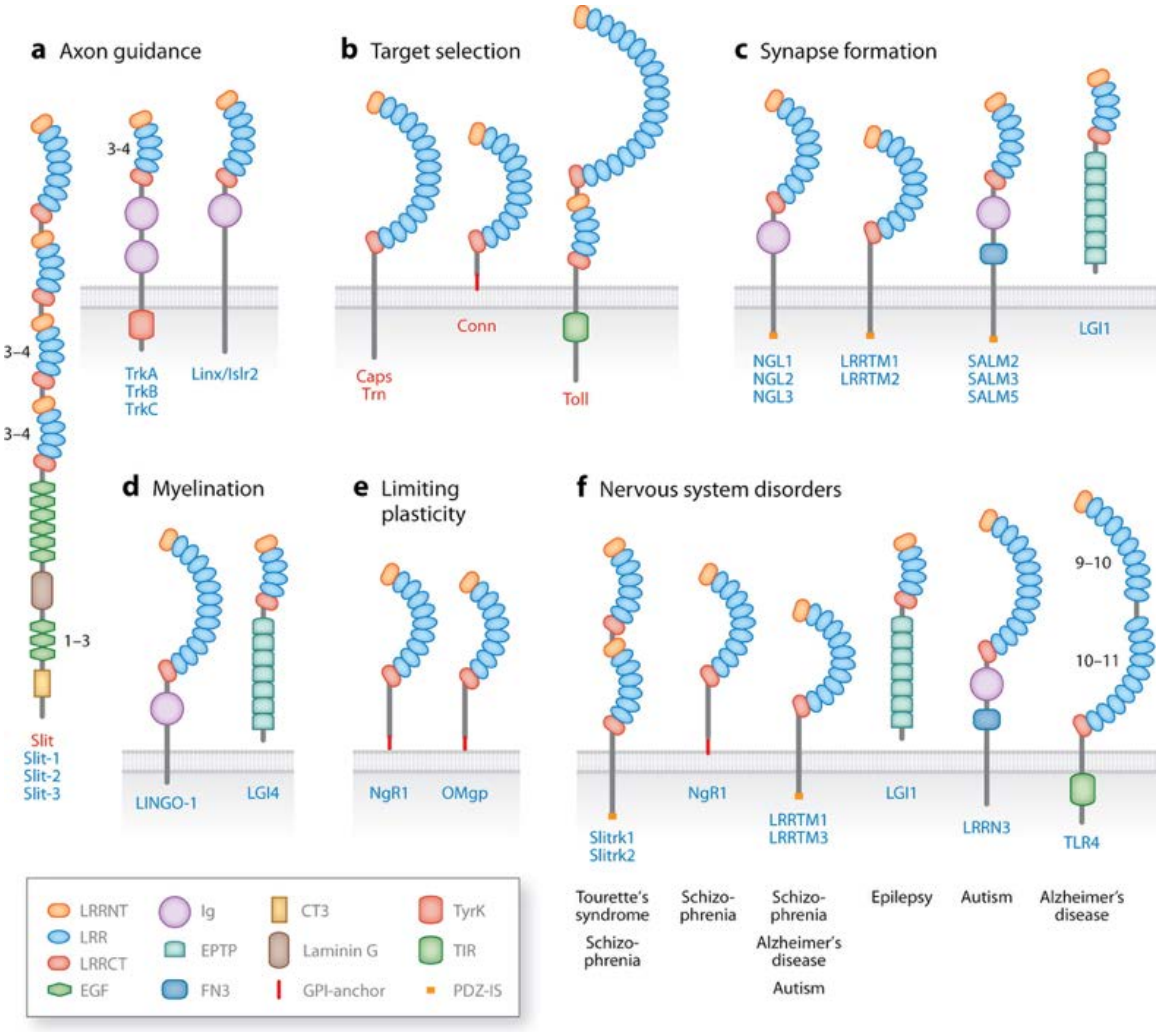


**Figure 1.8 Illustration of prominent eLRR proteins involved in the nervous system**

eLRR proteins function in many neuronal signaling pathways. This figure depicts some of the influential eLRR proteins that are involved in **a)** Axon guidance, **b)** neurite target selection, **c)** synapse formation, **d)** Myelination, **e)** Plasticity, and eLRRs that are implicated in **f)** Nervous System disorders. Modified from de Wit et al., 2011).

LRRTMs also play a role in mature synapses. If LRRTM1 or LRRTM2 are mutated in CA1 mouse hippocampal neurons, long-term potentiation (LTP) is blocked (Soler-Llavina et al., 2013). This can only be rescued through re-expression of their extracellular domain. LRRTM1 and LRRTM2 stabilize AMPA receptors in mature synapses, and therefore their loss prevents the increase in AMPA receptors that occurs during LTP (Bhouri et al., 2018). No known invertebrate homologs exist for this extracellular LRR (eLRR) family, however *C. elegans* do possess a group of proteins

(LRON proteins) with similar domain structure, which have been largely uncharacterized (de Wit et al., 2011).

Many other eLRR proteins have functions in the nervous system. The Slitrks, synaptic adhesion-like molecules (SALM), fibronectin leucine-rich repeat transmembrane protein (FLRT) and Netrin G ligands (NGLs) families all function in synaptogenesis and/or synaptic transmission (Figure 1.8; (de Wit and Ghosh, 2014). Other eLRR's such as the eLRR protein Caps and Toll receptors function in axon and dendrite target selection, where neural processes choose which neurons to synapse with (Figure 1.8b; de Wit et al., 2011; Rose et al., 1997). Importantly, a number of these eLRR genes have also been discovered to function in axon guidance.

### 1.5.2. Leucine-rich repeat proteins in axon guidance

As previously described, the secreted eLRR SLT-1/Slit has a well characterized role in axon guidance. More recently, other eLRR proteins have also been found to act in axon guidance pathways. In mouse thalamic neurons, FLRT3 actually functions in the Slit pathway in mice. FLRT3 is a transmembrane eLRR protein that also contains a fibronectin domain. In mice, it is a coreceptor to Robo1, and in the presence of Slit1, it promotes attraction to netrin by upregulating the DCC receptor (Leyva-Díaz et al., 2014). Intriguingly, FLRT2 and FLRT3 have also been shown to shed their extracellular domains and bind to Unc-5B and Unc-5D receptors as an inhibitory cue for mouse cortical axons (Yamagishi et al., 2011).

The TRK receptors, part of the cell-surface receptor tyrosine kinase (RTK) family, consist of a smaller LRR domain, with two immunoglobulin (IG) domains on its extracellular surface (Figure 1.8a). They also have an intracellular tyrosine kinase domain. Trk's are important neurotrophin receptors that function in neuron survival and synapse development (Barbacid, 1994; Huang and Reichardt, 2001). Their IG domain is important for binding neurotrophins, while their LRR domain modulates this ligand interaction (Ultsch et al., 1999; Windisch et al., 1995). Trk's have been shown to function in axon guidance through binding neurotrophins (de Wit et al., 2011; Segal, 2003). *in vitro*, TrkA is capable of turning growth cones toward a neurotrophin source (Gallo et al., 1997). *in vivo* TrkA is necessary for the segregation of axons into ocular dominance columns in cats (Cabelli et al., 1997). TrkA is also necessary for the

innervation of the skin by nociceptor sensory neurons in mice (Patel et al., 2000). Additionally, TrkA signaling functions in axon guidance within the mouse spinal cord, keeping nociceptor axons out of deep layers of the spinal cord (Guo et al., 2011). Furthermore, in *TrkC* mutants proprioceptor axons did not reach the spinal cord or their target muscles (T. D. Patel et al., 2003). Mouse mechanosensory neurons require TrkB for most of their axons to reach their correct hair follicle targets (Perez-Pinera et al., 2008). More generally, TrkB signaling is important for axonal branching (Gonzalez et al., 2016).

The eLRR Linx (also known as ISLR-2), has a similar ectodomain to the Trk's, though it has an atypical fibronectin domain and only one IG domain (Figure 1.8a; Homma et al., 2009). Linx interacts with TrkA to modulate its activity during axon guidance (Mandai et al., 2009). Linx can also act independently of neurotrophin receptors in thalamocortical axon navigation. Without Linx, many mouse thalamocortical axons do not properly navigate to their target destination and Linx expression in both guidepost cells and adjacent axons is important for guiding these axons (Abudureyimu et al., 2018; Mandai et al., 2014). Linx is also involved in retinal axon navigation through the optic chiasm of zebrafish (Panza et al., 2015). Multiple retinal axon guidance defects where observed in *Linx* mutants, including axons entering the opposite optic nerve and extending back toward the retina.

The NGLs play a role in circuit development, in both synapse formation and axon guidance. They are structurally similar to LRRTM's, but with an additional IG domain and a atypical fibronectin domain (Figure 1.8c; Homma et al., 2009). NGL-1 and NGL-2 bind to netrin-G1 and netrin-G2 respectively, and seem to function in axon guidance as well as synapse formation (Kim et al., 2006). The netrin-G family is structurally related to the axon guidance cue netrin, however they are GPI-anchored proteins. There is modest evidence that NGL-1/2 might be involved in axon guidance. In cultured thalamic neurons, NGL-1/netrin-G1 binding induced axons to grow across the NGL-1 containing substrate (Lin et al., 2003). More recently, NGL-2 has been found to be expressed in growth cones of a subset of neurons, horizontal cells, in the retina (Soto et al., 2013). In *ngl-2* mutant mice, these axons would extend aberrantly into the outer nuclear layer and would have overelaborate branches with less synapses. This seems to indicate a role for NGL-2 in inhibiting horizontal cell axons, likely after binding netrin-G2, which is present in the outer nuclear layer.

While studying axon regeneration after injury in rodents, other eLRR receptors were found to function in axon guidance. The Nogo Receptor 1 (NGR1; also called the Nogo-66 receptor) is a GPI-linked eLRR protein with only LRR motifs on its extracellular domain. NGR1 binds to Nogo (Nogo-66), a component of myelin, and it inhibits axon extension by inducing growth cone collapse (Fournier et al., 2001; Yamashita et al., 2005). Through its coreceptors P75 and Lingo-1, NGR1 binding to Nogo induces growth cone collapse through the Rho GTPase pathway (Filbin, 2003; Mi et al., 2004). The transmembrane coreceptor Lingo-1 is an eLRR protein as well, with a single IG domain. In later *in vitro* research, NGR1 was implicated in guiding axons through the mouse optic chiasm, likely through interactions with Nogo expressing radial glia (Schwab, 2010; J. Wang et al., 2008; Yu et al., 2020). Axons crossing the chiasm downregulate NGR1 to cross the midline. NGR1/Nogo signaling has also been demonstrated to be a repulsive adhesion cue in cultured neurons, as knocking it out increased axon fasciculation (Petrinovic et al., 2010).

Later, another transmembrane coreceptor for NGR1 was found, Amigo-3 (Amphoterin-induced gene and open reading frame 3), which also functions in the myelin induced growth cone inhibition pathway (Ahmed et al., 2013). The *Amigo* family of genes are also eLRRs, each containing 6 LRR domains and an IG domain. Another *Amigo* gene, *Amigo-1*, has been implicated in the homophilic fasciculation of axons in the zebrafish brain (Kuja-Panula et al., 2003; Zhao et al., 2014). *In vitro* experiments also showed that Amigo-1's presence on a substrate induced neurites to extend along it (Kuja-Panula et al., 2003). Thus, it also might also act as an attractive adhesive cue.

## 1.6. The extracellular-Leucine Rich Repeat-Only gene family

The extracellular-Leucine Rich Repeat-Only (LRON) family in *C. elegans* consists of 16 genes. These *lron* genes are characterized by only having LRRs on their extracellular domain (Figure 1.9). Most of these are single pass transmembrane proteins, but some are GPI-linked or secreted. While these genes share a general domain structure, due to rapid divergence during evolution most of them do not show much similarity at the sequence level, with each other or with comparable genes in other species (Dolan et al., 2007). However, the LRON family does share a similar protein structure with the LRRTM family in humans.

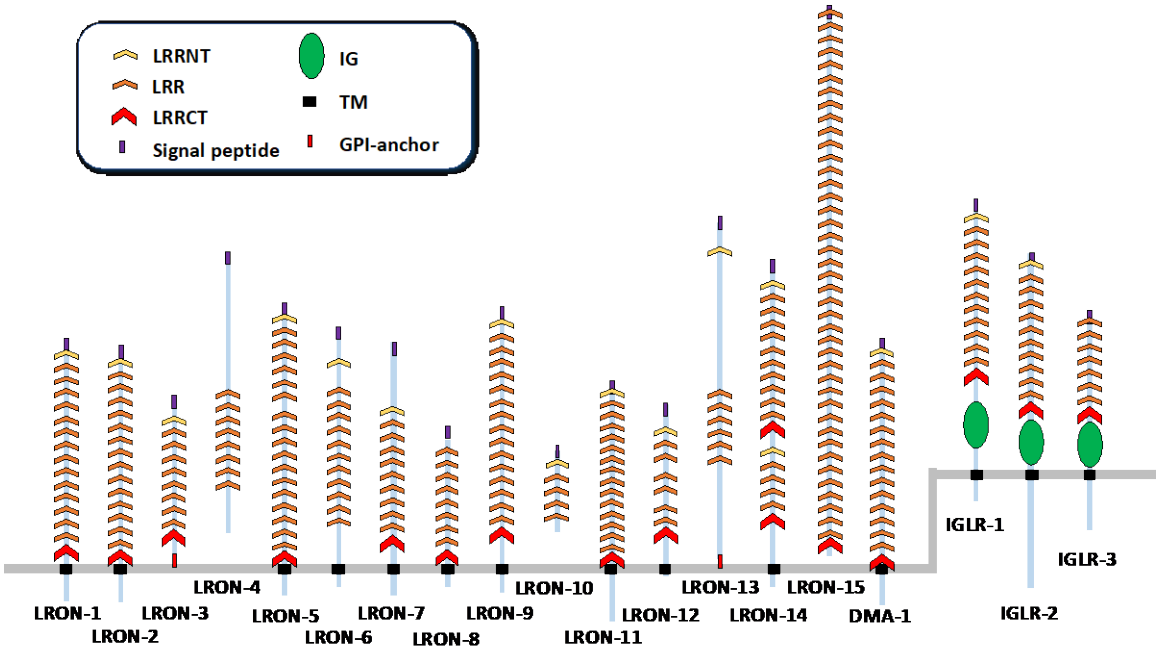


**Figure 1.9 Domain organization of the LRON and IGLR families**
This figure depicts the domain organization of the LRON and IGLR family proteins. LRR domains are depicted by orange chevrons, LRRNT caps are yellow chevrons, and LRRCT caps are red chevrons. IG domains are represented as green ovals. Transmembrane domains are in black, the signal peptides are purple, and GPI-anchors are red. These protein's domain organization was determined by consulting SMART, Interpro and Phobius domain predictions. For the LRR domains, I also comparing these results to the LRR domains predicted by LRRscan (Dolan et al., 2007).

Although there is evidence that some members of the *lron* family are expressed in neurons, most *lron* genes have not been studied (Liu and Shen, 2011; Packer et al., 2019). The exception is *dma-1*, which has been found to play an important role in dendrite guidance and branching in the PVD neuron (Figure 1.10). The PVD dendrites contain a thick primary dendritic branch running longitudinally across the animal. Secondary dendrite branches extend perpendicularly from this larger branch before themselves branching into 3' dendrites that run laterally, parallel to the primary dendrite. Finally, 4' dendrites branch outward at a 90-degree angle from the 3' dendrites to create a menorah shape. In PVD's dendrites, DMA-1 forms an adhesion complex with SAX-7/L1CAM and MNR-1 which are expressed in the adjacent hypodermis (Dong et al., 2013; X. Dong et al., 2016). This adhesion complex is important for the guidance of the primary and 3' dendrites along their longitudinal paths.

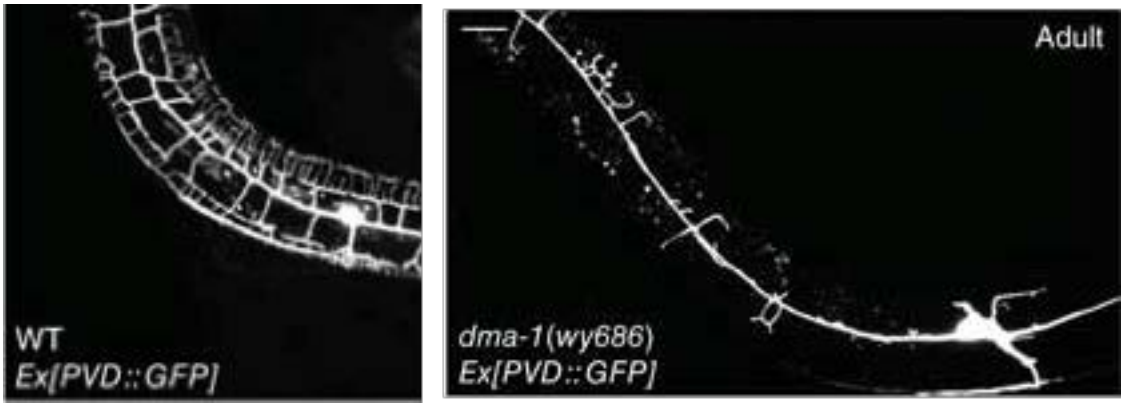


**Figure 1.10 Dendrites of the PVD neuron in wildtype and *dma-1*(*wy686*) mutants**
**a)** Wildtype PVD dendrites have four stages of dendritic branching events, eventually creating the menorah shape at its 4' branches. **b)** The PVD dendrites in a *dma-1*(*wy686*) mutant. The secondary dendrites are not able to properly form and few 3' dendrites are seen. (Modified from Liu and Shen, 2011).

Since DMA-1 promotes adhesion of the primary dendrites and the 3' dendrites to their longitudinal path, overexpression of DMA-1 actually results in a similar phenotype to *dma-1* mutants, because 2' dendrites are unable to escape the adhesive substrate (X. Dong et al., 2016). KPC-1/Furin is essential to temporally downregulate DMA-1 expression to allow extension of dendrites away from the adhesive SAX-7/MNR-1 substrate (X. Dong et al., 2016; Salzberg et al., 2014). It binds to DMA-1's extracellular domain and directs it into a late endosome for degradation.

Further research has revealed that DMA-1 signals via two, somewhat redundant pathways. DMA-1 signals intracellularly through its intracellular PDZ domain to form a complex with the Rac1 GEF TIAM-1 and ACT-4/actin (Tang et al., 2019; Zou et al., 2018). This complex links the DMA-1 adhesion complex with the actin cytoskeleton and is essential for the formation of 4' branches. It is possible that this interaction allows the adhesion complex to divert some of the force that is generated by the polymerizing f-actin pushing against the distal cell membrane. This would decrease the rate of depolymerization of f-actin, allowing it to extend the cell membrane along the adhesive substrate. Another possibility is that the strong binding of TIAM-1 to ACT-4 allows it to localize more ACT-4 distally when it is associated with DMA-1. Additionally, DMA-1 also signals through its extracellular domain binding HPO-30 which then recruits the WVE-1/Wave Regulatory Complex (WRC; Tang et al., 2019; Zou et al., 2018). The DMA-1/HPO-30 interaction is also important for the formation of 3' and 4' branches. Genetic

interactions indicate that this signaling pathway is parallel to the DMA-1/TIAM-1 pathway.

## 1.7. The *iglr* gene family

Another eLRR gene family in *C. elegans* that has not been studied in axon guidance is the ImmunoGlobulin and LRR domains (IGLR) family. The *iglr* family consists of three genes, which contain LRRs on their extracellular domain as well an IG-like motif. IG domains consist of two β-sheets, one on top of the other, and they facilitate protein-protein binding (Horstkorte and Fuss, 2012; Williams and Barclay, 1988). IGLR genes have a similar domain structure to some of the mammalian LRR and IG domain containing proteins, particularly the Amigos, though they have no known homologs (Homma et al., 2009). Both IGLR-1 and IGLR-2 expression has been observed in neurons (Kuo et al., 2020; Liu and Shen, 2011). Only IGLR-2 has been studied, and it has been discovered to act as a sensor of membrane fluidity in C. elegans (Devkota et al., 2021; Svensk et al., 2016). When the membrane becomes less rigid due to fatty acid saturation or cold temperature, it acts with PAQR/AdipoR1/2 to promote desaturation of fatty acids to return the membrane to homeostasis. IGLR-2 has also been implicated in *C. elegans* immune response, as well as being involved in pathogen avoidance behavior (Kuo et al., 2020). IGLR-1 knockdown has also been found in an RNAi screen to extend worms lifespan by 20%, though further study is required to establish why this occurs (Sutphin et al., 2017).

## 1.8. Thesis objective

The objective of this thesis is to determine if *lron* and *iglr* genes play a role in axon guidance. I focused on the VNC, where I could observe many different subsets of neurons with various fluorescent markers. I primarily used a pan-neuronal marker, and a marker that highlighted the PVPR and AVG pioneers. This allowed me to identify mutants with misguided axons within the VNC. I found several genes (*lron-3, lron-5*, *lron-8*, *lron-11*, *lron-14*, *iglr-1* and *iglr-2*) that, when mutated, had significant axon guidance defects. For most genes, the primary axon guidance defects observed were crossover defects, where axons inappropriately crossed from one VNC tract into the other. The exception was *iglr-2* where I observed penetrant defasciculation of the left

VNC. This occurs when the left tract axon bundle splits instead of remaining tightly fasciculated.

Of the genes I studied, *lron-11* had the highest penetrance of crossover defects. Therefore, I characterized *lron-11* further by utilizing command interneuron, AVK, HSN, DD/VD and DA/DB motor neuron markers. *lron-11* mutants had significant defects in many of these neuron subtypes, such as DD/VD neurites crossing into the left tract, and both DD/VD and DA/DB commissures navigating up the wrong side of the animal. Finally, I also looked for interaction between *lron-11* and other *lron* genes with significant axon guidance defects by creating the *lron-11*; *lron-14* and *lron-11*; *lron-3* double mutants. These results were inconclusive for the *lron-11*; *lron-14* double mutant as I only observed an additive increase in pan-neuronal axon guidance defects in the *lron-11*; *lron-14* double mutant, but not in the pioneer marker. The *lron-11*; *lron-3* double mutant displayed defects with similar penetrance to the *lron-11* mutant.

This research demonstrates that *lron-11* functions in the guidance of different types of axons in the *C. elegans* VNC. It also provides preliminary evidence for the involvement of other *lron* and *iglr* genes in axon guidance, particularly *iglr-2*.

# Chapter 2. Materials and methods

## 2.1. Maintenance and strains

I grew worms on Easiest Worm Media (EWM) plates seeded with OP50 *Escherichia coli*. The EWM mix is made up of 55g Tris-HCl, 24g Tris-OH, 310g Bacto Peptone, 800mg Cholesterol, and 200g NaCl. 5.9g of this mix was added to 18g agar and then H2O was added up to 1L's of total volume. Strains were typically grown and maintained at 20°C or 15°C, following standard procedures (Brenner, 1974).

I used these fluorescent markers to observe axons: *hdIs26[odr-2::CFP, sra-6::DsRed2] III*, *hdIs28[odr-2::CFP, sra-6::DsRed2]*, *hdIs29[odr-2::CFP, sra-6::DsRed2], evIs111[rgef-1::GFP] V*, *oxIs12[unc-47:GFPNTX;lin-15(+)] X*, *rhIs4[glr-1::GFP, dpy-20(+)] III*, *zdIs13[tph-1::gfp]*, *hdIs25[unc-129::CFP, unc-47::DsRed2]*, *hdIs54[flp-1::GFP]*, *evIs82A[unc-129::GFP] II*.

Below is a table of all the LRON and IGLR alleles I phenotyped (Table 2.1).

**Table 2.1 List of alleles and strains**

| Gene | chr | allele | strain | Mutation Type |
|---|---|---|---|---|
| *lron-1* | X | *gk5081* | VC4008 | ~3.5kb deletion of all exons + a ~5kb insertion* |
| *lron-3* | X | *ok2614* | RB1980 | ~2kb deletion of the final exon, including the C terminus |
| | X | *gk5319* | VC4233 | ~4kb deletion of exons 5-8 and part of exon 9 + ~5kb insertion* |
| *lron-4* | II | *gk5099* | VC4026 | ~2kb deletion of exons 3-8 and part of exon 9 + a ~5kb insertion* |
| *lron-5* | III | *gk959442* | VC41011 | A point mutation that induces a premature stop codon in exon 7, lacks its transmembrane domain |
| *lron-6* | I | *gk736335* | VC40637 | A point mutation that induces a premature stop codon in exon 10, lacks its transmembrane domain |
| *lron-7* | X | *gk5353* | VC4270 | ~2kb deletion of exons 4-10 and part of exons 3 and 11 + a ~5kb insertion* |
| *lron-8* | I | *gk5317* | VC4231 | ~5kb deletion of all exons + a ~5kb insertion* |

| Gene | chr | allele | strain | Mutation Type |
|---|---|---|---|---|
| *lron-10* | III | *gk5064* | VC3992 | ~2kb deletion of part of the exon 1, exon 2 and part of exon 3 + a ~5kb insertion* |
| *lron-11* | I | *gk5321* | VC4235 | ~ 3kb deletion of exon 3-5 and part of exon 6 + a ~5kb insertion* |
| | I | *ok2333* | VH2839 | ~1kb deletion of most of the last exon, including the transmembrane domain |
| *lron-12* | III | *gk187625* | VC20146 | A point mutation that induces a premature stop codon in exon 5, lacks its transmembrane domain |
| *lron-13* | III | *gkDf31* | VC3229 | ~800bp deletion of exon 5, frameshift mutation^ |
| *lron-14* | IV | *gk401715* | VC20783 | A point mutation that induces a premature stop codon in exon 6, lacks its transmembrane domain |
| *lron-15* | II | *gk918201* | VC40994 | A point mutation that induces a premature stop codon in exon 5 |
| *dma-1* | I | *wy686* | TV1624 | ~5kb deletion of all exons |
| *iglr-1* | X | *gk687851* | VC40547 | A point mutation that induces a premature stop codon in exon 6, lacks its transmembrane domain |
| *iglr-2* | III | *et34* | QC136 | A point mutation that induces a premature stop codon in exon 2, lacks its transmembrane domain |

*lron-2*, *lron-9* and *iglr-3* were not studied because mutations in these genes are lethal. *This insertion includes a myo-2::GFP marker, which is expressed in the pharynx and allows for the easy identification of the presence of this allele in an animal. ^This mutation was larger than predicted at Wormbase.org, which states that *gkDf31* is a 466bp deletion.

## 2.2. Crossing

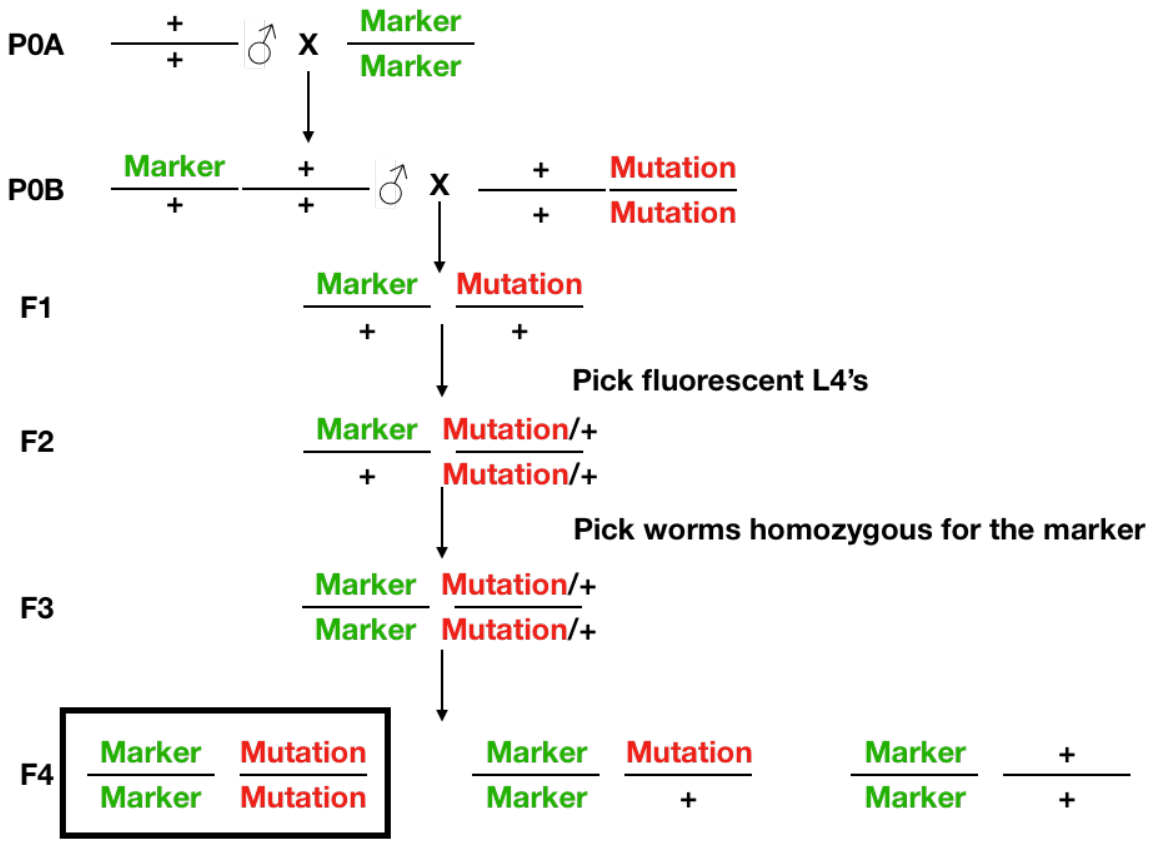


**Figure 2.1 Strategy for crossing fluorescent markers into mutants strains**
At the F1 stage, 5 fluorescent L4's were picked onto new plates. F3's were selected for by picking worms homozygous for the fluorescent marker. I then subcloned 20 worms from F3 plate that were homozygous for the marker. These F4's would then be genotyped to identify the homozygous mutant plates. Markers and alleles of interest were always present on different chromosomes.

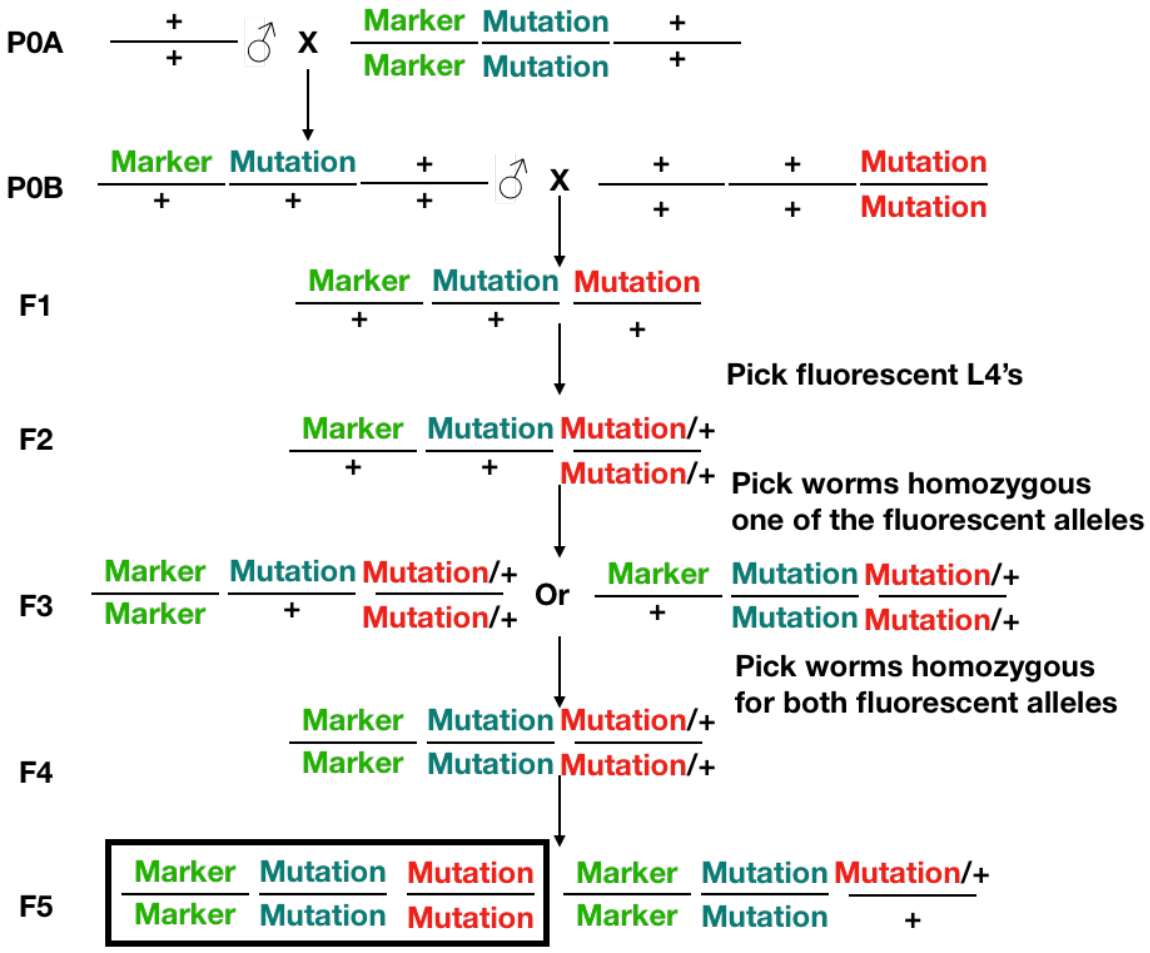


**Figure 2.2 Crossing scheme example for creating double mutants**
When creating double mutants, I started with one strain that contained a mutant allele and a marker allele, and another strain that contained a different mutant allele. One of these mutant alleles always contained a fluorescent pharyngeal marker (green mutation in the example). After crossing the strain with the marker with wildtype males, I would pick males to cross with the other mutant allele. I then picked 10 L4's from the F1 that had both fluorescent alleles. Next, I picked 15 worms that were homozygous for one of the fluorescent alleles from F2 plates with no males. After confirming which F3 plates were homozygous for one fluorescent allele, I then selected 30 worms, homozygous for the other fluorescent allele. Double homozygous F4 plates were subcloned from, up to a total of 80 plates. These plates were then genotyped for the nonfluorescent mutant allele. All alleles in these crosses were on different chromosomes.

## 2.3. Genotyping

Worms were collected by pipetting 40µl of M9 buffer (3 g KH2PO4, 6 g Na2HPO4, 5 g NaCl, 1 ml 1 M MgSO4, H2O to 1 litre) onto the plate, and transferring 20µl into a microcentrifuge tube. 20µl of 2X lysis buffer (containing 100ug/ml Proteinase K) was then added, and the solution was mixed with the pipette. The solution was frozen at -80°C for at least 15 minutes. A thermocycler was then used to run this

protocol: 1) 65°C for 90 minutes. 2) 95°C for 30 minutes. 3) 4°C pause. The lysate was stored at 4°C.

PCR was commonly used to identify plates that contain animals homozygous for the mutant allele. If the allele involves a deletion, I amplified the DNA with two primer pairs; one primer pair would flank the deletion, whereas the other would contain one primer inside the deletion. Typically, I used this protocol for each sample: 14.8µl water, 2.5µl TBA buffer (10X), 2.5µl dNTPs (2mM), 2.0µl MgCl2 (25mM), 1.0µl for the forward and reverse primer (10mM), 0.2µl self made-Taq, and 1.0 µl of template DNA (obtained from the lysis). The thermocycler protocol was thus: 1) 95°C for 5 minutes. 2) 95°C for 40 seconds. 3) Usually 55-60°C for 40 seconds. 4) 72°C for 90 seconds per 1kb being amplified. Steps 2, 3, and 4 were repeated 35 times. 5) 72°C for 10 minutes. 6) 4°C Pause. The PCR product was then stored at 4°C. Mutant alleles that were point mutation needed to be sent for sequencing. I sent all my sequencing samples premixed to Genewiz, following their sample preparation protocol. Table C1 contains all of the primers I used to genotype the various mutations analyzed in this study.

PCR products were run on agarose gels to discriminate the results. 1-1.5% agrose gels were made by adding agarose to TBE buffer (89mM Tris-Borate and 2mM EDTA) containing 0.5µg/ml of ethidium bromide. This mix was heated for 2 minutes, before being poured into a gel tray. After at least 45 minutes, the PCR products (mixed at a 2:1 ratio with DNA loading dye) was added to the wells and assessed via gel electrophoresis. For sequencing samples, 5µl of PCR product was run on the gel to verify that the PCR worked.

Some CRISPR generated mutations contained an insertion of GFP downstream of the *myo-2* promoter. The bright GFP fluorescence from these mutant animal's pharynx allowed for visual confirmation of the presence of this mutant allele. The presence of the mutation was usually confirmed via PCR as described previously.

## 2.4. Phenotyping

First, 5-10 L4s (depending on the strain) were picked onto each plate, and were grown for 5 days at 20°C. Then, I washed worms off these plates into microcentrifuge tubes with 2% 20mM sodium azide (diluted with M9). These were left for one hour to

induce paralysis. I mounted these worms on 3-4% agar pads. Fluorescent markers allowed visualization of subsets of axons with the Zeiss Axioscope using the 40X magnification objective. Axon guidance defects were only assessed in young adult and adult worms. ~100 worms were scored for each mutant allele with the pan-neuronal (*evIs111*) and pioneer markers (*hdIs26, hdIs28, or hdIs29*). These results were compared to data collected from the marker strain using the $\chi 2$ test for a 2x2 contingency table with the Yates correction, to determine if the mutant's axon guidance defects were significantly different from the marker strain. If a mutant allele displayed penetrant axon guidance defects, I would also phenotype that allele in additional interneuron and motor neuron subtypes, visualized with other fluorescent markers.

I took confocal images of *C. elegans* strains using a Zeiss Axioplan II microscope (Carl-Zeiss AG, Germany) connected to a Quorum WaveFX spinning disc system (Quorum Technologies, Canada). Stacks of confocal images with 0.2 to 0.5 µm distance between focal planes were recorded. Image acquisition and analysis was carried out by using Volocity software (Quorum Technologies, Canada), and were modified in Microsoft Powerpoint.

## 2.5. Expression construct

I used PCR to amplify the putative *lron-11* promoter region (3kb upstream of the start codon) and GFP from the pPD95.75 linearized plasmid. These primer pairs had overlapping tails. I ran a second PCR with nested primers to fuse these PCR products together. I ran this new PCR product on a gel, cut out the largest band and gel purified it with a Thermoscientific gel purification kit. This purified PCR product was injected into gravid hermaphrodites and their progeny were screened for GFP. GFP positive animals were observed using our confocal microscope to identify cells expressing GFP.

# Chapter 3. Results

## 3.1. Axon guidance defects in the ventral nerve cord of *lron* and *iglr* mutants

I used two fluorescent markers to observe mutants in the LRON and IGLR families for axon guidance defects. First, I used a pan-neuronal marker because it enables me to identify defects in any neuron subtype within the VNC or DNC. The second marker I used is a pioneer marker that lets me observe the important PVPR and AVG axons, which pioneer the left and right VNC tracts respectively. I observed the VNC of *lron* and *iglr* mutants with a pan-neuronal and pioneer marker and quantified the axon guidance defects I observed (Table 3.1). Null mutations in the *lron-2*, *lron-9* and *iglr-3* genes are lethal, so these genes were not phenotyped. Preliminary data collected by Saru Sandhu and Skyla Witt indicated that *lron-11* and *lron-3* mutants had significant VNC axon guidance defects. Therefore these mutant alleles were outcrossed before I phenotyped them.

Overall, I found significant axon guidance defects in several genes. *lron-11* has the most penetrant axon guidance defects (Table 3.1). *iglr-2*(*et34*) also had penetrant fasciculation defects in the left VNC. *lron-3*(*gk5319*), *lron-5*(*gk959442*), *lron-8*(*gk5317*), and *lron-14*(*gk401715*) also had significant axon guidance defects (Table 3.1). In the other *lron* and *iglr* genes I did not observe significant axon guidance defects (Appendix B).

**Table 3.1 *Iron* and *iglr* genes axon guidance defects summary**

| *Iron* and *iglr* Genes | Pan-neuronal VNC Defects | Pan-neuronal Marker Defects[4] | PVPR Defects | Pioneer Marker PVPR Defects | AVG Defects | Created with CRISPR/ Cas9^ | Out-crossed |
|---|---|---|---|---|---|---|---|
| *Iron-1*(*gk5081*) | 4% | 5% | 4% | 6%[1] | 0% | Yes | |
| *Iron-3*(*gk5319*) | 11%* | 5% | 17% | 10%[2] | 2% | Yes | Yes |
| *Iron-3*(*ok2614*) | 10% | 5% | 9% | 6%[1] | 0% | | Yes |
| *Iron-4*(*gk5099*) | 1% | 5% | 7% | 6%[1] | 0% | Yes | |
| *Iron-5*(*gk959442*) | 8% | 5% | 23%*** | 7%[3] | 1% | | |
| *Iron-6*(*gk736335*) | 3% | 5% | 3% | 7%[3] | 1% | | |
| *Iron-7*(*gk5353*) | 8% | 5% | 9% | 10%[2] | 2% | Yes | |
| *Iron-8*(*gk5317*) | 13%** | 5% | 4% | 7%[3] | 0% | Yes | |
| *Iron-10*(*gk5064*) | 6% | 5% | 11% | 7%[3] | 2% | Yes | |
| *Iron-11*(*ok2333*) | 29%*** | 5% | 15%* | 6%[1] | 4%** | | Yes |
| *Iron-11*(*gk5321*) | 28%*** | 5% | 19%*** | 6%[1] | 1% | Yes | |
| *Iron-12* (*gk187625*) | 10% | 5% | 4% | 7%[3] | 0% | | |
| *Iron-13*(*gkDf31*) | 7% | 5% | 7% | 7%[3] | 0% | | |
| *Iron-14* (*gk401715*) | 17%*** | 5% | 15% | 10%[2] | 0% | | |
| *Iron-15* (*gk918201*) | 7% | 5% | 5% | 6%[1] | 0% | | |
| *dma-1*(*wy686*) | 5% | 5% | 3% | 6%[1] | 0% | | |
| *iglr-1*(*gk687851*) | 11%* | 5% | 2% | 6%[1] | 0% | | |
| *iglr-2*(*et34*)^^ | 6% | 5% | 4% | 7%[3] | 0% | | Yes |

***p<0.001; **p<0.01; *p<0.05 ($\chi 2$ test). The data in this table does not include defasciculation defects. For pan-neuronal scoring, all genes were observed with the *evIs111* allele. The *evIs111* allele had an average of 5.1% pan-neuronal VNC defects in 787 worms. The *hdIs26* allele had an average of 6.4% PVPR defects in 294 worms. The *hdIs28* allele had an average of 9.8% PVPR defects in 163 animals. The *hdIs29* allele had an average of 6.9% PVPR defects in 159 animals. ^Mutant strains generated with CRISPR/Cas9 should not contain off target mutations. Therefore, these strains were usually not outcrossed (Au et al., 2019). ^^While *iglr-2*(*et34*) mutants did not have

significant penetrance for the axon guidance defects scored in this table, in the pan-neuronal marker these mutants did display significant fasciculation and early separation axon guidance defects (Table 3.38). [1] The pioneer marker used was *hdIs26*. [2] The pioneer marker used was *hdIs28.* [3] The pioneer marker used was *hdIs29*. [4] The marker used was *evIs111*.

### 3.1.1. *Iron-11* pan-neuronal and pioneer axon guidance phenotypes

In wildtype *C. elegans*, the VNC is composed of two parallel axon tracts (Figure 3.1a). Axons should not cross between these tracts. There is an exception at the very anterior end of the VNC where some axons from the head cross into the left tract, and at the posterior end where PVPR and PVQL cross from the right tract into the left tract. Otherwise, when an axon crosses over into the opposite tract this is classified as a crossover defect. If this occurs anterior or posterior to the vulva, it will be termed an anterior or posterior crossover.

I observed axons in strains with two *Iron-11* alleles, *Iron-11*(*ok2333*) and *Iron-11*(*gk5321*). The *Iron-11*(*ok2333*) strain has been outcrossed four times, and *Iron-11*(*gk5321*) was created via CRISPR, so probably does not contain off target mutations (Au et al., 2019). In both *Iron-11*(*ok2333*) and *Iron-11*(*gk5321*) mutant worms with the pan-neuronal marker, there is almost a 30% penetrance of axon guidance defects (Figure 3.1b) (Table 3.2). Most of the defects observed were crossover defects. These crossovers occurred in both the anterior and posterior halves of the VNC. In contrast, the marker strain only had 5% crossover defects. Both *Iron-11* alleles are predicted null mutants, involving deletions of at least the final exon which includes the transmembrane domain. As expected, both alleles displayed similar defect penetrance. For both *Iron-11* alleles, ~5% of mutants displayed dorsal nerve cord defasciculation, though only the *Iron-11*(*gk5321*) defects were significant (Figure 3.1c, 3.1d; Table 3.3).

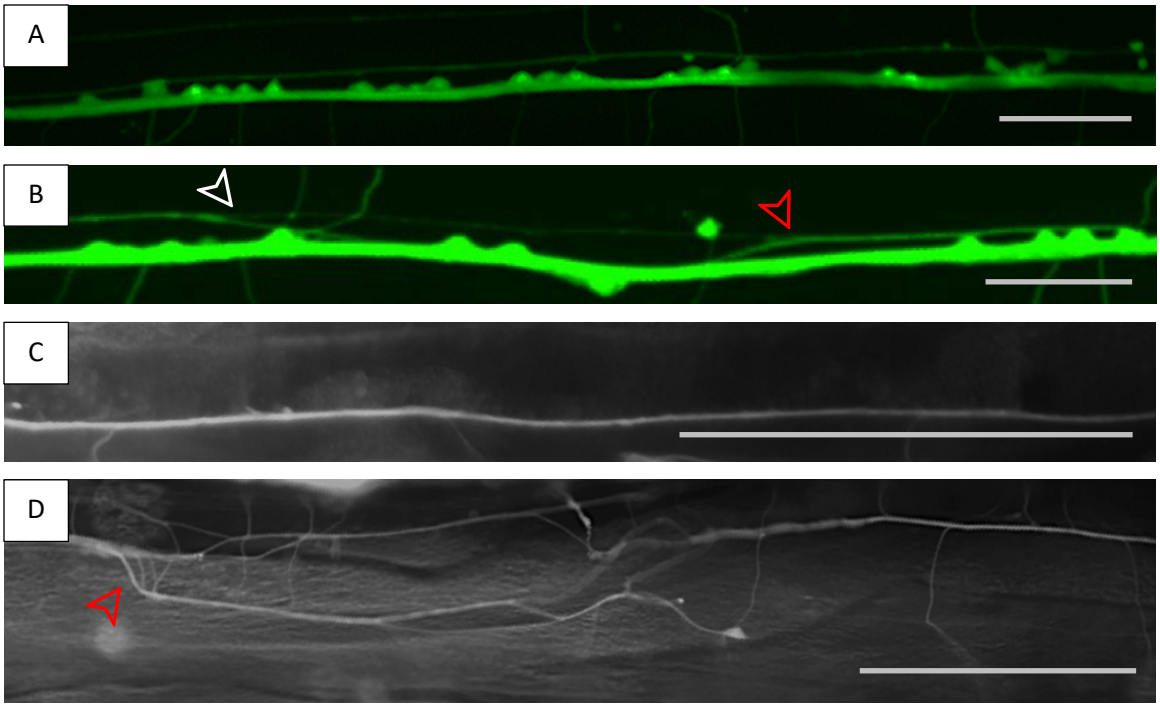


**Figure 3.1 *Iron-11* pan-neuronal axon guidance defects**
**a)** This is the VNC of a wildtype animal, visualized with the *evIs111* pan-neuronal marker. The right VNC is the thick green horizontal band with the motor neuron cell bodies adjacent to it. The left VNC tract is the faint green line that is just above the right tract, running parallel to it. **b)** This is the VNC of a *Iron-11* mutant animal. It displays a crossover defect where some of the axons in the left tract cross into the right tract (red arrow). In this image, these axons then appear to return to the left tract (white arrow). **c)** The wildtype DNC tract is a tightly fasciculated axon tract. **d)** This *Iron-11*(*gk5321*) animal has a DNC with a major defasciculation event (red arrow). The anterior side of the worm is towards the left of the image, the left side of the worm is toward the top of the image. Scale bars = 25µm. Marker used: *evIs111[rgef-1::GFP] V*.

There were also two other types of axon guidance defects observed, at a low frequency. Near the posterior end of the VNC, the left tract is formed when the PVPR pioneer axon leaves the right tract. In adults, the exact location PVPR leaves the right tract is slightly variable, however it should be close to the posterior end of the VNC (Figure 3.2a). A 'late separation' defect is adjudged when the PVPR axon leaves the right tract after extending at least halfway down the posterior half of the VNC in the right tract (Figure 3.2b). I saw under 5% penetrance of late separation in both *Iron-11* alleles (Table 3.2). Finally, if an axon leaves the VNC entirely, this is considered a 'leave VNC' event. With the *Iron-11* mutant alleles, I saw only one leave VNC event in each strain (Table 3.2).

**Table 3.2 *Iron-11* pan-neuronal VNC axon guidance defects**

| Ventral Nerve Cord | Marker Strain^ N = 787 | *Iron-11*(*ok2333*) N = 96 | *Iron-11*(*gk5321*) N = 96 |
|---|---|---|---|
| **No Defect** | 95% | 71%*** | 72%*** |
| **Anterior Crossover** | 2% | 15%*** | 19%*** |
| **Posterior Crossover** | 3% | 19%*** | 13%*** |
| **Late Separation** | 0% | 4%*** | 2% |
| **Leave VNC** | 0% | 1% | 1% |

***p<0.001; **p<0.01; *p<0.05 (χ2 test). ^The marker used was *evIs111[rgef-1::GFP]*.

**Table 3.3 *Iron-11* DNC axon guidance defects**

| Dorsal Nerve Cord | Marker Strain^ N = 245 | *Iron-11*(*ok2333*) N = 100 | *Iron-11*(*gk5321*) N = 98 |
|---|---|---|---|
| **No Defect** | 99% | 96% | 92%** |
| **Defasciculation** | 1% | 4% | 8%** |

***p<0.001; **p<0.01; *p<0.05 (χ2 test). ^The marker used was *evIs111[rgef-1::GFP]*.

In wildtype *C. elegans*, the PVPR axon pioneers the left tract of the VNC and the AVG axon pioneers the right tract (Figure 3.2a). As mentioned previously, the PVPR axon starts in the tail of the animal, then extends anteriorly. PVPR then pioneers the left tract, throughout the length of the VNC. In ~12% of *Iron-11* animals, PVPR crosses over the ventral midline into the right tract (Figure 3.2b; Table 3.4). When this occurs it usually will cross back into the left tract. Similar to the pan-neuronal marker, I also observed ~5% late separation events in *Iron-11* mutants (Table 3.4). Again, both *Iron-11* alleles displayed similar defect penetrance.

The AVG cell body is in VNC, near the head of the animal. Its axon extends posteriorly, pioneering the right VNC tract. This axon will extend the length of the VNC, always in the right tract. In *Iron-11* mutants AVG crosses into the left tract in less than 5% of animals (Figure 3.2e; Table 3.1).

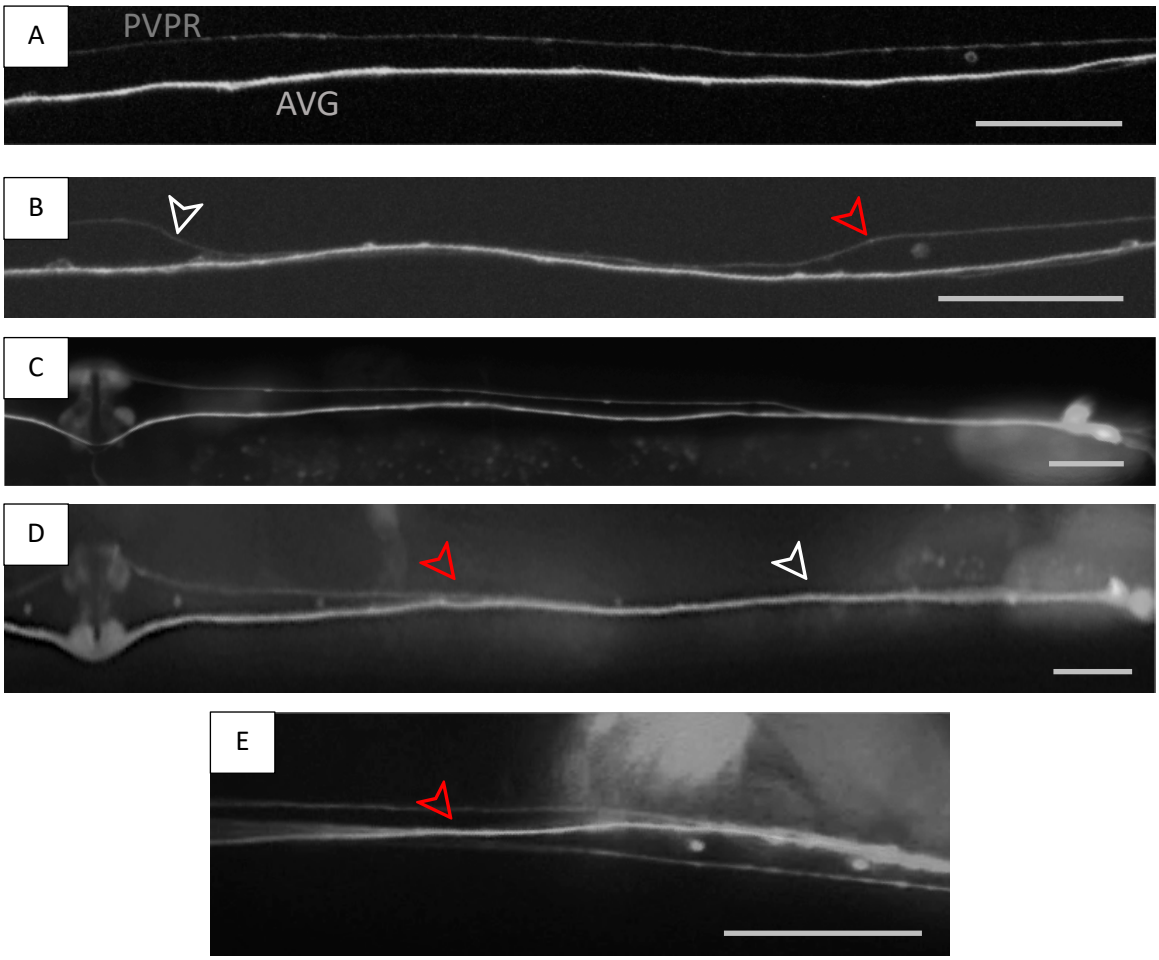


**Figure 3.2 *Iron-11* pioneer axon guidance defects**
**a)** The pioneer axons of the ventral nerve cord in a wildtype animal. PVPR is the fainter axon in the left tract. AVG is the brighter axon below it, in the right tract. **b)** A PVPR crossover (red arrow) in an *Iron-11*(*ok2333*) animal. The axon later crosses back into the left tract (white arrow). **c)** The posterior end of the VNC in a wildtype animal. PVPR quickly separates from the right tract to form the left tract. **d)** An *Iron-11*(*ok2333*) mutant with a late separation defect in PVPR (red arrow). PVPR only separates in this animal when it has almost reached the vulva. The white arrow shows approximately where PVPR should have separated. **e)** The AVG axon crossing into the left tract in a *Iron-11*(*ok2333*) mutant. The anterior side of the worm is towards the left of the image, the left side of the worm is toward the top of the image. Scale bars = 25μm. Marker used: *hdIs26[odr-2::CFP & sra-6::DsRed2] III*.

**Table 3.4 *Iron-11* PVPR defects**

| PVPR | Marker Strain^ N = 294 | *Iron-11*(*gk5321*)^^ N = 102 | *Iron-11*(*ok2333*) N = 110 |
|---|---|---|---|
| **No Defect** | 94% | 81%*** | 85%* |
| **Crossovers** | 6% | 13% | 10% |
| **Late Separation** | 1% | 5%* | 3% |

***p<0.001; **p<0.01; *p<0.05 (χ2 test). ^The marker used was *hdIs26[odr-2::CFP, sra-6::DsRed2]*. ^^The *Iron-11*(*gk5321*) data is actually from PVQL, which closely follows PVPR (Table B26; Durbin, 1987). This was used as a stand in for PVPR in this case because the microscope's optic fiber cable was damaged when collecting this data, making PVPR too faint to observe.

## 3.1.2. *Iron-11* HSN phenotypes

Since I found penetrant axon guidance defects in *Iron-11* mutants with the pan-neuronal marker, I wanted to investigate what other types of neurons were affected by *Iron-11* mutations. Therefore, I also observed *Iron-11* animals with AVK, command interneuron, HSN and DD/VD, DA/DB motor neuron markers. Both mutant alleles displayed similar phenotypes in the pan-neuronal and pioneer markers, so I only observed the *Iron-11*(*ok2333*) in these neurons.

There are two HSN neurons in *C. elegans*, HSNL and HSNR. Both reside dorsally above the VNC, just posterior of the vulva. HSNL is on the left side, HSNR is on the right. In wildtype animals, their axons travel ventrally into the left (HSNL) or right (HSNR) VNC tract (Figure 3.3a). Their axons then extend anteriorly along their respective tracts into the head of the animal.

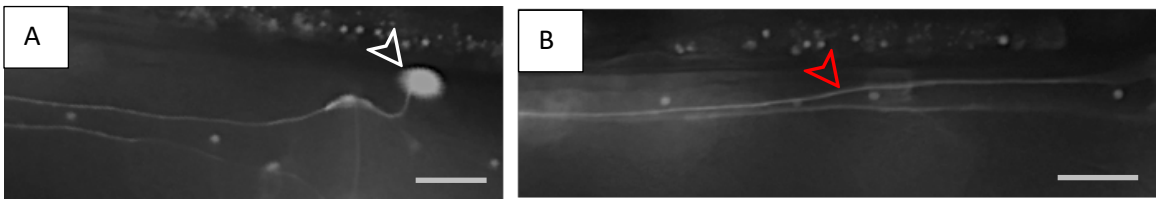


**Figure 3.3 *Iron-11*(*ok2333*) HSN defects**
**a)** HSNL's axon entering the VNC in a wildtype animal. The white arrow points to the HSNL cell body. **b)** The HSNL axon crossing into the right tract of a *Iron-11*(*ok2333*) worm. The anterior side of the worm is towards the left of the image, the left side of the worm is toward the top of the image. Scale bars = 25µm. Marker used: *zdIs13[tph-1::gfp]*.

In 17% of *Iron-11*(*ok2333*) animals the HSNL axon crosses into the right tract (Figure 3.3b; Table 3.5). However, this was not significant from the marker strain. Also, in *Iron-11*(*ok2333*) animals both HSNL and HSNR had a penetrance of pre-VNC deviation above 5% (Table 3.5). Pre-VNC defects were counted if the axon initially extended dorsally/posteriorly. Additionally, some axons would extend too far anteriorly before they turned ventrally to enter the VNC, which caused them to enter the VNC after the vulva. This was also considered a pre-VNC defect. These may be the result of axon guidance or axon outgrowth errors. Though these pre-VNC defects were not observed in the marker strain, these defects were not found to be significant.

**Table 3.5 *Iron-11*(*ok2333*) HSN defects**

| | HSNL | | HSNR | |
|---|---|---|---|---|
| | **Marker Strain^ N = 32** | ***Iron-11*(*ok2333*) N = 104** | **Marker Strain^ N = 64** | ***Iron-11*(*ok2333*) N = 105** |
| **No Defect** | 91% | 78% | 95% | 90% |
| **Crossover** | 9% | 17% | 5% | 1% |
| **Leave VNC** | 0% | 1% | 0% | 0% |
| **Pre-VNC deviations** | 0% | 6% | 0% | 8% |

The number of animals counted for HSNL and HSNR is different because the HSN cell bodies are located laterally of the VNC and it was difficult to observe both at once. Therefore, they were often counted separately. ^The marker used was *zdIs13[tph-1::gfp]*.

## 3.1.3. *Iron-11* AVK axon guidance phenotypes

The AVKL and AVKR neurons are located near the anterior end of the VNC (Figure 3.4a). They send their axons anteriorly into the head. The axons grow into the nerve ring before entering the VNC and extending posteriorly. AVKL enters the right axon tract, AVKR enters the left tract. Their axons terminate near the posterior end of the VNC. In a small proportion of *Iron-11*(*ok2333*) animals, under 10%, the AVKL and/or AVKR axon(s) leave the nerve ring and never enter the VNC (Figure 3.4b; Table 3.6). The axon will still travel posteriorly, but it otherwise appears to lack direction (Figure 3.4c). This phenotype was never observed in the marker strain but it is not statistically significant.

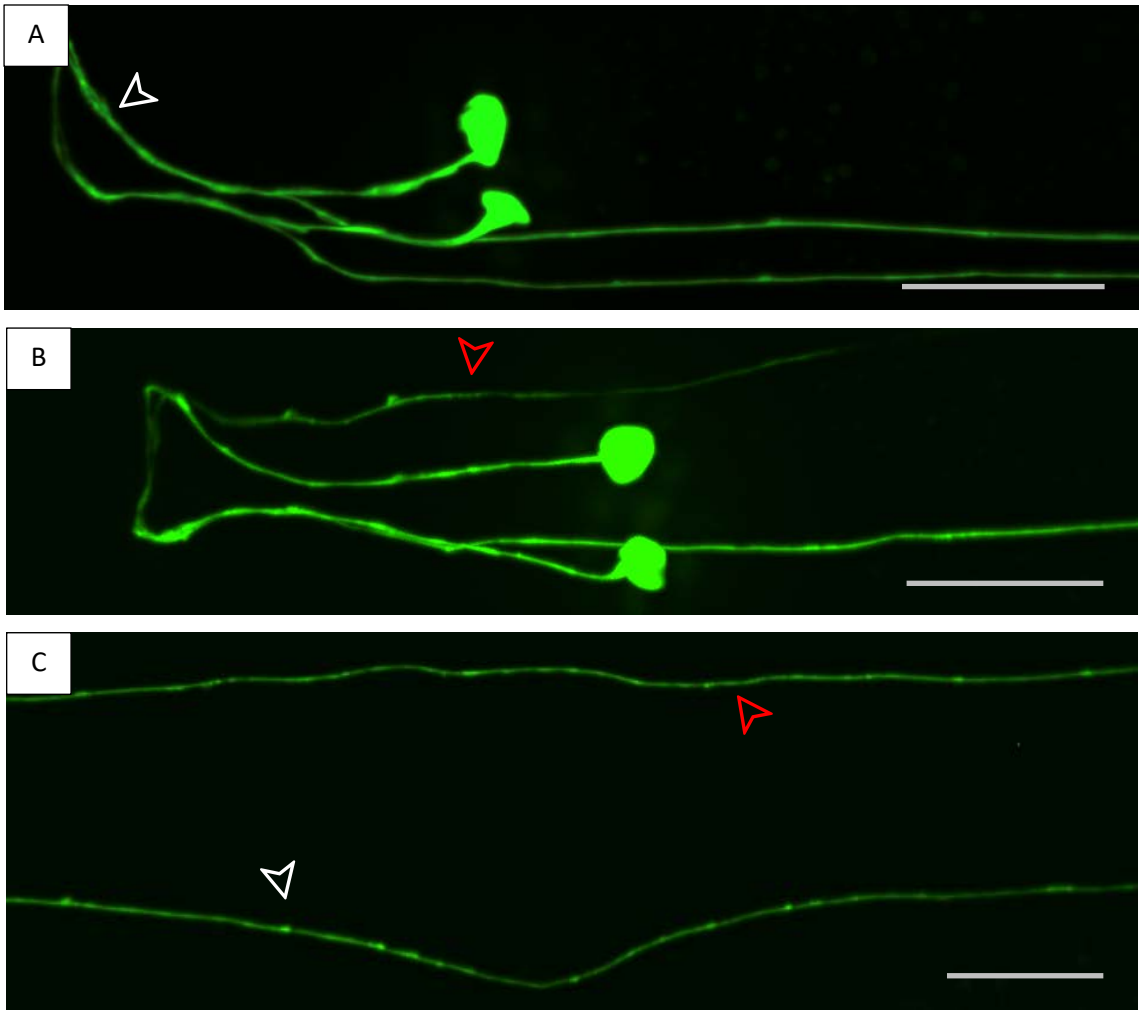


**Figure 3.4 *Iron-11*(*ok2333*) AVK axon guidance defects**
**a)** In a wildtype animal the AVK axons first extend anteriorly into the nerve ring, before extending posteriorly in the VNC. The white arrow points to the AVK cell bodies. **b)** This is a *Iron-11*(*ok2333*) animal where one of the AVK axons has left the nerve ring prematurely (red arrow). **c)** A *Iron-11*(*ok2333*) mutant where the AVKL axon prematurely left the nerve ring and extended posteriorly outside of the VNC (red arrow). The white arrow points to the AVKR axon in the VNC. The anterior side of the worm is towards the left of the image, the left side of the worm is toward the top of the image. Scale bars = 25µm. Marker used: *hdIs54[flp-1::GFP]*.

**Table 3.6 *Iron-11*(*ok2333*) AVK axon guidance defects**

| | AVKL | | AVKR | |
|---|---|---|---|---|
| | Marker Strain^ N = 53 | *Iron-11*(*ok2333*) N = 115 | Marker Strain^ N = 53 | *Iron-11*(*ok2333*) N = 115 |
| **No Defect** | 100% | 94% | 100% | 92% |
| **Crossover** | 0% | 1% | 0% | 1% |
| **Leave Nerve Ring** | 0% | 4% | 0% | 5% |
| **Leave VNC** | 0% | 1% | 0% | 1% |

^The marker used was *hdIs54[flp-1::GFP]*.

### 3.1.4. *Iron-11* command interneuron axon guidance phenotypes

Command interneurons enter the left or right VNC tract from the head, and travel posteriorly down its length (Figure 3.5a). The axons that enter the left tract will quickly crossover into the right tract at the very beginning of the VNC. This occurs anterior to the AVG cell body. In *Iron-11*(*ok2333*) mutants I saw axons cross into the left tract in 5% of animals (Table 3.7). Additionally, in 11% of mutant animals, some axons in the left tract were late to cross into the right tract; crossing only after passing the AVG cell body (Figure 3.5b; Table 3.7). This phenotype was statistically significant and was not observed in the marker strain.

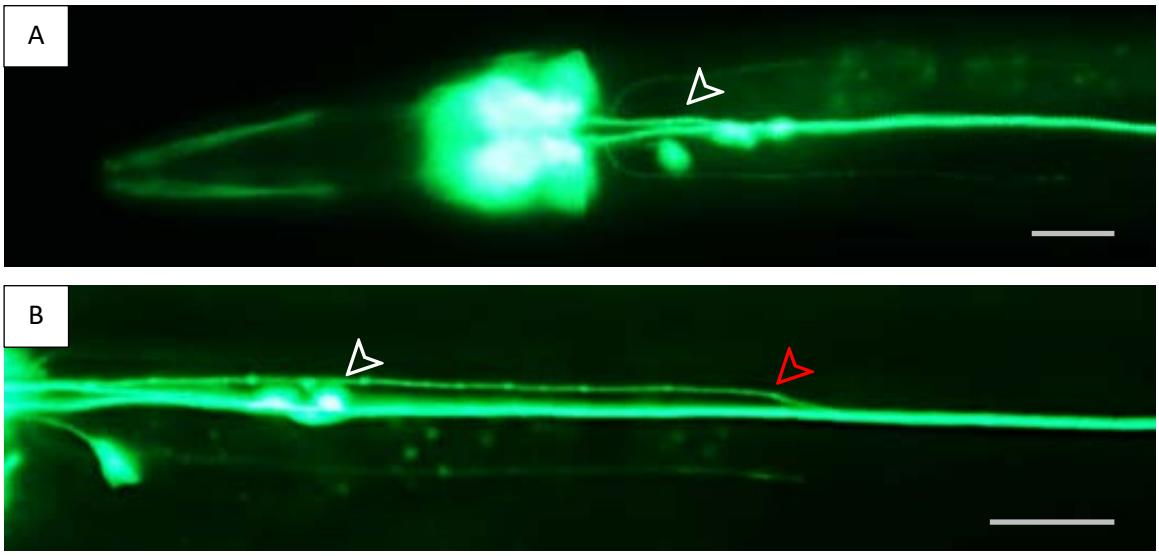


**Figure 3.5 *Iron-11*(*ok2333*) command interneuron axon guidance defects**
**a)** In the marker strain, command interneurons in the left tract immediately cross into the right tract (white arrow). **b)** In *Iron-11*(*ok2333*) animals, a subset of command interneurons in the left

tract would sometimes cross late, after the AVG cell body (red arrow). The white arrow points at the AVG cell body. The anterior side of the worm is towards the left of the image, the left side of the worm is toward the top of the image. Scale bars = 25µm. Marker used: *rhIs4[glr-1::GFP, dpy-20(+)] III*.

**Table 3.7 *Iron-11*(*ok2333*) command interneuron axon guidance defects**

| Command interneurons | Marker Strain^ N = 50 | *Iron-11*(*ok2333*) N = 97 |
|---|---|---|
| **No Defect** | 100% | 82%** |
| **Crossover** | 0% | 5% |
| **Late Crossover to Right Tract** | 0% | 11%* |
| **Leave VNC** | 0% | 1% |

***p<0.001; **p<0.01; *p<0.05 ($\chi 2$ test). ^The marker used was *rhIs4[glr-1::GFP, dpy-20(+)]*.

## 3.1.5. *Iron-11* DD/VD motor neuron phenotypes

In wildtype *C. elegans*, motor neurons send commissures dorsally to the DNC (Figure 3.6a). When motor neuron commissures begin to travel dorsally toward the dorsal nerve cord, they travel up either the left or the right side of the animal. Each neurons choice is consistent across wildtype animals. Almost all DD/VD commissures travel up the right side of the animal. In 55% of *Iron-11*(*ok2333*) mutants, at least one commissure went up the wrong side (Figure 3.6b, 3.6d; Table 3.9). This was statistically significant, though I also saw penetrant defects in the marker strain, where 34% of the animals had at least one DD/VD commissure on the wrong side. Finally, *Iron-11*(*ok2333*) and the marker strain had similar commissures guidance defects in dorsally extending DD/VD commissures (Table 3.8). These defects included premature termination and extending parallel to the VNC.

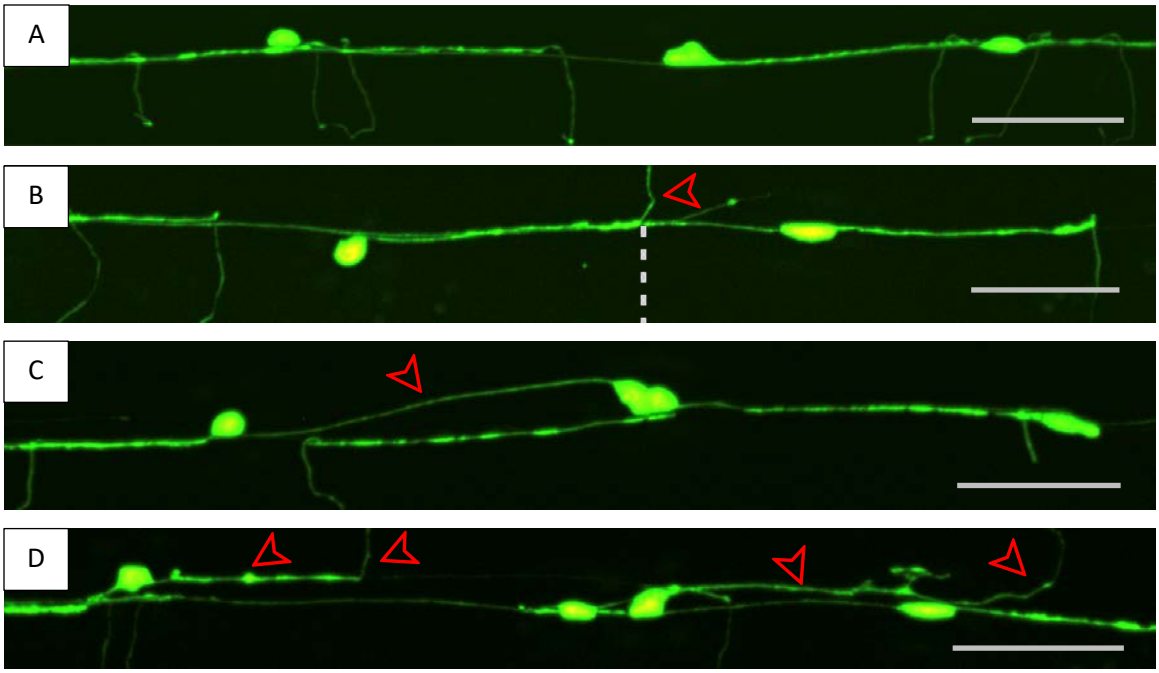


**Figure 3.6 *Iron-11*(*ok2333*) DD/VD VNC defects**
**a)** Wildtype DD/VD motor neurons sending commissures up the right side of the animal. **b)** A commissure going up the wrong side of the worm in a *Iron-11*(*ok2333*) mutant (red arrow). **c)** Errant neurite extending into the left tract in a *Iron-11*(*ok2333*) animal (red arrows). **d)** Errant neurites extending into the left tract and errant commissures extending up the wrong side of this *Iron-11*(*ok2333*) mutant (red arrows). The anterior side of the worm is towards the left of the image, the left side of the worm is toward the top of the image. Scale bars = 25µm. Marker used: *oxIs12[unc-47:GFPNTX;lin-15(+)] X*.

**Table 3.8 *Iron-11*(*ok2333*) DD/VD commissure guidance defects**

| DD/VD Motor Neurons | Marker Strain^ N = 51 | *Iron-11*(*ok2333*) N = 95 |
|---|---|---|
| **No Defect** | 86% | 87% |
| **Premature Termination** | 12% | 6% |
| **Parallel to VNC** | 6% | 6% |

^The marker used was *oxIs12[unc-47:GFPNTX;lin-15(+)]*.

**Table 3.9 *Iron-11*(*ok2333*) commissure polarity defects**

| DD/VD Motor Neurons | Marker Strain^ N = 58 | *Iron-11*(*ok2333*) N = 101 |
|---|---|---|
| **No Defect** | 66% | 45%* |
| **Single Commissure error** | 26% | 36% |
| **Two or Three Commissures errors** | 7% | 20% |

***p<0.001; **p<0.01; *p<0.05 (χ2 test). ^The marker used was *oxIs12[unc-47:GFPNTX;lin-15(+)]*.

Motor neurons send neurites exclusively into the right VNC in wildtype animals (Figure 3.6a). However, in 22% of *Iron-11*(*ok2333*) mutants, I observed neurites enter the left tract (Figure 3.6c, 3.6d; Table 3.10). If a neurite was in the left tract for more than two cell body lengths, I counted it as a defect.

**Table 3.10 *Iron-11*(*ok2333*) DD/VD motor neuron neurites in the left tract defect**

| DD/VD Motor Neurons | Marker Strain^ N = 58 | *Iron-11*(*ok2333*) N = 101 |
|---|---|---|
| **No Defect** | 97% | 78%** |
| **Neurite(s) in the Left Tract** | 3% | 22%** |

***p<0.001; **p<0.01; *p<0.05 (χ2 test). ^The marker used was *oxIs12[unc-47:GFPNTX;lin-15(+)]*.

I also often saw gaps in DNC in *Iron-11*(*ok2333*) animals (Figure 3.7b, 3.7c; Table 3.11). The DD/VD commissures in the dorsal nerve cord of wildtype animals together form a continuous tract (Figure 3.7a). In 23% of *Iron-11*(*ok2333*) mutants there is at least one gap in the DNC (Table 3.11). However, this was not significant when compared to the marker strain.

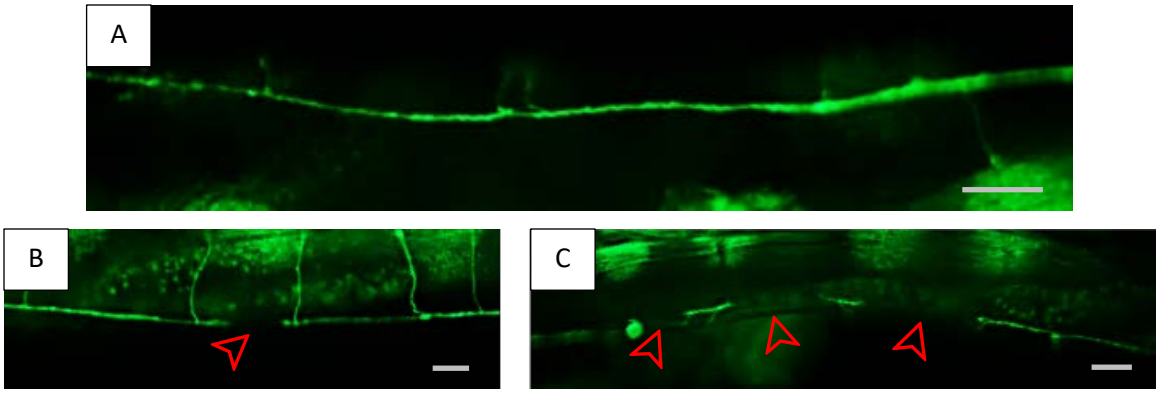


**Figure 3.7 *Iron-11*(*ok2333*) DD/VD motor neuron DNC defects**
**a)** Wildtype animals have a continuous DNC. **b-c)** *Iron-11*(*ok2333*) mutants with one or more gaps in their DNC. The anterior side of the worm is towards the left of the image, the left side of the worm is toward the top of the image. Scale bars = 25µm. Marker used: *oxIs12[unc-47:GFPNTX;lin-15(+)] X*.

**Table 3.11 *Iron-11*(*ok2333*) DD/VD DNC defects**

| DD/VD Motor Neurons | Marker Strain^ N = 54 | *Iron-11*(*ok2333*) N = 97 |
|---|---|---|
| **No Defect** | 91% | 77% |
| **One gap in the dorsal nerve cord** | 7% | 18% |
| **Multiple gaps in the dorsal nerve cord** | 2% | 5% |

^The marker used was *oxIs12[unc-47:GFPNTX;lin-15(+)]*.

## 3.1.6. *Iron-11* DA/DB motor neuron phenotypes

Just like the DD/VD motor neurons, DA/DB motor neurons send their commissures dorsally up either side of the animal, in a set pattern (Figure 3.8a). The marker strain was close to wildtype; commissures traveling up the wrong side of the worm was only 6% penetrant in these animals (Table 3.12). However, *Iron-11*(*ok2333*) mutants displayed a 75% penetrance of this commissure polarity defect (Figure 3.8b; Table 3.12).

The DB6 and DA6 motor neuron cell bodies are adjacent to each other and they send their commissure in opposite directions. While scoring the *Iron-11* mutant I observed that their cell body positions were sometimes not quite right. I also noticed a surprisingly high frequency of both neurons seeming to send their commissure the

wrong way in the same animal. Based on the small percentage of animals with only one of these commissures going the wrong way, I would expect a much smaller percentage of animals where both commissures happened to make the wrong decision, assuming these events are independent. This is likely the result of a cell migration defect that results in the cell bodies of DB6 and DA6 swapping position. Therefore, most occurrences with DB6 and DA6 commissure polarity defects coinciding in the same animal were counted as cell migration defects, not commissure polarity defects (Table 3.12). The penetrance of this defect was ~11% (Table 3.12).

I also observed extra neuron cell bodies in the VNC of three mutant animals (Figure 3.8c). This seems to be another cell migration defect caused by neurons from the head migrating posteriorly. Alternatively, this could be caused by additional cells expressing the fluorescent marker, which would be a cell identity defect.

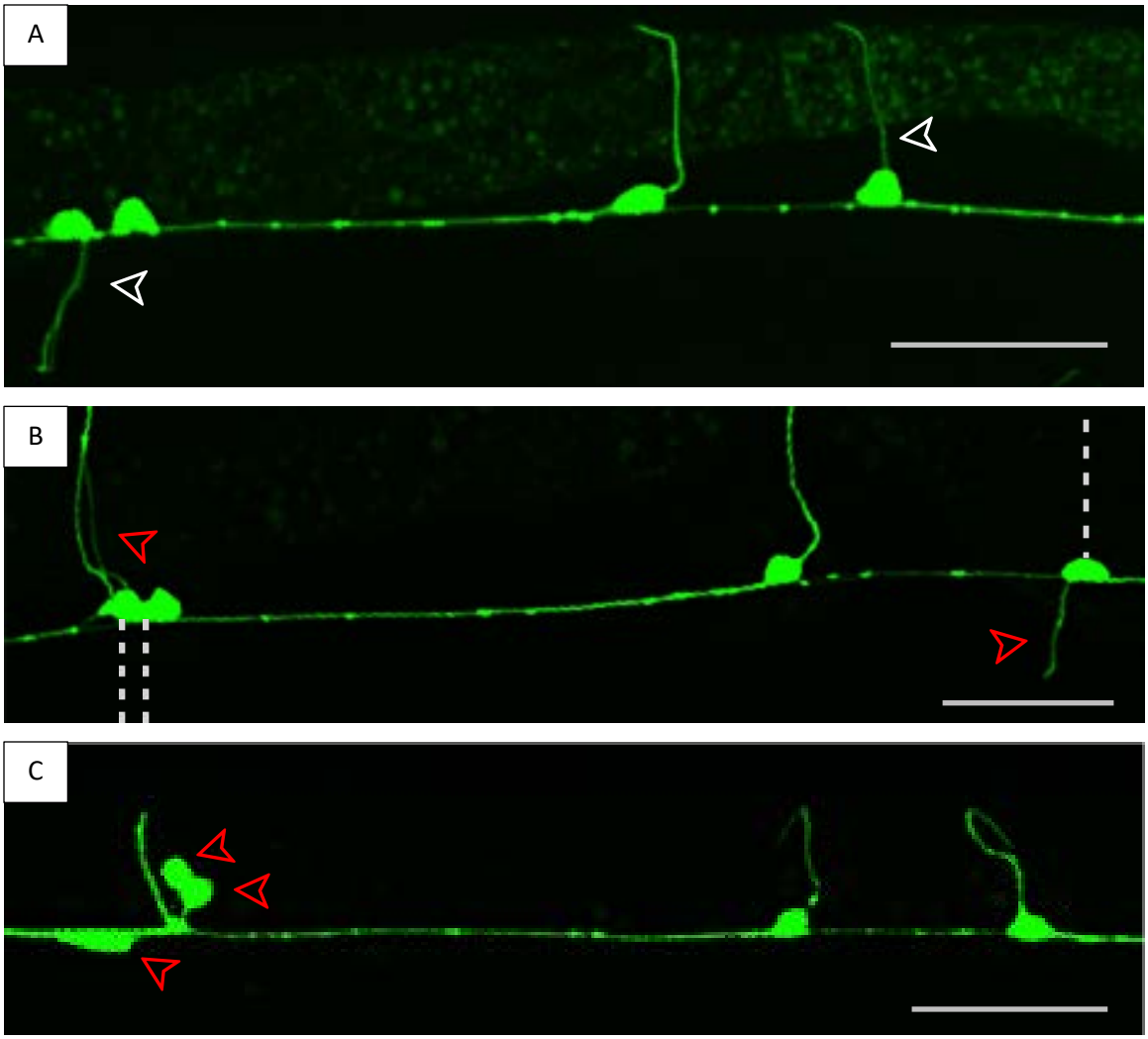


**Figure 3.8 *lron-11*(*ok2333*) DA/DB motor neuron defects**
All of these images contain the neurons DB3, DA2, DA3, DB4 in order, from left to right. **a)** Wildtype DA/DB motor neurons sending their commissures up the correct side of the animal. The left arrow points to the DB3/DA2 commissures traveling up the right side of the animal. The right arrow points to DB4's commissure traveling up the left side of the animal. **b)** In this *lron-11*(*ok2333*) mutant, the DB3/DA2 commissures (left arrow) and the DB4 commissure (right arrow) travel up the wrong side of the animal. **c)** In this *lron-11*(*ok2333*) worm, an extra cell body is illuminated in the VNC, and the DB3/DA2 commissures are traveling up the wrong side of the animal. The anterior side of the worm is towards the left of the image, the left side of the worm is toward the top of the image. Scale bars = 25µm. Marker used: *evIs82A[unc-129::GFP] II*.

**Table 3.12 *Iron-11*(*ok2333*) DA/DB motor neuron defects**

| | | Raw Data | Data Corrected for DB6/DA6 Cell Body Swap |
|---|---|---|---|
| **DA/DB Motor Neurons** | **Marker Strain^ N = 50** | ***Iron-11*(*ok2333*) N = 101** | ***Iron-11*(*ok2333*) N = 101** |
| **No Defect** | 94% | 22%*** | ~24%*** |
| **Single Commissure** | 4% | 32%*** | ~34%*** |
| **Two or Three Commissures** | 2% | 36%*** | ~35%*** |
| **Four or More Commissures** | 0% | 10% | ~7% |
| **Neurites in Left Tract** | 0% | 1% | 1% |
| **Neuron from Head** | 0% | 3% | 3% |
| **DB6/DA6 cell body swap** | 0% | N/A | ~11%* |

***p<0.001; **p<0.01; *p<0.05 ($\chi 2$ test). This table includes two columns that both describe the same *Iron-11*(*ok2333*) mutant dataset. The data in the 'Data Without Considering DB6/DA6 Cell Body Swap' column does not take into account any possible cell positioning defects between DB6 and DA6. The 'Data Corrected for DB6/DA6 Cell Body Swap' column does correct for the likelihood of the DB6/DA6 cell bodies swapping positions, which results in slightly fewer commissure polarity defects being counted. The 'Neuron from Head' and 'DB6/DA6 cell body swap' defects are not factored into calculating the percentage of animals with 'No Defect'. 'No Defect' means there are no neurite guidance defects. ^The marker used was *evIs82A[unc-129::GFP]*.

The individual motor neurons have a variable penetrance of commissure polarity defects. The DA4 neuron had the highest penetrance at 48%, which means it was essentially random which side of the animal this neuron's commissure extended up (Table 3.13). If a commissure extended into the VNC before extending up the wrong side, I considered this an axon guidance error. If the commissure extended immediately up the wrong side, directly from the cell body, this was considered an axon outgrowth error. Overall, these types of error each accounted for a similar number of commissure polarity defects. However, individual motor neurons usually made mostly axon outgrowth, or mostly axon guidance errors (Table 3.13).

**Table 3.13 *Iron-11*(*ok2333*) individual DA/DB motor neuron defects**

| *Iron-11* (*ok2333*) | DB3 | DA2 | DA3 | DB4 | DA4 | DB5 | DA5 | DB6* | DA6* | DB7 |
|---|---|---|---|---|---|---|---|---|---|---|
| **Wrong Side** | 13% | 13% | 25% | 17% | 48% | 5% | 6% | 4% | 10% | 8% |
| **Axon guidance error** | 0% | 0% | **21%** | 4% | **38%** | 1% | **5%** | 0% | 4% | 1% |
| **Axon outgrowth error** | **13%** | **13%** | 4% | **13%** | 10% | **4%** | 1% | **3%** | 5% | **7%** |

The most common type of error by each individual motor neuron is in bold. *This data has been corrected for the 'DB6/DA6 cell body swap' defect.

### 3.1.7. *Iron-11* expression construct

To determine where *Iron-11* is expressed, I used a PCR fusion strategy to combine the putative promoter region of *Iron-11* with GFP cDNA. Transgenic strains expressing this construct only showed faint GFP expression in a band of muscle cells and in a pair of sensory neurons in the head (data not shown). Further experiments using a CRISPR strategy to directly add GFP to the *Iron-11* locus are underway to determine the cellular expression of *Iron-11*.

### 3.1.8. *Iron-14* pan-neuronal and pioneer axon guidance phenotypes

In *Iron-14*(*gk401715*) mutants, I observed significant defects with the pan-neuronal marker (Table 3.14). I observed 12% crossovers penetrance in these mutants (Table 3.14). As well as 3% late separation defect penetrance, I also saw axons inappropriately leave the left VNC in 2% of these animals (Figure 3.9; Table 3.14). I did not see significant DNC defects in this mutant (Table 3.15). In the pioneer marker, *Iron-14*(*gk401715*) animals overall PVPR axon guidance were not significant from the marker strain (Table 3.16). However, I also saw PVPR leave the VNC with 2% penetrance in these animals, this is consistent with the pan-neuronal observations (Table 3.16).

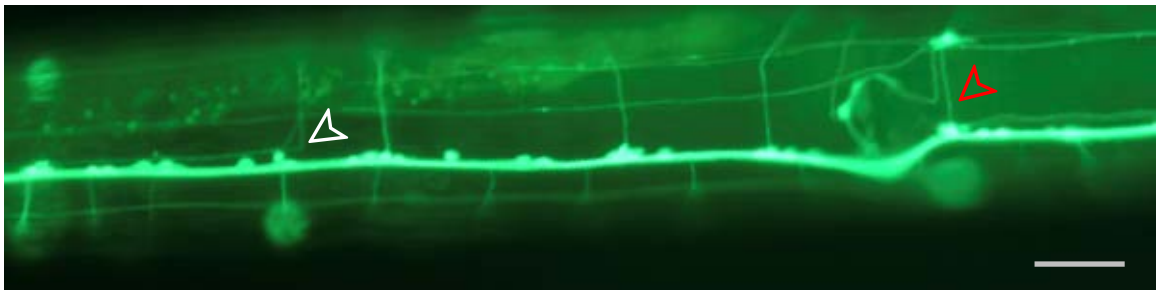

**Figure 3.9 Axons in the left tract leaving the VNC in an *Iron-14*(*gk401715*) mutant with the pan-neuronal marker**

In this *Iron-14*(*gk401715*) mutant, the axons in the left tract leave the VNC (red arrow) by traveling dorsally up the right side of the worm. Interestingly, the axons later manage to return to the left track (white arrow). The anterior side of the worm is towards the left of the image, the left side of the worm is toward the top of the image. Scale bar = 25µm. Marker used *evIs111[rgef-1::GFP] V*.

**Table 3.14 *Iron-14*(*gk401715*) pan-neuronal VNC axon guidance defects**

| Ventral Nerve Cord | Marker Strain^ N = 787 | *Iron-14*(*gk401715*) N = 88 |
|---|---|---|
| **No Defect** | 95% | 83%*** |
| **Anterior Crossover** | 2% | 6%* |
| **Posterior Crossover** | 3% | 10%** |
| **Late Separation** | 0% | 0% |
| **Leave VNC** | 0% | 2%** |

***p<0.001; **p<0.01; *p<0.05 (χ2 test). ^The marker used was *evIs111[rgef-1::GFP]*.

**Table 3.15 *Iron-14*(*gk401715*) DNC axon guidance defects**

| Dorsal Nerve Cord | Marker Strain^ N = 245 | *Iron-14*(*gk401715*) N = 95 |
|---|---|---|
| **No Defect** | 99% | 98% |
| **Defasciculation** | 1% | 2% |

^The marker used was *evIs111[rgef-1::GFP]*.

**Table 3.16 *Iron-14*(*gk401715*) PVPR axon guidance defects**

| PVPR | Marker Strain^ N = 163 | *Iron-14*(*gk401715*) N = 101 |
|---|---|---|
| **No Defect** | 90% | 85% |
| **Crossover** | 10% | 11% |
| **Late Separation** | 0% | 2% |
| **Leave VNC** | 0% | 2% |

^The marker used was *hdIs28[odr-2::CFP, sra-6::DsRed2]*.

## 3.1.9. *Iron-3* pan-neuronal and pioneer axon guidance phenotypes

I phenotyped two mutant alleles for *Iron-3*, with a pan-neuronal marker and a pioneer marker. Both of these mutant strains were 4X outcrossed before phenotyping. While both mutant alleles were predicted to be null alleles, *Iron-3*(*gk5319*) mutants displayed significant axon guidance defects in the pan-neuronal marker, but *Iron-3*(*ok2614*) animals did not display significant defects in the pan-neuronal marker or the pioneer marker (Table 3.1, 3.17, 3.19, 3.20, 3.21). However, the penetrance of pan-neuronal defects in both of these markers was very similar.

**Table 3.17 *Iron-3*(*gk5319*) pan-neuronal VNC axon guidance defects**

| Ventral Nerve Cord | Marker Strain^ N = 787 | *Iron-3*(*gk5319*) N = 102 |
|---|---|---|
| **No Defect** | 95% | 89%* |
| **Anterior Crossover** | 2% | 2% |
| **Posterior Crossover** | 3% | 8%* |
| **Late Separation** | 0% | 1% |

***p<0.001; **p<0.01; *p<0.05 ($\chi 2$ test). ^The marker used was *evIs111[rgef-1::GFP]*.

**Table 3.18 *Iron-3* DNC axon guidance defects**

| Dorsal Nerve Cord | Marker Strain^ N = 245 | *Iron-3*(*ok2614*) N = 100 | *Iron-3*(*gk5319*) N = 51 |
|---|---|---|---|
| **No Defect** | 99% | 97% | 100% |
| **Defasciculation** | 1% | 3% | 0% |

^The marker used was *evIs111[rgef-1::GFP]*.

**Table 3.19 *Iron-3*(*gk5319*) PVPR axon guidance defects**

| PVPR | Marker Strain^ N = 163 | *Iron-3*(*gk5319*) N = 96 |
|---|---|---|
| **No Defect** | 90% | 83% |
| **Crossover** | 10% | 15% |
| **Late Separation** | 0% | 1% |

^The marker used was *hdIs28[odr-2::CFP, sra-6::DsRed2]*.

**Table 3.20 *Iron-3*(*ok2614*) pan-neuronal VNC axon guidance defects**

| Ventral Nerve Cord | Marker Strain^ N = 787 | *Iron-3*(*ok2614*) N = 105 |
|---|---|---|
| **No Defect** | 95% | 90% |
| **Anterior Crossover** | 2% | 2% |
| **Posterior Crossover** | 3% | 6% |
| **Late Separation** | 0% | 2% |

^The marker used was *evIs111[rgef-1::GFP]*.

**Table 3.21 *Iron-3*(*ok2614*) PVPR axon guidance defects**

| PVPR | Marker Strain^ N = 294 | *Iron-3*(*ok2614*) N = 100 |
|---|---|---|
| **No Defect** | 94% | 91% |
| **Crossover** | 6% | 8% |
| **Late Separation** | 1% | 1% |

^The marker used was *hdIs26[odr-2::CFP, sra-6::DsRed2]*.

## 3.1.10. *Iron-5* pan-neuronal and pioneer axon guidance

In the pan-neuronal marker, *Iron-5*(*gk959442*) had no significant axon guidance defects (Table 3.22, 3.23). However, with the pioneer marker, I observed significant defects in PVPR axon guidance in this mutant (Table 3.24). The penetrance of defects was close to 25%. Crossovers were the most common defect, although I also saw PVPR leave the VNC four times (Table 3.24). Furthermore, I also saw 5% penetrance for PVPR 'no separation' defects, where the PVPR axon never separates from the right tract (Table 3.24). I only rarely see this defect in the marker strains.

**Table 3.22 *Iron-5*(*gk959442*) pan-neuronal VNC axon guidance defects**

| Ventral Nerve Cord | Marker Strain^ N = 787 | *Iron-5*(*gk959442*) N = 89 |
|---|---|---|
| **No Defect** | 95% | 92% |
| **Crossover** | 5% | 6% |
| **Late Separation** | 0% | 1% |
| **Leave VNC** | 0% | 1% |

^The marker used was *evIs111[rgef-1::GFP]*.

**Table 3.23 *Iron-5*(*gk959442*) DNC axon guidance defects**

| Ventral Nerve Cord | Marker Strain^ N = 245 | *Iron-5*(*gk959442*) N = 89 |
|---|---|---|
| **No Defect** | 99% | 100% |
| **Defasciculation** | 1% | 0% |

^The marker used was *evIs111[rgef-1::GFP]*.

**Table 3.24 *Iron-5*(*gk959442*) PVPR axon guidance defects**

| PVPR | Marker Strain^ N = 159 | *Iron-5*(*gk959442*) N = 94 |
|---|---|---|
| **No Defect** | 93% | 77%*** |
| **Crossover** | 6% | 13% |
| **Late Separation** | 1% | 1% |
| **Leave** | 0% | 4%* |
| **No Separation** | 0% | 5%* |

***p<0.001; **p<0.01; *p<0.05 ($\chi 2$ test). ^The marker used was *hdIs29[odr-2::CFP, sra-6::DsRed2]*.

## 3.1.11. *Iron-8* and *iglr-1* pan-neuronal and pioneer axon guidance phenotypes

*Iron-8*(*gk5317*) and *iglr-1*(*gk687851*) mutants displayed significant crossover defects in the pan-neuronal marker (Table 3.25, 3.28). Most of these defects were crossovers. However, they did not have significant defects in pioneer neurons, when compared to the marker strains (Table 3.27, 3.29). These mutants also did not display any DNC defects (Table 3.26).

**Table 3.25 *Iron-8*(*gk5317*) pan-neuronal VNC axon guidance defects**

| Ventral Nerve Cord | Marker Strain^ N = 787 | *Iron-8*(*gk5317*) N = 100 |
|---|---|---|
| **No Defect** | 95% | 87%** |
| **Anterior Crossover** | 2% | 5% |
| **Posterior Crossover** | 3% | 7% |
| **Late Separation** | 0% | 2% |

***p<0.001; **p<0.01; *p<0.05 ($\chi 2$ test). ^The marker used was *evIs111[rgef-1::GFP]*.

**Table 3.26 *Iron-8*(*gk5317*) and *iglr-1*(*gk687851*) DNC defects**

| Dorsal Nerve Cord | Marker Strain^ N = 245 | *Iron-8*(*gk5317*) N = 65 | *iglr-1* (*gk687851*) N = 80 |
|---|---|---|---|
| **No Defect** | 99% | 100% | 100% |
| **Defasciculation** | 1% | 0% | 0% |

^The marker used was *evIs111[rgef-1::GFP]*.

**Table 3.27 *Iron-8*(*gk5317*) PVPR axon guidance defects**

| PVPR | Marker Strain^ N = 159 | *Iron-8* (*gk5317*) N = 81 |
|---|---|---|
| **No Defect** | 93% | 96% |
| **Crossover** | 6% | 1% |
| **Late Separation** | 1% | 1% |
| **Leave VNC** | 0% | 0% |

^The marker used was *hdIs29[odr-2::CFP, sra-6::DsRed2]*.

**Table 3.28 iglr-1(gk687851) pan-neuronal VNC axon guidance defects**

| Ventral Nerve Cord | Marker Strain^ N = 787 | *iglr-1*(*gk687851*) N = 100 |
|---|---|---|
| **No Defect** | 95% | 89%* |
| **Anterior Crossover** | 2% | 3% |
| **Posterior Crossover** | 3% | 6% |
| **Late Separation** | 0% | 1% |

***p<0.001; **p<0.01; *p<0.05 ($\chi 2$ test). ^The marker used was *evIs111[rgef-1::GFP]*.

**Table 3.29 *iglr-1*(*gk687851*) PVPR axon guidance defects**

| PVPR | Marker Strain^ N = 294 | *iglr-1*(*gk687851*) N = 100 |
|---|---|---|
| **No Defect** | 94% | 98% |
| **Crossover** | 6% | 0% |
| **Late Separation** | 1% | 2% |

^The marker used was *hdIs26[odr-2::CFP, sra-6::DsRed2]*.

## 3.1.12. *Iron-11*; *Iron-3* double mutant axon guidance phenotypes

I created double mutants of *Iron-11*(*ok2333*) and *Iron-3*(*gk5319*) with either pan-neuron or pioneer markers. In the pan-neuronal marker double mutant I observed ~30% VNC axon guidance defects, consisting mostly of crossover defects (Table 3.30). This is similar to the *Iron-11*(*ok2333*) single mutant. I also observed 7% DNC defasciculation, which is also not significantly different from the *Iron-11*(*ok2333*) single mutant (Table 3.31).

With the pioneer marker I observed I observed 16% penetrance PVPR defects in the double mutant, 15% were crossovers (Table 3.32). This was not significantly different from either of the single mutants. These results indicate that if *Iron-3* functions in axon guidance, it functions in the same pathway as *Iron-11*.

**Table 3.30 *Iron-11*(*ok2333*); *Iron-3*(*gk5319*) pan-neuronal VNC axon guidance defects**

| Ventral Nerve Cord | Marker Strain^ N = 787 | *Iron-3*(*gk5319*) N = 102 | *Iron-11*(*ok2333*) N = 96 | *Iron-11*(*ok2333*); *Iron-3*(*gk5319*) N = 102 |
|---|---|---|---|---|
| **No Defect** | 95% | 89% | 71% | 74% |
| **Anterior Crossover** | 2% | 2% | 15% | 19% |
| **Posterior Crossover** | 3% | 8% | 19% | 13% |
| **Late Separation** | 0% | 1% | 4% | 1% |

The χ2 test was only used to compare the *Iron-11*(*ok2333*); *Iron-3*(*gk5319*) double mutant, with the *Iron-11*(*ok2333*) single mutant. ^The marker used was *evIs111[rgef-1::GFP]*.

**Table 3.31 *Iron-11*(*ok2333*); *Iron-3*(*gk5319*) DNC axon guidance defects**

| Dorsal Nerve Cord | Marker Strain^ N = 245 | *Iron-11* (*ok2333*) N = 100 | *Iron-3* (*gk5319*) N = 51 | *Iron-11*(*ok2333*); *Iron-3*(*gk5319*) N = 98 |
|---|---|---|---|---|
| **No Defect** | 99% | 96% | 100% | 93% |
| **Defasciculation** | 1% | 4% | 0% | 7% |

The χ2 test was only used to compare the *Iron-11*(*ok2333*); *Iron-3*(*gk5319*) double mutant, with the *Iron-11*(*ok2333*) single mutant. ^The marker used was *evIs111[rgef-1::GFP]*.

**Table 3.32 *Iron-11*(*ok2333*); *Iron-3*(*gk5319*) PVPR axon guidance defects**

| PVPR | Marker Strain^ N = 294 | *Iron-3*(*gk5319*) N = 96 | *Iron-11*(*ok2333*) N = 103 | *Iron-3*(*gk5319*); *Iron-11*(*ok2333*) N = 100 |
|---|---|---|---|---|
| **No Defect** | 94% | 83% | 81% | 84% |
| **Crossover** | 6% | 15% | 15% | 15% |
| **Late Separation** | 1% | 1% | 4% | 1% |
| **AVG Crossover** | 0% | 2% | 4% | 5% |

The χ2 test was only used to compare the *Iron-11*(*ok2333*); *Iron-3*(*gk5319*) double mutant, with the *Iron-11*(*ok2333*) single mutant. The 'AVG Crossover' row was not included when calculating in the percentage of 'Wildtype' animals. The 'Wildtype' row only refers to the PVPR axon. ^The marker in this table was *hdIs26[odr-2::CFP, sra-6::DsRed2]*. However, *Iron-3*(*gk5319*) was scored with *hdIs28[odr-2::CFP, sra-6::DsRed2]*.

### 3.1.13. *Iron-11*; *Iron-14* double mutant axon guidance phenotypes

I found 44% penetrance of axon guidance defects in the VNC of *Iron-11*(*gk5321*); *Iron-14*(*gk401715*) double mutants, viewed with a pan-neuronal marker (Table 3.33). The most common defects were crossovers and late separation defects. The double mutant's defect penetrance was significantly higher than either of the single mutants (Figure 3.10). I also saw a significant increase in DNC defects in the double mutant (Table 3.34). These results indicate that *Iron-11* and *Iron-14* function in separate axon guidance pathways.

In the pioneer marker, I found a 27% penetrance for PVPR defects in the double mutant (Table 3.35). This was mostly crossover defects. The double mutant's PVPR defect penetrance was not significant when compared to the *Iron-11*(*gk5321*) single mutant (Figure 3.11). This suggests that *Iron-14* might function in the same axon guidance pathway as *Iron-11* in PVPR axon guidance or that *Iron-14* might not function in PVPR axon guidance at all.

**Table 3.33 *Iron-11*(*gk5321*); *Iron-14*(*gk401715*) pan-neuronal VNC axon guidance defects**

| Ventral Nerve Cord | Marker Strain^ N = 787 | *Iron-14*(*gk401715*) N = 88 | *Iron-11*(*gk5321*) N = 96 | *Iron-11*(*gk5321*); *Iron-14*(*gk401715*) N = 90 |
|---|---|---|---|---|
| **No Defect** | 95% | 83% | 72% | 56%* |
| **Anterior Crossover** | 2% | 6% | 19% | 18% |
| **Posterior Crossover** | 3% | 9% | 13% | 18% |
| **Late Separation** | 0% | 3% | 2% | 13%** |
| **Leave VNC** | 0% | 2% | 1% | 0% |

***p<0.001; **p<0.01; *p<0.05 (χ2 test). The χ2 test was only used to compare the *Iron-11*(*gk5321*); *Iron-14*(*gk401715*) double mutant, with the *Iron-11*(*gk5321*) single mutant. ^The marker used was *evIs111[rgef-1::GFP]*.

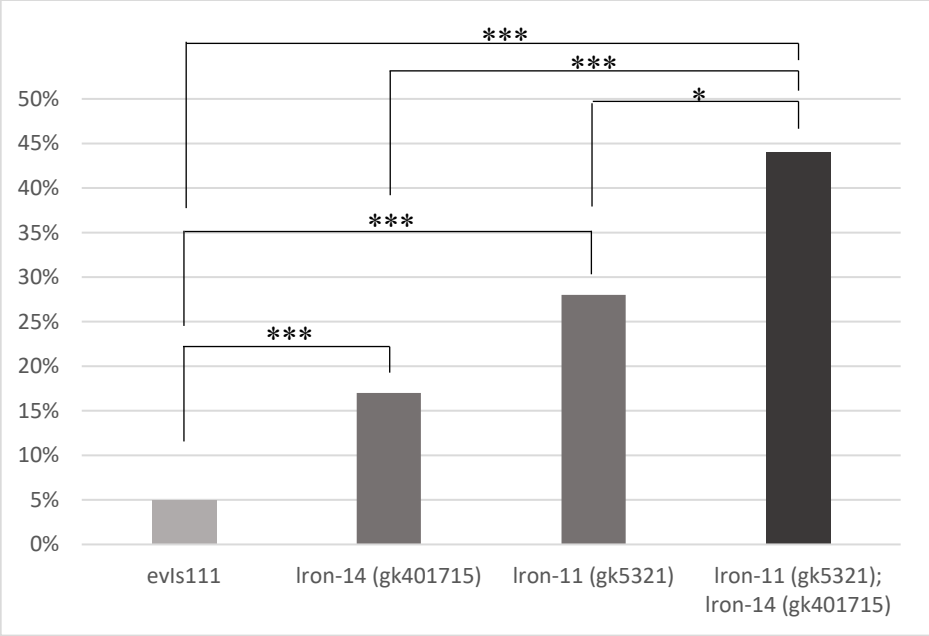


**Figure 3.10 *Iron-11*(*gk5321*); *Iron-14*(*gk401715*) pan-neuronal VNC axon guidance defects**

Both the *Iron-11*(*gk5321*) and *Iron-14*(*gk401715*) mutants have significantly more pan-neuronal axon guidance defects than the *evIs111* marker strain. The *Iron-11*(*gk5321*); *Iron-14*(*gk401715*) double mutant has significantly more defects than either single mutant, or the marker strain. ***p<0.001; **p<0.01; *p<0.05 (χ2 test).

**Table 3.34 *Iron-11*(*gk5321*); *Iron-14*(*gk401715*) DNC axon guidance defects**

| Dorsal Nerve Cord | Marker Strain^ N = 245 | *Iron-14*(*gk401715*) N = 95 | *Iron-11*(*gk5321*) N = 98 | *Iron-11*(*gk5321*); *Iron-14* (*gk401715*) N = 100 |
|---|---|---|---|---|
| **No Defect** | 99% | 98% | 92% | 81%* |
| **Defasiculation** | 1% | 2% | 7% | 12% |
| **DNC off track** | 0% | 0% | 1% | 7% |

***p<0.001; **p<0.01; *p<0.05 (χ2 test). The χ2 test was only used to compare the *Iron-11*(*gk5321*); *Iron-14*(*gk401715*) double mutant, with the *Iron-11*(*gk5321*) single mutant. ^The marker used was *evIs111[rgef-1::GFP]*.

**Table 3.35 *lron-11*(*gk5321*); *lron-14*(*gk401715*) PVPR axon guidance defects**

| PVPR | Marker Strain^ N = 294 | *lron-14* (*gk401715*) N = 101 | *lron-11*(*gk5321*) PVQL N = 102 | *lron-11*(*gk5321*); *lron-14* (*gk401715*) N = 106 |
|---|---|---|---|---|
| **No Defect** | 94% | 85% | 82% | 73% |
| **PVPR Crossovers** | 6% | 11% | 13% | 22% |
| **Late Separation** | 1% | 2% | 5% | 3% |
| **Leave VNC** | 0% | 2% | 0% | 2% |
| **AVG Crossovers** | 0% | 0% | 1% | 4% |

The χ2 test was only used to compare the *lron-11*(*gk5321*); *lron-14*(*gk401715*) double mutant, with the *lron-11*(*gk5321*) single mutant. The *lron-11*(*gk5321*) data was collected from observations of PVQL instead of PVPR. ^The marker used was *hdIs26[odr-2::CFP, sra-6::DsRed2].* However, *lron-14*(*gk401715*) was scored with *hdIs28[odr-2::CFP, sra-6::DsRed2].*

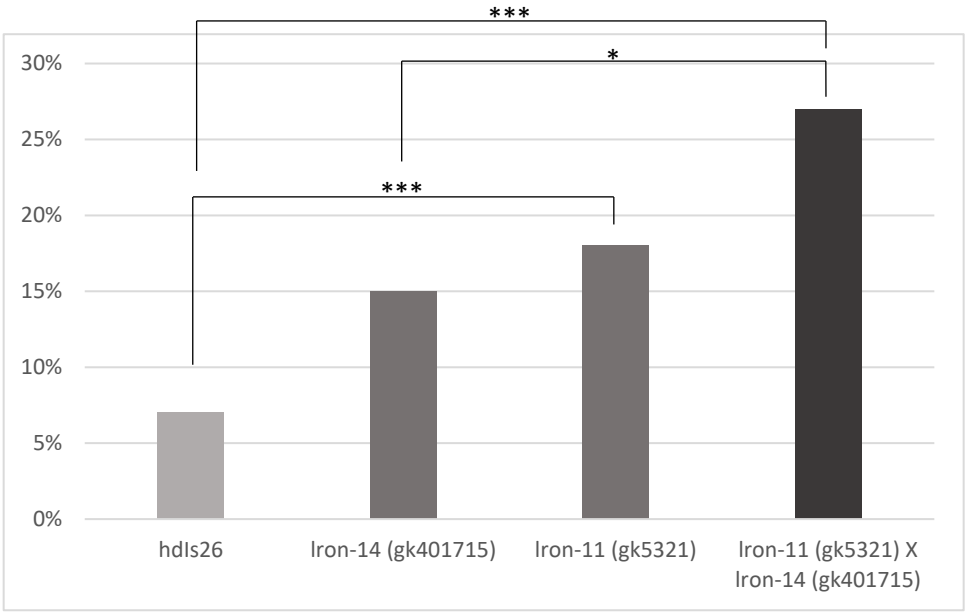


**Figure 3.11 *lron-11*(*gk5321*); *lron-14*(*gk401715*) PVPR axon guidance defects**
The *lron-11*(*gk5321*) mutant has significantly more PVPR (PVQL was counted in place of PVPR, see the table note for Table 3.4. for an explanation) axon guidance defects than the marker strain (*hdIs26*). *lron-14*(*gk401715*)'s PVPR defects are not significant from either the marker strain, or the *lron-11* single mutant. The *lron-11*(*gk5321*); *lron-14*(*gk401715*) double mutant did not have significantly more PVPR defects than the *lron-11*(*gk5321*) single mutant. ***p<0.001; **p<0.01; *p<0.05 (χ2 test).

### 3.1.14. *iglr-2* pan-neuronal and pioneer axon guidance phenotypes

Observed with the pan-neuronal marker, *iglr-2*(*et34*) animals do not have significant crossover defects or DNC defects (Table 3.36, Table 3.37). However, *iglr-2*(*et34*) worms did have highly penetrant defasciculation of the left VNC (Figure 3.12b, 3.12c; Table 3.38). I counted a split of the left VNC to be a defasciculation event. Importantly, I ignored defasciculation occurred only at the very anterior end of the VNC, anterior of the AVG cell body, and at the vulva bulge in the middle of the VNC. This is because occasional defasciculation in these locations in the marker strain did occur. I also observed significant early separation defects. Unlike late separation, early separation occurs when the left tract separates from the right tract before the cluster of 3-4 motor neuron cell bodies near the end of the VNC where it would normally diverge (Figure 3.13b). Defasciculation and early separation defects are separated into their own table, so that *iglr-2*(*et34*) mutant's other defects in Table 3.36 can be compared with data collected from other strains. I did not collect quantitative data on defasciculation or early separation in most other mutant strains, since they only displayed these defects infrequently, at frequencies that seemed similar to the marker strain.

I did not see significant defects in the pioneer marker, likely because defasciculation of the left tract cannot be observed in this marker (Table 3.39). However, I did see a single instance of PVQL producing what appears to be a second axon (Figure A1). I also infrequently observed an additional neurite sprout from one of the PVQ neurons, but I did not quantify this phenotype (Figure A1).

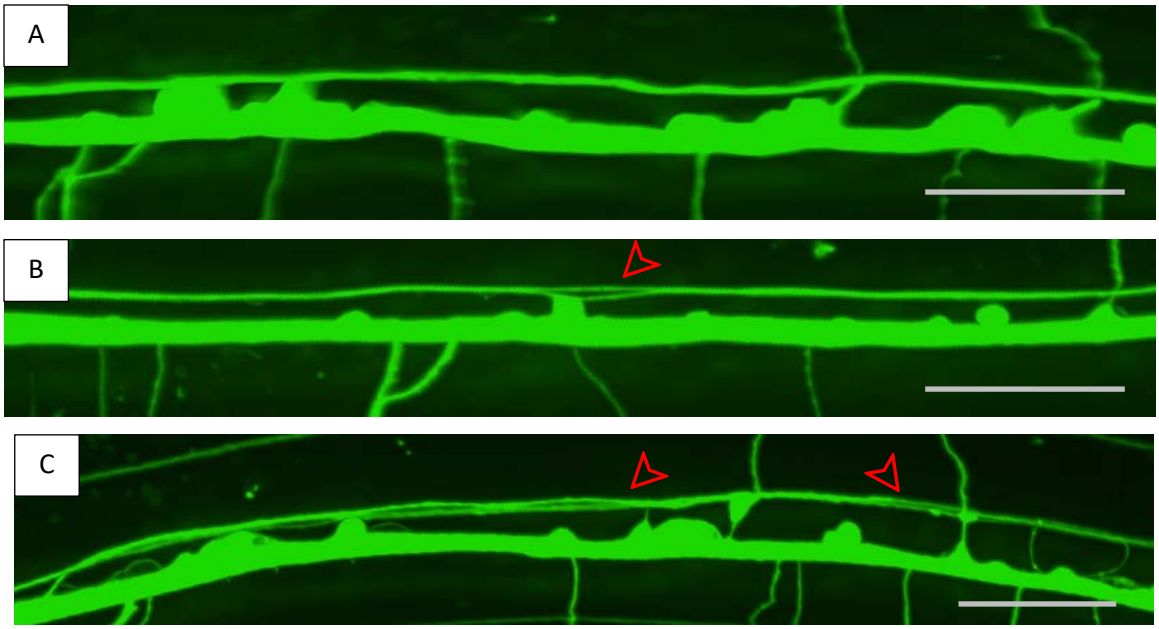


**Figure 3.12 *iglr-2*(*et34*) VNC left tract defasciculation**
**a)** This is the VNC of a wildtype animal. The left tract is tightly fasciculated. **b)** In this *iglr-2*(*et34*) animal the left tract has briefly defasciculated (red arrow). **c)** This *iglr-2*(*et34*) mutant's left VNC tract has defasciculated (red arrows). The anterior side of the worm is towards the left of the image, the left side of the worm is toward the top of the image. Scale bars = 25µm. Marker used: *evIs111[rgef-1::GFP] V*.

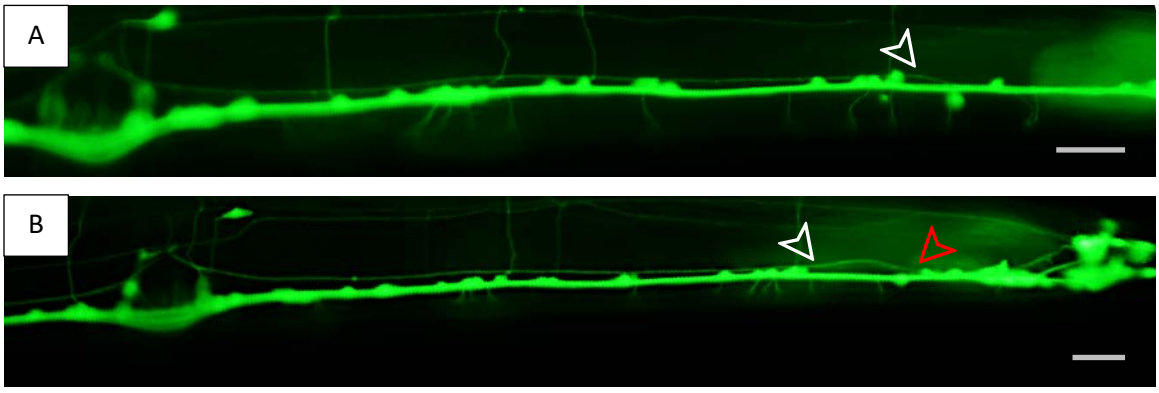


**Figure 3.13 *iglr-2*(*et34*) left VNC tract early separation**
**a)** A wildtype animal with the left VNC tact separating at the cluster of 3-4 motor neuron cell bodies (white arrow). **b)** In this *iglr-2*(*et34*) mutant, the left tract separates early from the right tract (red arrow), before the motor neuron cell body cluster (white arrow). The anterior side of the worm is towards the left of the image, the left side of the worm is toward the top of the image. Scale bars = 25µm. Marker used: *evIs111[rgef-1::GFP] V*.

**Table 3.36 *iglr-2*(*et34*) pan-neuronal VNC axon guidance defects**

| Ventral Nerve Cord | Marker Strain^ N = 787 | *iglr-2*(*et34*) N = 104 |
|---|---|---|
| **No Defect** | 95% | 94% |
| **Anterior Crossover** | 2% | 4% |
| **Posterior Crossover** | 3% | 3% |
| **Late Separation** | 0% | 1% |

^The marker used was *evIs111[rgef-1::GFP]*.

**Table 3.37 *iglr-2*(*et34*) DNC axon guidance defects**

| Dorsal Nerve Cord | Marker Strain^ N = 245 | *iglr-2*(*et34*) N = 100 |
|---|---|---|
| **No Defect** | 99% | 100% |
| **Defasciculation** | 1% | 0% |

***p<0.001; **p<0.01; *p<0.05 ($\chi 2$ test). ^The marker used was *evIs111[rgef-1::GFP]*.

**Table 3.38 *iglr-2*(*et34*) VNC left tract defasciculation**

| Left Ventral Nerve Cord | Marker Strain^ N = 50 | *iglr-2*(*et34*) N = 104 |
|---|---|---|
| **No Defect** | 90% | 13%*** |
| **Defasciculation** | 6% | 86%*** |
| **Early Separation** | 4% | 27%** |

***p<0.001; **p<0.01; *p<0.05 ($\chi 2$ test). ^The marker used was *evIs111[rgef-1::GFP]*.

**Table 3.39 *iglr-2*(*et34*) PVPR axon guidance defects**

| PVPR | Marker Strain^ N = 159 | *iglr-2*(*et34*) N = 93 |
|---|---|---|
| **No Defect** | 93% | 96% |
| **Crossover** | 6% | 2% |
| **Late Separation** | 1% | 1% |
| **Leave** | 0% | 0% |

^The marker used was *hdIs29[odr-2::CFP, sra-6::DsRed2]*.

# Chapter 4. Discussion

## 4.1. *Iron* genes' function in axon guidance

eLRR genes are extracellular or transmembrane proteins that contain LRR repeats on their extracellular domain. Many eLRR genes function in neurodevelopment, including SLT-1/Slit which is an important axon guidance cue (Dickson and Gilestro, 2006; Hao et al., 2001; Rothberg et al., 1990). Other eLRRs such as NGR1, Trks, FLRT3 and NGL's have also been found to function as receptors, co-receptors and even as ligands (de Wit et al., 2011; Lin et al., 2003; Yamagishi et al., 2011). However, these genes require further study to fully understand their role in axon guidance pathways (Chen et al., 2006; de Wit et al., 2011). Furthermore, many eLRR genes have not been studied in the context of axon guidance.

The *C. elegans Iron* gene family consists of eLRR genes that contain only LRRs in their extracellular domain. These *Iron* genes encode mostly single-pass transmembrane proteins, though some are GPI-linked or secreted. *Iron* genes have not been studied in any context, including in axon guidance. The exception is *dma-1*, which has been well studied in its role as an adhesion receptor in dendrite guidance (Liu and Shen, 2011; Tang et al., 2019; Zou et al., 2018).

eLRR genes in *C. elegans*, particularly those with only LRR domains, have diverged rapidly during evolution and rarely display sequence similarity with themselves, or similarly structured genes in other species (Dolan et al., 2007). Since many *C. elegans* genes with mammalian homologs already have somewhat divergent sequences due to their separate evolutionary history, this makes identifying *Iron* homologs very difficult. Additionally, there are many genes that also contain LRR domains along with other motifs that have a relatively high degree of sequence similarity with *Iron* genes based solely off of having large LRR domains. Therefore, homologs for *Iron* genes in mammals have not yet been identified. However, *Iron* genes do share a similar structure to the *LRRTM* gene family in mammals. *LRRTM*'s also encodes single-pass transmembrane protein's containing only LRRs on their extracellular domain.

I investigated the *Iron* family to identify if any of these genes function in axon guidance in the *C. elegans*' VNC. My data suggests that *Iron-11* functions in axon

guidance, in several different types of neurons (Table 3.1). Other *Iron* genes, particularly *Iron-14*, have significant axon guidance defects but require further research to confirm their role in this process. Genes that didn't display axon guidance defects when screened with pan-neuronal and pioneer markers could still have axon guidance functions in neurons that were not analysed in this study. For example, it is possible these genes guide axons in lateral axon tracts or within the head, which were outside the scope of my research.

### 4.1.1. PVPR axon guidance

PVPR is the interneuron that pioneers the left tract of the VNC. I found significant, ~12%, crossover defects in PVPR with both *Iron-11* alleles (Table 3.1, 3.4). I also observed ~5% of the late separation defect, where PVPR stays in the right tract for too long. Despite the low penetrance, this was also significant since the marker strain only rarely (<1% penetrance) displayed this phenotype. *Iron-5* was the only other *Iron* gene that displayed significant PVPR defects (Table 3.1, 3.19, 3.24). However, *Iron-5*(*gk959442*) did not have significant pan-neuronal axon guidance defects. This conflicts with the pioneer data since PVPR defects should be observed in the pan-neuronal marker. However, this *Iron-5* mutant strain, VC41011, contains many additional mutations and has not been outcrossed. Therefore, the *Iron-5* strain crossed with the global marker will be homozygous for different background mutations than the *Iron-5* strain containing the pioneer marker. The difference in background mutations could account for the discrepancy between the pan-neuronal and pioneer marker axon guidance defects. This suggests that *Iron-5* does not guide the PVPR axon, though the outcrossed *Iron-5* strain should be phenotyped to confirm this.

Both studied *Iron-3* alleles are putative null alleles contain large deletions. Preliminary work on a *Iron*-3(*ok2614*) strain found significant axon guidance defects, but this strain hadn't been outcrossed. Neither of the alleles I studied displayed significant PVPR axon guidance defects (Table 3.1, 3.19, 3.21). However, *Iron-3*(*gk5319*) did have significant pan-neuronal defects that were mostly left tract crossovers, which are often indicative of PVPR crossovers (Table 3.1, 3.17, 3.20). However, the penetrance of defects was still quite low, at 11%. I created *Iron-3*; *Iron-11* double mutants which displayed pan-neuronal and PVPR defects that were comparable to the *Iron-11* single mutant (Table 3.30, 3.32). Therefore, *Iron-3* could act in the same PVPR axon guidance

pathway as *lron-11*, which has similar PVPR defects to *lron-3*(*gk5319*) (Table 3.4). However, the much more likely explanation is that *lron-3* doesn't actually function in axon guidance in the VNC and that the significant pan-neuronal defects for one *lron-3* allele were a false positive result.

*lron-14*(*gk401715*) displayed 15% PVPR defects, but this was not significant when compared with the marker strain (Table 3.1, 3.16). *lron-14* did have significant pan-neuronal defects, the majority of which involved defects in axons of the left tract which often indicative of PVPR defects (Table 3.1, 3.14). Also, consistent in both the pan-neuronal and in PVPR, 2% of *lron-14* mutants had axons in their left tract leave the VNC (Figure 3.9). Based on these results, I phenotyped the *lron-11*; *lron-14* double mutant in both the pan-neuronal and pioneer marker. I observed axon guidance defects in the pan-neuronal marker that were significantly more penetrant than either of the single mutants (Figure 3.10; Table 3.33, 3.34). This indicates that *lron-11* and *lron-14* have an additive genetic interaction and function in separate pathways. However, the increase in PVPR axon guidance defects in the double mutant was not significant when compared to the *lron-11*(*gk5321*) mutant (Figure 3.11; Table 3.35). This suggests that *lron-14* and *lron-11* might function in the same pathway, which is somewhat contradictory to the pan-neuronal data, or it could mean that only *lron-11* functions in PVPR axon guidance. The *lron-14*(*gk401715*) mutant's low penetrance of axon guidance defects could be making it harder to statistically detect an additive genetic interaction or it is possible that *lron-14*(*gk401715*) doesn't actually function in axon guidance in the VNC. To resolve this, *lron-14*(*gk401715*) should be outcrossed to determine if background mutations are causing this discrepancy, and to verify that it acts in axon guidance.

Interestingly, there appear to be many axon guidance pathways involved in PVPR axon guidance. The cadherins *cdh-4*, and *fmi-1*, as well as the *lin-17*/*frizzled* receptor display the largest PVPR defects, with a crossover penetrance of over 50% (Schmitz et al., 2008; Steimel et al., 2010). However other axon guidance genes have also been implicated. The ephrin's guidance pathway functions to inhibit many axons, including PVPR, from crossing the ventral midline (Boulin et al., 2006). The ephrin receptor is expressed in the extending growth cone, and ephrins and the IgCAM *wrk-1* signal from the surface of motor neuron cell bodies along the midline. *sax-3/robo* mutants display a high PVPR crossover penetrance as well (inferred from PVQL

defects), however this appears to be largely independent of its usual ligand *slt-1*/*Slit* (Boulin et al., 2006; Zallen et al., 1998). Additionally, *unc-6/netrin*, which is secreted by ventral cells, also results in penetrant PVPR axon guidance defects when mutated (Hutter, 2003). Finally, there are two PVPR axon guidance pathways mediated by heparan sulfate modified proteins. Heparan sulfate modifying enzymes *hst-2* and *hse-5* mutants have ~50% PVPR crossover defects, though the protein they are modifying has not been identified (Bülow and Hobert, 2004). *hst-6* may modify the HSPG *sdn-1* which acts in a parallel PVPR axon guidance pathway (Rhiner et al., 2005). Further work is required to determine if any of these axon guidance genes act in the same pathway or whether these are all separate axon guidance pathways.

With the data currently available, it is impossible to accurately determine which of these pathways *lron-11* might be a part of, if any. The *lron-11* single mutant PVPR crossover defects I observed were more moderate than in most of these other known axon guidance genes. The exception is the ephrin *vab-2,* which also has PVPR defects under 20% (Boulin et al., 2006). However, I have not found evidence of LRR domains interacting with ephrins or their receptors; the RTK eLRR TrkB binds ephA, but the LRR domain was not required for this interaction (Marler et al., 2008). Therefore, there is not strong evidence to support *lron* genes functioning in this ephrin pathway. However, there is strong evidence that the addition of heparan sulfate to neurexin is necessary for its proper binding with the eLRR-only proteins LRRTM1 and LRRTM2 to induce synaptogenesis (Ko et al., 2009; Yamagata et al., 2018; P. Zhang et al., 2018). Furthermore, heparan sulfate is also required for a functional interaction between LRRTM4 and glycipans, a heparan sulfate proteoglycan (HSPG) (de Wit et al., 2013). So, it is possible LRON proteins like LRON-11 bind HSPGs. However, LRRTMs are not known homologs of *lron* genes, so this is a somewhat tenuous connection.

Robo receptors have been shown to interact with several different eLRR proteins. As previously stated, SAX-3/Robo receptor binds the eLRR protein SLT-1/Slit, and the ligand's LRR domain is essential for this interaction (Battye et al., 2001; Hao et al., 2001). Zebrafish eLRR-only LRRTM1, which has a similar ectodomain to the LRON proteins, has been shown to bind to Robo2 *in-vitro* (Söllner and Wright, 2009). In *Drosophila*, eLRR-only protein Leucine Rich Repeat Trans-membrane protein (LRT), seems to bind Robo during muscle cell migration (Gilsohn and Volk, 2010). Interestingly, in mice the eLRR protein FLRT3 binds to Robo1 with its intracellular

domain, where it promotes netrin attraction by upregulating UNC-40/DCC in the presence of SLT-1/Slit, combining these axon guidance pathways (Leyva-Díaz et al., 2014). Therefore, it is possible that LRON-11 is another eLRR protein that bind SAX-3/Robo. However, *lron-11*'s expression pattern has not been verified, and double mutants between *lron-11* and *sax-3* would have to be created to provide evidence for an interaction between these genes.

Finally, there is evidence of eLRR proteins interacting with the netrin receptors UNC-40/DCC and UNC-5. I already mentioned that FLRT3 can upregulate UNC-40/DCC expression, though how this occurs is unclear. However, it is also known that FLRT3 binds UNC-5b in *Xenopus* as an inhibitory cue for cell adhesion (Karaulanov et al., 2009). This interaction primarily utilizes FLRT3's LRR domain, demonstrating that UNC-5 receptors can bind LRRs. More relevantly, FLRT2 and FLRT3 bind UNC-5D receptors as an inhibitory cue during mouse cortical neuron axon guidance (Yamagishi et al., 2011). Intriguingly, these FLRTs shed their ectodomain and act as a secreted cue in this axon guidance pathway. This cleavage does not require their fibronectin domain, so some *lron* genes might be capable of shedding their extracellular domains as well. UNC-5 does function in the pioneer AVG's axon guidance, but it has not been studied in PVPR (Bhat and Hutter, 2016).

While the axon guidance pathways that *lron-11* is acting in cannot currently be identified, research on other similar eLRRs is informative as to what genes it might interact with. *lron-11* has a similar structure to *dma-1*, which functions as an adhesion receptor, so it is possible it could also act cell autonomously as an adhesion receptor. However, although all the *lron* genes have been grouped into the same family based on shared characteristics, they do not cluster together if you compare their amino acid sequences (Dolan et al., 2007). Also, *lron-11*'s PVPR defects seem more likely to be caused by signaling defects rather than adhesion defects, since PVPR is a pioneer axon. Therefore, *lron-11* might act as receptors for extracellular guidance cues. DMA-1 is capable of transmitting signals through its intracellular domain, and through cis-binding of other transmembrane proteins, suggesting other *lron* genes might be capable of this as well (Tang et al., 2019; Zou et al., 2018). Additionally, there is RNA-seq evidence that *lron-11* is expressed in neurons during axon extension and could therefore function cell autonomously, though this requires further evidence to be confirmed (Packer et al., 2019). I created a transcriptional expression construct by fusing the 3kb

upstream of the *lron-11* start codon to GFP. However, with this reporter I only observed faint expression in a band of muscle, and in a pair of sensory neurons in the head. An explanation for this low and limited expression could be that *lron-11*'s introns contain enhancer elements that are important in its expression. *lron-11*'s first two introns are very large, consisting of ~900 and ~2000 base pairs respectively. In *C. elegans*, as well as other organisms, large early introns often play an important role in enhancing gene expression. Therefore, further experiments, such as with a transcriptional reporter that includes *lron-11*'s promoter and its introns, are required to determine if *lron-11* is expressed cell-autonomously by PVPR and could be functioning as a signal transducing receptor.

### 4.1.2. AVG axon guidance

I observed significant AVG crossover defects in *lron-11*(*ok2333*) mutants, but with only ~5% penetrance (Table 3.1). I only saw 1% axon guidance defects in *lron-11*(*gk5321*) animals (Table 3.1). In the *lron-11*; *lron-14* and *lron-11*; *lron-3* double mutants I observed 4% and 5% AVG crossover defects (Table 3.32, 3.35). The *lron-11*; *lron-14* double mutant with the pioneer marker contained the *lron-11*(*gk5321*) allele, and the *lron-11*; *lron-3* animals with the pioneer marker contained the *lron-11*(*ok2333*) allele.

It is unsurprising that I observed such low penetrance of AVG crossovers since AVG is not greatly affected by single mutations in known axon guidance genes, likely due to redundant signaling pathways. For example, *unc-6*/*netrin* and *unc-5* mutants also display low, <10%, AVG crossover penetrance (Bhat and Hutter, 2016). However, when they are combined with a *nid-1*/*nidogen* mutation, a gene which encodes part of the basement membrane, the ~40% crossover penetrance of the double mutant is much higher than either single mutant (Bhat and Hutter, 2016). NID-1/nidogen is required for the correct navigation of longitudinal axons, though it is not required for basement membrane assembly (Ackley et al., 2003; Kim and Wadsworth, 2000). This demonstrates that UNC-6 and UNC-5 do function in AVG axon guidance, despite low penetrance of defects in the single mutants. Therefore, *lron-11* mutant's low penetrance of crossover defects could still be an indication that *lron-11* has a role in AVG axon guidance.

### 4.1.3. AVK axon guidance

AVKL and AVKR are interneurons situated near the anterior end of the VNC. They send their axons anteriorly into the nerve ring before they enter the VNC traveling posteriorly (Figure 3.4a). AVKL's axon enters the right tract, AVKR's enters the left. In *lron-11*(*ok2333*) mutants, I rarely observed any crossover defects in AVK axons (Table 3.6). This is not unexpected, since different axons often rely on different guidance pathways. For example, mutations in the ephrin pathway and in *hst-2*, *hst-6* and *sdn-1* have crossover defects in other interneurons like PVPR, but not in AVK (Boulin et al., 2006; Bülow and Hobert, 2004). The AVK axon does display crossover and VNC leave defects in *sdn-1* and *fmi-1* (Rhiner et al., 2005; Steimel et al., 2010). In *lron-11*(*ok2333*) animals I did observe AVKL and/or AVKR axons prematurely leave the nerve ring in ~10% of animals (Figure 3.4b; Table 3.6). When this occurred, the AVK axon typically wanders posteriorly, and it would never enter the VNC (Figure 3.4c). Although I did not observe this defect in the marker strain, these results are not statistically significant due to the low penetrance of the defect and because only 53 animals were scored for the marker strain. More animals need to be scored to determine if this is a *lron-11* mutant phenotype.

### 4.1.4. Command interneuron axon guidance

Command interneurons axons enter the VNC at the anterior end. While initially command interneuron axons enter the VNC in both the left and right tract, the axons in the left tract will all crossover very early on, before the AVG cell body (Figure 3.5a). The axons then extend posteriorly along the right tract. In *lron-11*(*ok2333*) animals, I only saw 5% penetrance of crossovers into the left tract (Table 3.7). So, *lron-11* doesn't appear to play a major role in guiding command interneurons along the VNC. Notably, *sdn-1* mutants display no command interneuron defects, despite significant PVPR and AVK crossover defect (Rhiner et al., 2005). Ephrin and FMI-1 however do function in command interneuron axon guidance (Boulin et al., 2006; Steimel et al., 2010). In *lron-11*(*ok2333*) mutants I did observed axons in the left tract extend past the AVG cell body before crossing over in ~10% of animals, which I never observed in the marker strain and was statistically significant (Figure 3.5b; Table 3.7). This might indicate a modest role for *lron-11* in guiding command interneurons as they enter the VNC.

### 4.1.5. HSN axon guidance

The HSN motor neuron's cell bodies reside slightly dorsal of either side of the VNC and are just posterior of the vulva (Figure 3.3a). HSNL is on the left side, where it sends its axon ventrally into the left VNC. HSNR sends its axon into the right tract. The HSN axons then travel anteriorly along the VNC. Mutations in several known axon guidance genes cause HSN axon guidance defects. This includes the ephrin pathway, since *vab-2 and wrk-1* mutants have 15-20% HSN crossover defects (Boulin et al., 2006). *sax-3* mutants have the largest defects, with ~50% penetrance of HSN crossovers (Zallen et al., 1998). Finally, mutations in all three heparan sulfate modifying enzymes *hst-2*, *hse-5* and *hst-6* and in *sdn-1* result in significant HSN crossover (Bülow and Hobert, 2004; Rhiner et al., 2005). *lron-11*(*ok2333*) mutants had 17% penetrance of crossovers in HSNL (Figure 3.3b; Table 3.5). This was not significant and since the PVPR axon sometimes leaves the left tract in *lron-11*(*ok2333*) animals, it is possible that the HSNL axon is simply following this pioneer axon when it crosses over (Table 3.4). Therefore, *lron-11* doesn't appear to guide the HSN axons in the VNC.

### 4.1.6. DD/VD motor neuron neurite guidance

Motor neurons cell bodies are present along the ventral midline and they send their neurites only into the right tract of the VNC. They send their commissures dorsally to the DNC, up either the left side or the right side of the animal, in a consistent pattern. Most DD/VD commissures are sent up the right side of the animal. In 55% of *lron-11*(*ok2333*) mutants, at least one commissure extends up the wrong side of the animal and in 20% of animals there are more than two errant commissures (Figure 3.6b; Table 3.9). This commissure polarity defect was significant, but it should be noted that the marker strain had 34% penetrance of commissure polarity defects (Table 3.9).

Commissure polarity defects cannot be easily interpreted as an adhesion defect. Therefore, this suggests LRON-11 might not act as an adhesion receptor like DMA-1, at least for commissure polarity. However, there is some evidence for adhesion, or at least cell-cell contact, being important for commissure polarity. First, the cadherin adhesion receptor *cdh-4* also has over 50% penetrant DD/VD commissure polarity defects (Schmitz et al., 2008). Further evidence comes from AVG ablation experiments. When AVG is ablated early, its axon is not able to pioneer the right tract, resulting in the right

axon tract becoming highly defasciculated (Durbin, 1987). Interestingly AVG ablation also causes a high penetrance of commissure polarity defects, in both DD/VD and DA/DB motor neuron commissures (Hutter, 2003). Therefore, adhesion to AVG or other neighbouring axons in the right tract might be important for the establishment of left-right polarity in motor neurons. Other mutants such as *fmi-1*, *unc-6* and *sax-3* also display DD/VD commissure polarity defect, although their penetrance is less than 50% (Hutter, 2003; Steimel et al., 2010). *unc-6* and *sax-3* mutants having commissure polarity defects suggests that there is at least some signaling component in determining commissure polarity. Heparan sulfate also appears to be involved in this process, with *hst-2* and *hse-5* animals having ~25% penetrant defects (Bülow and Hobert, 2004).

The *lron-11*(*ok2333*) mutant allele did not impair DD/VD commissure's ability to navigate dorsally to reach the DNC (Table 3.8). In wildtype animals, once these commissures reach the DNC, they should form a continuous tract (Figure 3.7a). Gaps in the DNC were observed in 23% of *lron-11* mutants, however this was not significant compared to the marker strain (Figure 3.7b, 3.7c; Table 3.11).

Interestingly, in the pan-neuronal marker I did observe significant defects in the DNC of *lron-11* mutants, but only with the *gk5321* allele. In both mutant alleles, part of DNC defasciculated in ~5% of animals (Figure 3.1d; Table 3.3). Intriguingly, despite the *lron-14*(*gk401715*) single mutant only having 2% penetrance of DNC defasciculation, the *lron-11*; *lron-14* double mutant had 19% penetrance for DNC defects (Table 3.15, 3.34). This included the DNC bending ventrally in some animals (Table 3.34). The *lron-11*; *lron-14* double mutant's DNC defects were highly significant from the marker strain, as were also significant from both the *lron-11* single mutant strains (Table 3.34). This suggests that both *lron-11* and *lron-14* might play minor roles in DNC fasciculation. The cause of this defasciculation defect could be impaired adhesion between the commissures within the DNC, which is thought to be the cause of the ~50% penetrance of DNC defasiculation defects observed in the cadherin *cdh-4* mutants (Schmitz et al., 2008).

Alternatively, *lron-11*'s commissure polarity defects could be causing this disorganization in the DNC. As mentioned previously, mutations in a heparan sulfate pathway induce commissure polarity defects (Bülow and Hobert, 2004). Mutations in the heparan sulfate modifying enzymes *hst-2* and *hse-5* mutants also cause ~25% DNC

defasciculation penetrance and *sdn-1* mutants have 15% defects (Bülow and Hobert, 2004). *cdh-4* mutants also have both commissure polarity defects and DNC defasciculation defect (Schmitz et al., 2008). Therefore, *lron-11* could be functioning as an adhesion receptor during DNC fasciculation, and/or its function in commissure polarity could be indirectly impacting the organization of the DNC, resulting in defasciculation.

In addition to commissure defects, I observed DD/VD neurites extend aberrantly into the left tract in 22% of *lron-11*(*ok2333*) animals (Figure 3.6c, 3.6d; Table 3.10). This occurred due to a crossover event, or due to an outgrowth error that results in the neurite starting in the left tract. I observed both of these events in *lron-11* mutants and the penetrance of this defect was statistically significant from the marker strain. I only counted this as a defect if the neurite(s) stayed in the left tract for at least two motor neuron cell body lengths.

DD/VD neurites crossing into the left tract could be cause by loss of adhesion to other neurites in the right tract. This loss of adhesion could cause a neurite to occasionally cross the ventral midline when it otherwise would have stayed bound to the right tract. This is thought to be the cause of the cadherins *cdh-4* and *fmi-1*'s ~25% DD/VD neurite crossover phenotype (Schmitz et al., 2008; Steimel et al., 2010). However, because some of the neurites initially outgrew into the left tract, this suggests that *lron-11* plays a signaling role in DD/VD neurites outgrowth. Therefore, the neurites crossing into the left tract could also be interpreted as a signaling defect. For instance, if neurites are no longer able to recognise a repulsive signal at the ventral midline, they will crossover more frequently. Loss of known axon guidance signaling pathway components has been implicated in DD/VD neurite crossovers. For example, mutants lacking the axon guidance cue *unc-6* have a DD/VD neurite crossover penetrance of 42% (Hutter, 2003). Additionally, *sax-3* functions as a receptor in a separate axon guidance signaling pathway, and mutations in *sax-3* have a DD/VD crossover penetrance of 30% (Hutter, 2003). *hst-2* and *hse-5* were shown to have penetrant 'VNC defasciculation' defects in DD/VD motor neurons as well (Bülow and Hobert, 2004). These observations suggest that DD/VD neurite guidance might require both adhesion and signaling for proper guidance along the VNC.

Based on this data, *Iron-11* could be functioning purely as a receptor for axon guidance signals or it could have a fasciculation function in these neuron's neurites. More research to discover other genes *Iron-11* is interacting with is required to determine what role it is playing in DD/VD neurites navigation. Of the genes with similar DD/VD motor neuron defects, *Iron-11* seems most likely to function in the *sax-3*/*Robo* or heparan sulfate pathways. This is because many eLRR protein's LRR domains have been shown to bind to SAX-3/Robo and heparan sulfate modified proteins, including binding Robo in axon guidance signaling pathways (Battye et al., 2001; de Wit et al., 2013; Gilsohn and Volk, 2010; Hao et al., 2001; Leyva-Díaz et al., 2014; Söllner and Wright, 2009; P. Zhang et al., 2018). Creation of double mutants to test for genetic interactions would elucidate any interaction between these genes.

### 4.1.7. DA/DB motor neuron neurite guidance

The DA/DB motor neuron neurites make similar axon guidance decisions to DD/VD motor neuron neurites. Neurites extend into the right VNC, and the commissures choose to travel up the left or right side of the animal to the DNC. However, fewer genes have been implicated in DA/DB neurite guidance, so they seem to not rely entirely on the same guidance pathways that DD/VD motor neurons use. In *Iron-11*(*ok2333*) mutants, I did not observe neurites in the left tract when observing these neurons (Table 3.12). However, I did see a 75% penetrance of at least one commissure polarity defect in these mutant animals (Figure 3.8; Table 3.12). Additionally, 40% of *Iron-11* animals had at least two commissures traveling up the wrong side, and 7% had more than four (Table 3.12). Interestingly, the *Iron-11* mutation had different effects across DA/DB neurons (Table 3.13). DA4 was defective in ~50% of animals, which is the same as if it was choosing randomly. So, without functional *Iron-11* DA4 seems unable to polarize along the left-right axis. Conversely, the posterior-most neurons counted, DB5, DA5, DB6, DA6 and DB7, were only slightly affected, with commissure polarity defects in 10% or less of mutants. *Iron-11*'s commissure polarity defect cannot be classified purely as an axon outgrowth or axon guidance defect, since both were predominant in different motor neurons (Table 3.13). For example, the DA4 commissure traveled along the VNC briefly before turning up the wrong side of the animal for the majority of commissure polarity defects observed. However, for all DB3 and DA2 defects, the commissures outgrew directly from the wrong side of the cell body. This suggests *Iron-11* is required to

different degrees and even in different processes (commissure guidance and outgrowth) in various DA/DB motor neurons. Interestingly, mutations in heparan sulfate modifying enzymes and in *sdn-1* also have divergent effects on the different DA/DB commissures. In this case, the DA2 and DB3 commissures almost completely lost their left-right polarity in *hst-2*; *hst-6* double mutants, and in *sdn-1* mutants (Bülow et al., 2008). No other commissure was heavily impacted. Together, these results suggest that different DA/DB motor neurons rely on different axon guidance pathways to polarize along the left-right axis. DA2 and DB3 seem to rely on a heparan sulfate pathway, whereas DA4 relies on *lron-11*.

*sax-3* is the only other axon guidance gene with high penetrance of DA/DB commissure polarity defects, with 70% of animals having errant commissures (Hutter, 2003). *fmi-1* and *unc-6* also have commissure polarity defects, but these are only ~20% penetrant (Hutter, 2003; Steimel et al., 2010). This is additional evidence that *lron-11* could be acting in a *sax-3*/*Robo* signaling pathway. As previously noted, both *lron-11* and *sax-3* mutants have display axon guidance defects in PVPR and in DD/VD motor neurons, and have few crossovers in command interneurons (Table 3.4, 3.5, 3.7, 3.9, 3.10; Hutter, 2003; Zallen et al., 1998). It should be noted that *sax-3* mutant's defects in PVPR and HSN are much more highly penetrant than in *lron-11* mutants. However, this does not mean *lron-11* can't be functioning in the same pathway. *sax-3* could act in multiple axon guidance signaling pathways or other genes could have a redundant role to *lron-11* in this pathway. Regardless, more research is required to demonstrate an interaction between *lron* genes and *sax-3*.

### 4.1.8. Other possible *lron* gene functions

While I didn't observe axon guidance defects in some *lron* genes, they could still function in axon guidance outside of the VNC. However, it is likely most of them have other functions. Some of these *lron* genes are expressed in neurons, so they, like many other eLRRs, could act in synapse formation or function (Figure 1.8; Liu and Shen, 2011; Packer et al., 2019). This includes the LRRTM family, which has only LRRs on their extracellular domain and in mammals has the most comparable protein structure to the LRON family. LRRTM2 is an important binding partners for neurexin and recruits synaptic proteins in the postsynaptic membrane to induce excitatory synapse differentiation in both the pre- and postsynaptic membranes (de Wit et al., 2009; Ko et

al., 2009; Linhoff et al., 2009; Yamagata et al., 2018). LRRTM4 also induces synaptic differentiation, but by binding the heparan sulfate proteoglycan glypicans (de Wit et al., 2013). Both neurexin and glypicans have homologs in *C. elegans* that function in synapses, so these homologs are good candidates for binding partners of the LRON proteins that are expressed in neurons (Ackley et al., 2003; Lázaro-Peña et al., 2018; Reissner et al., 2013). The Slitrks also function in synaptic differentiation through binding LAR family receptor protein tyrosine phosphatases (Yim et al., 2013). Furthermore, the IG containing eLRR NGL family functions in excitatory synapse formation as well (Kim et al., 2006). The SALM (synaptic adhesion-like molecules) family, which contain LRR, IG and fibronectin domains, also function in synaptogenesis, as well as in synapse maturation and neurite outgrowth (Ko et al., 2006; Nam et al., 2011). In *Drosophila*, the eLRR Caps is expressed in both the pre- and postsynaptic membranes where it mediates axon and dendrite target selection through hetero- or homophilic binding (Hong et al., 2009; Kohsaka and Nose, 2009; Shinza-Kameda et al., 2006). Toll receptors also have a function in target selection, as they inhibit motor neuron synaptic initiation in *Drosophila* (Rose et al., 1997). This demonstrates that eLRRs commonly play a role in synapse development, so neuronal expressed *Iron* genes that did not display axon guidance defects could instead function in synapses.

eLRR genes also have diverse functions outside of nervous system development. *Iron* genes not expressed in developing neurons could potentially act in these processes. This includes functions in innate immunity (Nürnberger et al., 2004) pain (Wadachi and Hargreaves, 2006) heart function (Li et al., 2017) modulation of voltage-gated channels (Peltola et al., 2011) as hormone receptors (Van Loy et al., 2008) muscle regeneration (K. Zhang et al., 2018) stem cell regulation (Rafidi et al., 2013) and modulation of cell growth (Böttcher et al., 2004; Ghiglione et al., 1999; Zhang et al., 2005). Additionally, in *Drosophila* the Toll receptor functions during embryonic development, playing a key role in the creation of the dorsal-ventral polarity of the embryo (Anderson et al., 1985). Interestingly, Toll receptors have also been found to initiate apoptosis in neurons (Ma et al., 2006). Finally, eLRR's have roles in synapse function. LRRTM1 and LRRTM2 stabilize AMPA receptors in the postsynaptic membrane (Bhouri et al., 2018). When they are mutated, the normal increase of AMPA receptors required for LTP is prevented. Other eLRR proteins, such as Slitrk5, have also been found to have synaptic transmission or memory functions (Bando et al., 2005;

Shmelkov et al., 2010). eLRR proteins also function in myelination, though this process does not occur in *C. elegans* (Bermingham et al., 2006; Mi et al., 2005). There are undoubtably more undiscovered functions of eLRR genes, since this group of genes has not been as well characterized (Dolan et al., 2007).

## 4.2. *iglr* genes' function in axon guidance

Most of the eLRR genes that are known to function in axon guidance contain IG domains in addition to their LRR domains (Figure 1.8). The Trks, which have relatively few LRR domains and contain two IG domains, have an important role in neuron survival and in synapse development (Barbacid, 1994; Huang and Reichardt, 2001). In addition, all three Trks have been implicated in guiding a variety of axons in several model organisms (Cabelli et al., 1997; Gallo et al., 1997; Guo et al., 2011; Patel et al., 2000; T. D. Patel et al., 2003; Perez-Pinera et al., 2008). Linx is transmembrane protein with LRRs, one IG domain, and a fibronectin domain (Homma et al., 2009). It modulates TrkA's activity during sensory and motor axon guidance in mice (Mandai et al., 2009). It also functions in mouse thalamocortical axons, their guidepost cells, and in axons navigating through the optic chiasm of zebrafish (Abudureyimu et al., 2018; Mandai et al., 2014; Panza et al., 2015). These functions are independent of TrkA. Lingo-1 and Amigo-3, which both contain a LRR domain and a single IG domain, function as coreceptors to the eLRR NGR1 to induce axon repulsion from myelin (Ahmed et al., 2013; Mi et al., 2004). Additionally, Amigo-1 has been found to enable fasciculation through homophilic binding (Kuja-Panula et al., 2003; Zhao et al., 2014).

The *C. elegans*' *iglr* genes are single-pass transmembrane proteins containing eLRRs and a single IG domain. Transcriptional and translational reporter experiments provide evidence that *iglr-1* and *iglr-2* are being expressed in neurons (Kuo et al., 2020; Liu and Shen, 2011). Like the genes just described, their LRRs are closest to their N terminus, with the IG domain's being closer to the transmembrane domain (Figure 1.8). It has been proposed that all human LRR and IG containing proteins, including the Trks, Lingos and Amigos, evolved from a single ancestor gene (Mandai et al., 2009). However, similar to the *Iron* family, the *iglr* genes have no identified homologs, though *iglr-2* does cluster with the uncharacterized *Drosophila* gene *CG16974* (Dolan et al., 2007). However, *iglr* genes do have the same domain organization as the *Lingo* and *Amigo* mammalian gene families, which both cluster together due to their sequence

similarity (Mandai et al., 2009; Ulian-Benitez et al., 2017). These genes' extracellular domains are also made up of a single IG domain and LRRs and they are also single-pass transmembrane proteins. Genes in both of these families have been implicated in axon guidance (Ahmed et al., 2013; Kuja-Panula et al., 2003; Mi et al., 2004; Zhao et al., 2014). Given that eLRR and IG containing genes with similar domain structure to *iglr* genes function in axon guidance, some *iglr* genes could have a similar function.

### 4.2.1. Pan-neuronal and pioneer crossover defects

I analyzed *iglr-1*(*gk687851*) and *iglr-2*(*et34*) mutants for VNC axon guidance defects with pioneer and pan-neuronal markers. I did observe significant pan-neuronal defects in *iglr-1* animals, though these were only 11% penetrant (Table 3.1). Also, although most of these crossovers were from axons in the left tract, *iglr-1*(*gk687851*) mutants didn't have display significant PVPR defects. This indicates that this is either a false positive result or *iglr-1* plays a minor role in AVKR or HSNL axon guidance. I did not observe significant crossover defects in the *iglr-2* mutants.

### 4.2.2. Left VNC fasciculation defects

Intriguingly, in *iglr-2*(*et34*) mutants, I observed apparent fasciculation defects in the left VNC in the pan-neuronal marker (Figure 3.12). The left tract split in 86% of *iglr-2* animals, compared with just 6% of wildtype animals (Table 3.38). In contrast, I did not notice any defasciculation of the right tract. However, any defasciculation of the right tract that isn't major (involving crossovers) is difficult to observe due to the number of axons in the right tract (Chisholm et al., 2016). Fasciculation defects can prevent axons from synapsing with their proper targets because most synapses in *C. elegans* form *en passant* between adjacent neurites (Hall and Russell, 1991; White et al., 1986).

While *iglr-2* mutants seem to have a fasciculation defect in the left tract, there are other explanations. Half of the fasciculation events observed started anterior of the AVG cell body. The cell bodies near AVG and in the head together produce an excess of fluorescence that makes it difficult to observe the faint left tract at the anterior end of the VNC. This makes it difficult to identify if this is a real split in the left tract or if an anterior axon is simply crossing over gradually from the right tract to the left. Another explanation is that axons from the head or neurites from motor neurons could be

inappropriately extending into the left VNC. Since these axons are not meant to navigate along this fascicle, they might not fasciculate properly with the axons in this bundle. Further analysis in a motor neuron marker could identify if any motor neuron neurites are extending into the left tract, which could also be caused by a fasciculation defect. However, for the rest of this discussion I will assume that this is primarily a left VNC fasciculation defect.

I also noticed significant, ~30%, early separation defects in the *iglr-2*(*et34*) mutants (Table 3.38). This occurs when the left tract leaves the right tract abnormally early, before the cluster of motor neuron cell bodies near the end of the VNC (Figure 3.13). This is hard to interpret, since the PVPR axon forms the left tract almost immediately after outgrowing (Durbin, 1987). Its only later in development that the start of the left tract is shifted anteriorly, presumably due to additional growth and cell rearrangement that occurs later in development. So, this defect presumable is caused by an alteration of these developmental processes in this region, not due to an axon guidance error.

The left VNC consists of only four axons, the pioneer PVPR, as well as PVQL, HSNL and AVKR (Figure 1.5). PVQL in particular is known to fasciculate tightly to PVPR (Durbin, 1987; Hutter, 2003). HSNL requires either PVQL or PVPR to navigate along the left tract properly (Garriga et al., 1993). AVKR appears to be able to navigate along the left tract without the PVPR or PVQL axon being constantly present, although it still fasciculates tightly to PVPR when it is in the left tract (Steimel et al., 2010). Since all of the follower axons depend on PVPR, directly or indirectly, to form a tight fascicle, the most likely cause of *iglr-2*'s defasciculation would be loss of adhesion between the pioneer PVPR and one or more of the followers. This could be demonstrated by creating a double mutant of *iglr-2* and another gene such as *sax-3* which has high penetrance for PVPR crossovers but has no PVPR/PVQL fasciculation defects (Hutter, 2003). With a pioneer marker this would enable observation of defasciculation between PVPR/PVQL if PVQL doesn't follow PVPR during its crossovers.

Only mutations in two genes have been proven to disrupt fasciculation between PVPR and its followers, the cadherin *fmi-1* and the *lin-17*/*frizzled* receptor (Steimel et al., 2010). These genes act in the same pathway for PVPR/PVQL fasciculation, and likely directly bind each other because in *Drosophila*, *fmi-1*'s homolog *Flamingo*/*Starry night*

directly interacts with *Frizzled* in the planar cell polarity pathway (W.-S. Chen et al., 2008; Steimel et al., 2010). The defasciculation results from this paper cannot be directly compared to my results, since their measure of defasciculation was different. *fmi-1* mutants not only have left VNC fasciculation defects, they also have frequent PVPR crossover events (Steimel et al., 2010). Therefore, in this paper fasciculation was measured by comparing the number of times PVQL crossed with PVPR, to the number of times PVQL crossed without PVPR. Since *iglr-2* animals don't have crossovers, this type of analysis was not possible. Interestingly, *fmi-1*'s crossover defect was found to be independent of its fasciculation defect. *fmi-1* mutants rescued with FMI-1 lacking its extracellular cadherin domains rescued the fasciculation defects, but not the crossover defects (Steimel et al., 2010). Conversely, the extracellular domain was required to rescue the crossover defect. Perhaps, as it doesn't have crossover defects, *iglr-2* is functioning solely in the *fmi-1*/*lin-17* fasciculation pathway.

However, proteins with IGLR-2's domain structure such as the Lingo's, Amigo's or Trk's have not been found to interact with cadherins or with frizzled receptors, though this could be due to a dearth of research on some of these proteins. For example, the *Drosophila* gene *CG16974*, which clusters with *iglr-2*, has not been studied (Dolan et al., 2007). Many eLRR proteins with a single IG domain have not been characterized in axon guidance.

Alternatively, since fasciculation between PVQL and PVPR was only disrupted in ~60% of crossovers, other fasciculation pathway(s) must exist (Steimel et al., 2010). Therefore, IGLR-2 could act in a parallel pathway to promote fasciculation. There is some evidence of eLRR proteins with a single IG domain acting in fasciculation. In *Drosophila*, Kekkon1 has been shown to promote fasciculation in central nervous system axon tracts, though how this occurs has not been elucidated (Speicher et al., 1998). Like IGLR-2, Kekkons have extracellular LRR domains with a single IG domain. Interestingly, Kekkons cluster with the Trk receptors which contain an extra IG domain as well as an intracellular tyrosine kinase domain, instead of with the Lingo and Amigo families which have a single IG domain and more closely resemble IGLR proteins domain structure (Mandai et al., 2009; Ulian-Benitez et al., 2017). As mentioned previously, all three Trk receptors have been implicated in axon guidance, in multiple different types of neurons (Cabelli et al., 1997; Gallo et al., 1997; Guo et al., 2011; Patel et al., 2000; T. D. Patel et al., 2003; Perez-Pinera et al., 2008). This demonstrates that

proteins with only extracellular LRRs and IG domains can operate in axon guidance and fasciculation. However, Trks have a divergent domain structure compared to IGLR genes, so this data doesn't provide strong evidence for IGLR proteins also functioning in these processes.

Unfortunately, there are only a limited number of studies on the *Lingo* and *Amigo* families, which more closely resemble *iglr* genes. Both Lingo-1 and Amigo-3 have been found to function as coreceptors in axon inhibition in the NGR1 axon guidance pathway, however they have not been well characterized outside of this pathways function in inhibiting axon regeneration or extension (Filbin, 2003; Mi et al., 2004). However, there have been several papers published on Amigo-1 which are relevant to my IGLR-2 data. Presence of the Amigo-1 ectodomain in solution causes defasciculation of axons from neurons grown *in vitro* (Kuja-Panula et al., 2003). A possible explanation could be that soluble Amigo-1 is binding the Amigo-1 in the axon's membrane, preventing it from dimerizing with another Amigo-1 in adjacent axons. Further research supports this, revealing that Amigo proteins can form homophilic bonds between their LRR domains (Kajander et al., 2011). Finally, knockdown of Amigo-1 was shown to cause defasciculation in the developing zebrafish brain (Zhao et al., 2014). Embryos injected with constructs expressing Amigo-1's ectodomain also had fasciculation defects, similar to the *in vitro* results. This provides further evidence that Amigo-1 homophilic binding is necessary for Amigo-1 induced fasciculation. Furthermore, Amigo-1 was found to be expressed in the growth cone, as well as along axon fascicles (Zhao et al., 2014). While these studies aren't on verified IGLR homologs, they do demonstrate that the LRR and single IG ectodomain structure can promote the fasciculation of axons through homophilic binding. Perhaps, like Amigo-1, IGLR-2 is also engaging in homophilic binding to fasciculate left VNC axons together, independent of other adhesion molecules. Double mutants between *fmi-1* and *iglr-2* could elucidate whether *iglr-2* functions in PVPR/PVQL axon guidance, and if so, whether it functions in *fmi-1*'s pathway or not.

### 4.2.3. Conclusion

I analysed the *Iron* and *iglr* gene families for axon guidance defects within the VNC. I discovered significant axon guidance defects with a pan-neuronal marker in four *Iron* mutants (*Iron-3, Iron-8*, *Iron-11*, and *Iron-14*) and in two *iglr* mutants (*iglr-1* and *iglr-*

*2*). In these mutant animals, the primary defect was axons crossing into the opposite VNC tract. The exception is *iglr*-2, which did not have crossover defects but instead had penetrant defasciculation defects in the left axon tract. Additionally, *lron-5*, and *lron-11* animals were found to have significant crossover defects in the pioneer PVPR axon. Overall, *lron-11* mutants had the highest penetrance of crossover defects in these markers. Further observation of *lron-11* animals found modest defects in command interneurons and potentially in the AVK interneurons, as well as highly penetrant defects in the DD/VD and DA/DB motor neurons.

My results reveal that *lron-11* functions in axon guidance in several types of neurons. However, it is not currently understood what role *lron-11* is playing in axon guidance. Based on *lron-11*'s structure and its mutants' crossover and commissure polarity defects, it seems to be acting cell autonomously, possibly as an adhesion and/or signaling transducing receptor, although some defects do not seem to be caused by lack of adhesion. Further expression and genetic interaction data will be required to validate that it functions cell autonomously as an axon guidance receptor, and to identify what axon guidance pathway(s) it participates in. My observations also suggest that *iglr-2* acts in axon guidance, possible by functioning in axon fasciculation. *iglr-2* should be further studied by analysing mutants in other neurons such as motor neurons and by crossing *iglr-2* with a mutant that has PVPR crossovers so that potential PVPR/PVQL defasciculation is observable. While *lron-5*, *lron-8*, *lron-14* and *iglr-1* mutants also displayed significant axon guidance defects, these will have to be outcrossed (except for *lron-8*, which was scored with the CRISPR-generated allele *gk5317*) and further characterized to verify and characterize their roll in axon guidance.

Uncovering new genes involved in axon guidance in *C. elegans* deepens our understanding of how this 'simple' nervous system is created. Being able to comprehend how such a comparatively simple neural network is built is a good first step to being able to understand our own brain's development. This work could have more direct implications for mammalian research as well, since many of the signaling pathways in the critical developmental process of axon guidance are conserved. In mammals, many eLRR genes have not been well characterized, partially due to the limitations of working with complex and expensive model organisms. Now, identification of the genes and signaling pathways that eLRR genes like *lron-11* interact with during axon guidance can be done in the high-throughput model organism *C. elegans*. This

could provide candidate genes for researchers searching for genes interacting with similar mammalian eLRR genes during axon guidance.  All life on earth is connected through their shared evolutionary past, and we can use this to our advantage.

# References


Abudureyimu, S., Asai, N., Enomoto, A., Weng, L., Kobayashi, H., Wang, X., Chen, C., Mii, S., Takahashi, M., 2018. Essential Role of Linx/Islr2 in the Development of the Forebrain Anterior Commissure. Sci Rep 8, 7292. https://doi.org/10.1038/s41598-018-24064-0

Ackley, B.D., Kang, S.H., Crew, J.R., Suh, C., Jin, Y., Kramer, J.M., 2003. The basement membrane components nidogen and type XVIII collagen regulate organization of neuromuscular junctions in Caenorhabditis elegans. J Neurosci 23, 3577–3587.

Ahmed, Z., Douglas, M.R., John, G., Berry, M., Logan, A., 2013. AMIGO3 is an NgR1/p75 co-receptor signalling axon growth inhibition in the acute phase of adult central nervous system injury. PLoS One 8, e61878. https://doi.org/10.1371/journal.pone.0061878

Anderson, K.V., Bokla, L., Nüsslein-Volhard, C., 1985. Establishment of dorsal-ventral polarity in the Drosophila embryo: the induction of polarity by the Toll gene product. Cell 42, 791–798. https://doi.org/10.1016/0092-8674(85)90275-2

Arvanitis, D., Davy, A., 2008. Eph/ephrin signaling: networks. Genes Dev 22, 416–429. https://doi.org/10.1101/gad.1630408

Au, V., Li-Leger, E., Raymant, G., Flibotte, S., Chen, G., Martin, K., Fernando, L., Doell, C., Rosell, F.I., Wang, S., Edgley, M.L., Rougvie, A.E., Hutter, H., Moerman, D.G., 2019. CRISPR/Cas9 Methodology for the Generation of Knockout Deletions in Caenorhabditis elegans. G3 Genes|Genomes|Genetics 9, 135–144. https://doi.org/10.1534/g3.118.200778

Baker, K.A., Moore, S.W., Jarjour, A.A., Kennedy, T.E., 2006. When a diffusible axon guidance cue stops diffusing: roles for netrins in adhesion and morphogenesis. Curr Opin Neurobiol 16, 529–534. https://doi.org/10.1016/j.conb.2006.08.002

Bando, T., Sekine, K., Kobayashi, S., Watabe, A.M., Rump, A., Tanaka, M., Suda, Y., Kato, S., Morikawa, Y., Manabe, T., Miyajima, A., 2005. Neuronal leucine-rich repeat protein 4 functions in hippocampus-dependent long-lasting memory. Mol Cell Biol 25, 4166–4175. https://doi.org/10.1128/MCB.25.10.4166-4175.2005

Bao, Z., Murray, J.I., 2011. Mounting Caenorhabditis elegans embryos for live imaging of embryogenesis. Cold Spring Harb Protoc 2011. https://doi.org/10.1101/pdb.prot065599

Barbacid, M., 1994. The Trk family of neurotrophin receptors. J Neurobiol 25, 1386–1403. https://doi.org/10.1002/neu.480251107

Battye, R., Stevens, A., Perry, R.L., Jacobs, J.R., 2001. Repellent signaling by Slit requires the leucine-rich repeats. J Neurosci 21, 4290–4298.

Bella, J., Hindle, K.L., McEwan, P.A., Lovell, S.C., 2008. The leucine-rich repeat structure. Cell Mol Life Sci 65, 2307–2333. https://doi.org/10.1007/s00018-008-8019-0

Bermingham, J.R., Shearin, H., Pennington, J., O'Moore, J., Jaegle, M., Driegen, S., van Zon, A., Darbas, A., Ozkaynak, E., Ryu, E.J., Milbrandt, J., Meijer, D., 2006. The claw paw mutation reveals a role for Lgi4 in peripheral nerve development. Nat Neurosci 9, 76–84. https://doi.org/10.1038/nn1598

Bhat, J.M., Hutter, H., 2016. Pioneer Axon Navigation Is Controlled by AEX-3, a Guanine Nucleotide Exchange Factor for RAB-3 in Caenorhabditis elegans. Genetics 203, 1235–1247. https://doi.org/10.1534/genetics.115.186064

Bhat, J.M., Pan, J., Hutter, H., 2015. PLR-1, a putative E3 ubiquitin ligase, controls cell polarity and axonal extensions in C. elegans. Dev Biol 398, 44–56. https://doi.org/10.1016/j.ydbio.2014.11.008

Bhouri, M., Morishita, W., Temkin, P., Goswami, D., Kawabe, H., Brose, N., Südhof, T.C., Craig, A.M., Siddiqui, T.J., Malenka, R., 2018. Deletion of LRRTM1 and LRRTM2 in adult mice impairs basal AMPA receptor transmission and LTP in hippocampal CA1 pyramidal neurons. Proc Natl Acad Sci U S A 115, E5382–E5389. https://doi.org/10.1073/pnas.1803280115

Blanchette, C.R., Perrat, P.N., Thackeray, A., Bénard, C.Y., 2015. Glypican Is a Modulator of Netrin-Mediated Axon Guidance. PLoS Biol 13, e1002183. https://doi.org/10.1371/journal.pbio.1002183

Blanchette, C.R., Thackeray, A., Perrat, P.N., Hekimi, S., Bénard, C.Y., 2017. Functional Requirements for Heparan Sulfate Biosynthesis in Morphogenesis and Nervous System Development in C. elegans. PLoS Genet 13, e1006525. https://doi.org/10.1371/journal.pgen.1006525

Blockus, H., Chédotal, A., 2016. Slit-Robo signaling. Development 143, 3037–3044. https://doi.org/10.1242/dev.132829

Böttcher, R.T., Pollet, N., Delius, H., Niehrs, C., 2004. The transmembrane protein XFLRT3 forms a complex with FGF receptors and promotes FGF signalling. Nat Cell Biol 6, 38–44. https://doi.org/10.1038/ncb1082

Boulin, T., Pocock, R., Hobert, O., 2006. A novel Eph receptor-interacting IgSF protein provides C. elegans motoneurons with midline guidepost function. Curr Biol 16, 1871–1883. https://doi.org/10.1016/j.cub.2006.08.056

Bourikas, D., Pekarik, V., Baeriswyl, T., Grunditz, A., Sadhu, R., Nardó, M., Stoeckli, E.T., 2005. Sonic hedgehog guides commissural axons along the longitudinal axis of the spinal cord. Nat Neurosci 8, 297–304. https://doi.org/10.1038/nn1396

Bouzigues, C., Morel, M., Triller, A., Dahan, M., 2007. Asymmetric redistribution of GABA receptors during GABA gradient sensing by nerve growth cones analyzed by single quantum dot imaging. Proc Natl Acad Sci U S A 104, 11251–11256. https://doi.org/10.1073/pnas.0702536104

Brenner, S., 1974. The genetics of Caenorhabditis elegans. Genetics 77, 71–94.

Broadbent, I.D., Pettitt, J., 2002. The C. elegans hmr-1 gene can encode a neuronal classic cadherin involved in the regulation of axon fasciculation. Curr Biol 12, 59–63. https://doi.org/10.1016/s0960-9822(01)00624-8

Brose, K., Bland, K.S., Wang, K.H., Arnott, D., Henzel, W., Goodman, C.S., Tessier-Lavigne, M., Kidd, T., 1999. Slit proteins bind Robo receptors and have an evolutionarily conserved role in repulsive axon guidance. Cell 96, 795–806. https://doi.org/10.1016/s0092-8674(00)80590-5

Bruce, F.M., Brown, S., Smith, J.N., Fuerst, P.G., Erskine, L., 2017. DSCAM promotes axon fasciculation and growth in the developing optic pathway. Proc Natl Acad Sci U S A 114, 1702–1707. https://doi.org/10.1073/pnas.1618606114

Bugyi, B., Carlier, M.-F., 2010. Control of actin filament treadmilling in cell motility. Annu Rev Biophys 39, 449–470. https://doi.org/10.1146/annurev-biophys-051309-103849

Bülow, H.E., Hobert, O., 2004. Differential sulfations and epimerization define heparan sulfate specificity in nervous system development. Neuron 41, 723–736. https://doi.org/10.1016/s0896-6273(04)00084-4

Bülow, H.E., Tjoe, N., Townley, R.A., Didiano, D., van Kuppevelt, T.H., Hobert, O., 2008. Extracellular sugar modifications provide instructive and cell-specific information for axon-guidance choices. Curr Biol 18, 1978–1985. https://doi.org/10.1016/j.cub.2008.11.023

Cabelli, R.J., Shelton, D.L., Segal, R.A., Shatz, C.J., 1997. Blockade of endogenous ligands of trkB inhibits formation of ocular dominance columns. Neuron 19, 63–76. https://doi.org/10.1016/s0896-6273(00)80348-7

Cammarata, G.M., Bearce, E.A., Lowery, L.A., 2016. Cytoskeletal social networking in the growth cone: How +TIPs mediate microtubule-actin cross-linking to drive axon outgrowth and guidance. Cytoskeleton (Hoboken) 73, 461–476. https://doi.org/10.1002/cm.21272

Cang, J., Feldheim, D.A., 2013. Developmental mechanisms of topographic map formation and alignment. Annu Rev Neurosci 36, 51–77. https://doi.org/10.1146/annurev-neuro-062012-170341

Chan, C.E., Odde, D.J., 2008. Traction dynamics of filopodia on compliant substrates. Science 322, 1687–1691. https://doi.org/10.1126/science.1163595

Chen, W.-S., Antic, D., Matis, M., Logan, C.Y., Povelones, M., Anderson, G.A., Nusse, R., Axelrod, J.D., 2008. Asymmetric homotypic interactions of the atypical cadherin flamingo mediate intercellular polarity signaling. Cell 133, 1093–1105. https://doi.org/10.1016/j.cell.2008.04.048

Chen, Y., Aulia, S., Li, L., Tang, B.L., 2006. AMIGO and friends: an emerging family of brain-enriched, neuronal growth modulating, type I transmembrane proteins with leucine-rich repeats (LRR) and cell adhesion molecule motifs. Brain Res Rev 51, 265–274. https://doi.org/10.1016/j.brainresrev.2005.11.005

Chen, Z., Gore, B.B., Long, H., Ma, L., Tessier-Lavigne, M., 2008. Alternative splicing of the Robo3 axon guidance receptor governs the midline switch from attraction to repulsion. Neuron 58, 325–332. https://doi.org/10.1016/j.neuron.2008.02.016

Chilton, J.K., 2006. Molecular mechanisms of axon guidance. Dev Biol 292, 13–24. https://doi.org/10.1016/j.ydbio.2005.12.048

Chin-Sang, I.D., George, S.E., Ding, M., Moseley, S.L., Lynch, A.S., Chisholm, A.D., 1999. The ephrin VAB-2/EFN-1 functions in neuronal signaling to regulate epidermal morphogenesis in C. elegans. Cell 99, 781–790. https://doi.org/10.1016/s0092-8674(00)81675-x

Chin-Sang, I.D., Moseley, S.L., Ding, M., Harrington, R.J., George, S.E., Chisholm, A.D., 2002. The divergent C. elegans ephrin EFN-4 functions inembryonic morphogenesis in a pathway independent of the VAB-1 Eph receptor. Development 129, 5499–5510. https://doi.org/10.1242/dev.00122

Chisholm, A.D., Hutter, H., Jin, Y., Wadsworth, W.G., 2016. The Genetics of Axon Guidance and Axon Regeneration in Caenorhabditis elegans. Genetics 204, 849–882. https://doi.org/10.1534/genetics.115.186262

Clevers, H., 2006. Wnt/beta-catenin signaling in development and disease. Cell 127, 469–480. https://doi.org/10.1016/j.cell.2006.10.018

Cox, E.A., Tuskey, C., Hardin, J., 2004. Cell adhesion receptors in C. elegans. J Cell Sci 117, 1867–1870. https://doi.org/10.1242/jcs.01177

de Wit, J., Ghosh, A., 2014. Control of neural circuit formation by leucine-rich repeat proteins. Trends Neurosci 37, 539–550. https://doi.org/10.1016/j.tins.2014.07.004

de Wit, J., Hong, W., Luo, L., Ghosh, A., 2011. Role of leucine-rich repeat proteins in the development and function of neural circuits. Annu Rev Cell Dev Biol 27, 697–729. https://doi.org/10.1146/annurev-cellbio-092910-154111

de Wit, J., O'Sullivan, M.L., Savas, J.N., Condomitti, G., Caccese, M.C., Vennekens, K.M., Yates, J.R., Ghosh, A., 2013. Unbiased discovery of glypican as a receptor for LRRTM4 in regulating excitatory synapse development. Neuron 79, 696–711. https://doi.org/10.1016/j.neuron.2013.06.049

de Wit, J., Sylwestrak, E., O'Sullivan, M.L., Otto, S., Tiglio, K., Savas, J.N., Yates, J.R., Comoletti, D., Taylor, P., Ghosh, A., 2009. LRRTM2 interacts with Neurexin1 and regulates excitatory synapse formation. Neuron 64, 799–806. https://doi.org/10.1016/j.neuron.2009.12.019

Devkota, R., Henricsson, M., Borén, J., Pilon, M., 2021. The C. elegans PAQR-2 and IGLR-2 membrane homeostasis proteins are uniquely essential for tolerating dietary saturated fats. Biochim Biophys Acta Mol Cell Biol Lipids 1866, 158883. https://doi.org/10.1016/j.bbalip.2021.158883

Dickson, B.J., 2002. Molecular mechanisms of axon guidance. Science 298, 1959–1964. https://doi.org/10.1126/science.1072165

Dickson, B.J., Gilestro, G.F., 2006. Regulation of commissural axon pathfinding by slit and its Robo receptors. Annu Rev Cell Dev Biol 22, 651–675. https://doi.org/10.1146/annurev.cellbio.21.090704.151234

Dolan, J., Walshe, K., Alsbury, S., Hokamp, K., O'Keeffe, S., Okafuji, T., Miller, S.F.C., Tear, G., Mitchell, K.J., 2007. The extracellular leucine-rich repeat superfamily; a comparative survey and analysis of evolutionary relationships and expression patterns. BMC Genomics 8, 320. https://doi.org/10.1186/1471-2164-8-320

Dominici, C., Moreno-Bravo, J.A., Puiggros, S.R., Rappeneau, Q., Rama, N., Vieugue, P., Bernet, A., Mehlen, P., Chédotal, A., 2017. Floor-plate-derived netrin-1 is dispensable for commissural axon guidance. Nature 545, 350–354. https://doi.org/10.1038/nature22331

Dong, B., Moseley-Alldredge, M., Schwieterman, A.A., Donelson, C.J., McMurry, J.L., Hudson, M.L., Chen, L., 2016. EFN-4 functions in LAD-2-mediated axon guidance in Caenorhabditis elegans. Development 143, 1182–1191. https://doi.org/10.1242/dev.128934

Dong, X., Chiu, H., Park, Y.J., Zou, W., Zou, Y., Özkan, E., Chang, C., Shen, K., 2016. Precise regulation of the guidance receptor DMA-1 by KPC-1/Furin instructs dendritic branching decisions. Elife 5. https://doi.org/10.7554/eLife.11008

Dong, X., Liu, O.W., Howell, A.S., Shen, K., 2013. An extracellular adhesion molecule complex patterns dendritic branching and morphogenesis. Cell 155, 296–307. https://doi.org/10.1016/j.cell.2013.08.059

Durbin, R.M., 1987. Studies on the development and organisation of the nervous system of Caenorhabditis elegans (Ph.D.). University of Cambridge.

Fan, L., Kovacevic, I., Heiman, M.G., Bao, Z., 2019. A multicellular rosette-mediated collective dendrite extension. Elife 8. https://doi.org/10.7554/eLife.38065

Filbin, M.T., 2003. Myelin-associated inhibitors of axonal regeneration in the adult mammalian CNS. Nat Rev Neurosci 4, 703–713. https://doi.org/10.1038/nrn1195

Fournier, A.E., GrandPre, T., Strittmatter, S.M., 2001. Identification of a receptor mediating Nogo-66 inhibition of axonal regeneration. Nature 409, 341–346. https://doi.org/10.1038/35053072

Gallo, G., Lefcort, F.B., Letourneau, P.C., 1997. The trkA receptor mediates growth cone turning toward a localized source of nerve growth factor. J Neurosci 17, 5445–5454.

Garriga, G., Desai, C., Horvitz, H.R., 1993. Cell interactions control the direction of outgrowth, branching and fasciculation of the HSN axons of Caenorhabditis elegans. Development 117, 1071–1087.

George, S.E., Simokat, K., Hardin, J., Chisholm, A.D., 1998. The VAB-1 Eph receptor tyrosine kinase functions in neural and epithelial morphogenesis in C. elegans. Cell 92, 633–643. https://doi.org/10.1016/s0092-8674(00)81131-9

Ghiglione, C., Carraway, K.L., Amundadottir, L.T., Boswell, R.E., Perrimon, N., Duffy, J.B., 1999. The transmembrane molecule kekkon 1 acts in a feedback loop to negatively regulate the activity of the Drosophila EGF receptor during oogenesis. Cell 96, 847–856. https://doi.org/10.1016/s0092-8674(00)80594-2

Gilsohn, E., Volk, T., 2010. Fine tuning cellular recognition: The function of the leucine rich repeat (LRR) trans-membrane protein, LRT, in muscle targeting to tendon cells. Cell Adh Migr 4, 368–371. https://doi.org/10.4161/cam.4.3.11606

Gonzalez, A., Moya-Alvarado, G., Gonzalez-Billaut, C., Bronfman, F.C., 2016. Cellular and molecular mechanisms regulating neuronal growth by brain-derived neurotrophic factor. Cytoskeleton (Hoboken) 73, 612–628. https://doi.org/10.1002/cm.21312

Grigoryan, T., Wend, P., Klaus, A., Birchmeier, W., 2008. Deciphering the function of canonical Wnt signals in development and disease: conditional loss- and gain-of-function mutations of beta-catenin in mice. Genes Dev 22, 2308–2341. https://doi.org/10.1101/gad.1686208

Grossman, E.N., Giurumescu, C.A., Chisholm, A.D., 2013. Mechanisms of ephrin receptor protein kinase-independent signaling in amphid axon guidance in Caenorhabditis elegans. Genetics 195, 899–913. https://doi.org/10.1534/genetics.113.154393

Gumbiner, B.M., 1996. Cell adhesion: the molecular basis of tissue architecture and morphogenesis. Cell 84, 345–357. https://doi.org/10.1016/s0092-8674(00)81279-9

Guo, T., Mandai, K., Condie, B.G., Wickramasinghe, S.R., Capecchi, M.R., Ginty, D.D., 2011. An evolving NGF-Hoxd1 signaling pathway mediates development of divergent neural circuits in vertebrates. Nat Neurosci 14, 31–36. https://doi.org/10.1038/nn.2710

Gysi, S., Rhiner, C., Flibotte, S., Moerman, D.G., Hengartner, M.O., 2013. A network of HSPG core proteins and HS modifying enzymes regulates netrin-dependent guidance of D-type motor neurons in Caenorhabditis elegans. PLoS One 8, e74908. https://doi.org/10.1371/journal.pone.0074908

Hall, D.H., Russell, R.L., 1991. The posterior nervous system of the nematode Caenorhabditis elegans: serial reconstruction of identified neurons and complete pattern of synaptic interactions. J Neurosci 11, 1–22.

Hao, J.C., Yu, T.W., Fujisawa, K., Culotti, J.G., Gengyo-Ando, K., Mitani, S., Moulder, G., Barstead, R., Tessier-Lavigne, M., Bargmann, C.I., 2001. C. elegans slit acts in midline, dorsal-ventral, and anterior-posterior guidance via the SAX-3/Robo receptor. Neuron 32, 25–38. https://doi.org/10.1016/s0896-6273(01)00448-2

Harris, R., Sabatelli, L.M., Seeger, M.A., 1996. Guidance cues at the Drosophila CNS midline: identification and characterization of two Drosophila Netrin/UNC-6 homologs. Neuron 17, 217–228. https://doi.org/10.1016/s0896-6273(00)80154-3

Hedgecock, E.M., Culotti, J.G., Hall, D.H., 1990. The unc-5, unc-6, and unc-40 genes guide circumferential migrations of pioneer axons and mesodermal cells on the epidermis in C. elegans. Neuron 4, 61–85. https://doi.org/10.1016/0896-6273(90)90444-k

Heidemann, S.R., Lamoureux, P., Buxbaum, R.E., 1990. Growth cone behavior and production of traction force. J Cell Biol 111, 1949–1957. https://doi.org/10.1083/jcb.111.5.1949

Herculano-Houzel, S., 2009. The human brain in numbers: a linearly scaled-up primate brain. Front Hum Neurosci 3, 31. https://doi.org/10.3389/neuro.09.031.2009

Hilgetag, C.C., Barbas, H., 2009. Are there ten times more glia than neurons in the brain? Brain Struct Funct 213, 365–366. https://doi.org/10.1007/s00429-009-0202-z

Hill, E., Broadbent, I.D., Chothia, C., Pettitt, J., 2001. Cadherin superfamily proteins in Caenorhabditis elegans and Drosophila melanogaster. J Mol Biol 305, 1011–1024. https://doi.org/10.1006/jmbi.2000.4361

Hilliard, M.A., Bargmann, C.I., 2006. Wnt signals and frizzled activity orient anterior-posterior axon outgrowth in C. elegans. Dev Cell 10, 379–390. https://doi.org/10.1016/j.devcel.2006.01.013

Hindges, R., McLaughlin, T., Genoud, N., Henkemeyer, M., O'Leary, D.D.M., 2002. EphB forward signaling controls directional branch extension and arborization required for dorsal-ventral retinotopic mapping. Neuron 35, 475–487. https://doi.org/10.1016/s0896-6273(02)00799-7

Holland, S.J., Gale, N.W., Mbamalu, G., Yancopoulos, G.D., Henkemeyer, M., Pawson, T., 1996. Bidirectional signalling through the EPH-family receptor Nuk and its transmembrane ligands. Nature 383, 722–725. https://doi.org/10.1038/383722a0

Homma, S., Shimada, T., Hikake, T., Yaginuma, H., 2009. Expression pattern of LRR and Ig domain-containing protein (LRRIG protein) in the early mouse embryo. Gene Expr Patterns 9, 1–26. https://doi.org/10.1016/j.gep.2008.09.004

Hong, K., Hinck, L., Nishiyama, M., Poo, M.M., Tessier-Lavigne, M., Stein, E., 1999. A ligand-gated association between cytoplasmic domains of UNC5 and DCC family receptors converts netrin-induced growth cone attraction to repulsion. Cell 97, 927–941. https://doi.org/10.1016/s0092-8674(00)80804-1

Hong, W., Zhu, H., Potter, C.J., Barsh, G., Kurusu, M., Zinn, K., Luo, L., 2009. Leucine-rich repeat transmembrane proteins instruct discrete dendrite targeting in an olfactory map. Nat Neurosci 12, 1542–1550. https://doi.org/10.1038/nn.2442

Horstkorte, R., Fuss, B., 2012. Chapter 9 - Cell Adhesion Molecules, in: Brady, S.T., Siegel, G.J., Albers, R.W., Price, D.L. (Eds.), Basic Neurochemistry (Eighth Edition). Academic Press, New York, pp. 165–179. https://doi.org/10.1016/B978-0-12-374947-5.00009-2

Huang, E.J., Reichardt, L.F., 2001. Neurotrophins: Roles in Neuronal Development and Function. Annu Rev Neurosci 24, 677–736. https://doi.org/10.1146/annurev.neuro.24.1.677

Hutter, H., 2006. Fluorescent reporter methods. Methods Mol Biol 351, 155–173. https://doi.org/10.1385/1-59745-151-7:155

Hutter, H., 2003. Extracellular cues and pioneers act together to guide axons in the ventral cord of C. elegans. Development 130, 5307–5318. https://doi.org/10.1242/dev.00727

Hutter, H., Vogel, B.E., Plenefisch, J.D., Norris, C.R., Proenca, R.B., Spieth, J., Guo, C., Mastwal, S., Zhu, X., Scheel, J., Hedgecock, E.M., 2000. Conservation and novelty in the evolution of cell adhesion and extracellular matrix genes. Science 287, 989–994. https://doi.org/10.1126/science.287.5455.989

Inatani, M., Irie, F., Plump, A.S., Tessier-Lavigne, M., Yamaguchi, Y., 2003. Mammalian brain morphogenesis and midline axon guidance require heparan sulfate. Science 302, 1044–1046. https://doi.org/10.1126/science.1090497

Ishii, N., Wadsworth, W.G., Stern, B.D., Culotti, J.G., Hedgecock, E.M., 1992. UNC-6, a laminin-related protein, guides cell and pioneer axon migrations in C. elegans. Neuron 9, 873–881. https://doi.org/10.1016/0896-6273(92)90240-e

Johnson, K.G., Ghose, A., Epstein, E., Lincecum, J., O'Connor, M.B., Van Vactor, D., 2004. Axonal heparan sulfate proteoglycans regulate the distribution and efficiency of the repellent slit during midline axon guidance. Curr Biol 14, 499–504. https://doi.org/10.1016/j.cub.2004.02.005

Kajander, T., Kuja-Panula, J., Rauvala, H., Goldman, A., 2011. Crystal Structure and Role of Glycans and Dimerization in Folding of Neuronal Leucine-Rich Repeat Protein AMIGO-1. Journal of Molecular Biology 413, 1001–1015. https://doi.org/10.1016/j.jmb.2011.09.032

Karaulanov, E., Böttcher, R.T., Stannek, P., Wu, W., Rau, M., Ogata, S., Cho, K.W.Y., Niehrs, C., 2009. Unc5B interacts with FLRT3 and Rnd1 to modulate cell adhesion in Xenopus embryos. PLoS One 4, e5742. https://doi.org/10.1371/journal.pone.0005742

Katidou, M., Tavernarakis, N., Karagogeos, D., 2013. The contactin RIG-6 mediates neuronal and non-neuronal cell migration in Caenorhabditis elegans. Dev Biol 373, 184–195. https://doi.org/10.1016/j.ydbio.2012.10.027

Keleman, K., Ribeiro, C., Dickson, B.J., 2005. Comm function in commissural axon guidance: cell-autonomous sorting of Robo in vivo. Nat Neurosci 8, 156–163. https://doi.org/10.1038/nn1388

Kennedy, T.E., Serafini, T., de la Torre, J.R., Tessier-Lavigne, M., 1994. Netrins are diffusible chemotropic factors for commissural axons in the embryonic spinal cord. Cell 78, 425–435. https://doi.org/10.1016/0092-8674(94)90421-9

Kennerdell, J.R., Fetter, R.D., Bargmann, C.I., 2009. Wnt-Ror signaling to SIA and SIB neurons directs anterior axon guidance and nerve ring placement in C. elegans. Development 136, 3801–3810. https://doi.org/10.1242/dev.038109

Kidd, T., Bland, K.S., Goodman, C.S., 1999. Slit is the midline repellent for the robo receptor in Drosophila. Cell 96, 785–794. https://doi.org/10.1016/s0092-8674(00)80589-9

Kim, S., Burette, A., Chung, H.S., Kwon, S.-K., Woo, J., Lee, H.W., Kim, K., Kim, H., Weinberg, R.J., Kim, E., 2006. NGL family PSD-95-interacting adhesion molecules regulate excitatory synapse formation. Nat Neurosci 9, 1294–1301. https://doi.org/10.1038/nn1763

Kim, S., Wadsworth, W.G., 2000. Positioning of longitudinal nerves in C. elegans by nidogen. Science 288, 150–154. https://doi.org/10.1126/science.288.5463.150

Ko, J., Fuccillo, M.V., Malenka, R.C., Südhof, T.C., 2009. LRRTM2 functions as a neurexin ligand in promoting excitatory synapse formation. Neuron 64, 791–798. https://doi.org/10.1016/j.neuron.2009.12.012

Ko, J., Kim, S., Chung, H.S., Kim, K., Han, K., Kim, H., Jun, H., Kaang, B.-K., Kim, E., 2006. SALM synaptic cell adhesion-like molecules regulate the differentiation of excitatory synapses. Neuron 50, 233–245. https://doi.org/10.1016/j.neuron.2006.04.005

Kobe, B., Deisenhofer, J., 1994. The leucine-rich repeat: a versatile binding motif. Trends Biochem Sci 19, 415–421. https://doi.org/10.1016/0968-0004(94)90090-6

Kobe, B., Kajava, A.V., 2001. The leucine-rich repeat as a protein recognition motif. Curr Opin Struct Biol 11, 725–732. https://doi.org/10.1016/s0959-440x(01)00266-4

Koh, C.-G., 2006. Rho GTPases and their regulators in neuronal functions and development. Neurosignals 15, 228–237. https://doi.org/10.1159/000101527

Kohsaka, H., Nose, A., 2009. Target recognition at the tips of postsynaptic filopodia: accumulation and function of Capricious. Development 136, 1127–1135. https://doi.org/10.1242/dev.027920

Kuja-Panula, J., Kiiltomäki, M., Yamashiro, T., Rouhiainen, A., Rauvala, H., 2003. AMIGO, a transmembrane protein implicated in axon tract development, defines a novel protein family with leucine-rich repeats. Journal of Cell Biology 160, 963–973. https://doi.org/10.1083/jcb.200209074

Kuo, C.-J., Hsu, Y.-C., Wang, S.-T., Liou, B.-Y., Lim, S.B.-Y., Chen, Y.-W., Chen, C.-S., 2020. IGLR-2, a Leucine-Rich Repeat Domain Containing Protein, Is Required for the Host Defense in Caenorhabditis elegans. Front Immunol 11, 561337. https://doi.org/10.3389/fimmu.2020.561337

Kuwajima, T., Yoshida, Y., Takegahara, N., Petros, T.J., Kumanogoh, A., Jessell, T.M., Sakurai, T., Mason, C., 2012. Optic chiasm presentation of Semaphorin6D in the context of Plexin-A1 and Nr-CAM promotes retinal axon midline crossing. Neuron 74, 676–690. https://doi.org/10.1016/j.neuron.2012.03.025

Lázaro-Peña, M.I., Díaz-Balzac, C.A., Bülow, H.E., Emmons, S.W., 2018. Synaptogenesis Is Modulated by Heparan Sulfate in Caenorhabditis elegans. Genetics 209, 195–208. https://doi.org/10.1534/genetics.118.300837

Lee, A.C., Suter, D.M., 2008. Quantitative analysis of microtubule dynamics during adhesion-mediated growth cone guidance. Dev Neurobiol 68, 1363–1377. https://doi.org/10.1002/dneu.20662

Lee, J.-S., von der Hardt, S., Rusch, M.A., Stringer, S.E., Stickney, H.L., Talbot, W.S., Geisler, R., Nüsslein-Volhard, C., Selleck, S.B., Chien, C.-B., Roehl, H., 2004. Axon sorting in the optic tract requires HSPG synthesis by ext2 (dackel) and extl3 (boxer). Neuron 44, 947–960. https://doi.org/10.1016/j.neuron.2004.11.029

Lemke, G., Reber, M., 2005. Retinotectal mapping: new insights from molecular genetics. Annu Rev Cell Dev Biol 21, 551–580. https://doi.org/10.1146/annurev.cellbio.20.022403.093702

Levy-Strumpf, N., Culotti, J.G., 2014. Netrins and Wnts function redundantly to regulate antero-posterior and dorso-ventral guidance in C. elegans. PLoS Genet 10, e1004381. https://doi.org/10.1371/journal.pgen.1004381

Leyva-Díaz, E., del Toro, D., Menal, M.J., Cambray, S., Susín, R., Tessier-Lavigne, M., Klein, R., Egea, J., López-Bendito, G., 2014. FLRT3 is a Robo1-interacting protein that determines Netrin-1 attraction in developing axons. Curr Biol 24, 494–508. https://doi.org/10.1016/j.cub.2014.01.042

Li, R., Fang, J., Huo, B., Su, Y.-S., Wang, J., Liu, L.-G., Hu, M., Cheng, C., Zheng, P., Zhu, X.-H., Jiang, D.-S., Wei, X., 2017. Leucine-rich repeat neuronal protein 4 (LRRN4) potentially functions in dilated cardiomyopathy. Int J Clin Exp Pathol 10, 9925–9933.

Limerick, G., Tang, X., Lee, W.S., Mohamed, A., Al-Aamiri, A., Wadsworth, W.G., 2018. A Statistically-Oriented Asymmetric Localization (SOAL) Model for Neuronal Outgrowth Patterning by Caenorhabditis elegans UNC-5 (UNC5) and UNC-40 (DCC) Netrin Receptors. Genetics 208, 245–272. https://doi.org/10.1534/genetics.117.300460

Lin, J.C., Ho, W.-H., Gurney, A., Rosenthal, A., 2003. The netrin-G1 ligand NGL-1 promotes the outgrowth of thalamocortical axons. Nat Neurosci 6, 1270–1276. https://doi.org/10.1038/nn1148

Linhoff, M.W., Laurén, J., Cassidy, R.M., Dobie, F.A., Takahashi, H., Nygaard, H.B., Airaksinen, M.S., Strittmatter, S.M., Craig, A.M., 2009. An unbiased expression screen for synaptogenic proteins identifies the LRRTM protein family as synaptic organizers. Neuron 61, 734–749. https://doi.org/10.1016/j.neuron.2009.01.017

Liu, O.W., Shen, K., 2011. The transmembrane LRR protein DMA-1 promotes dendrite branching and growth in C. elegans. Nat Neurosci 15, 57–63. https://doi.org/10.1038/nn.2978

Long, H., Sabatier, C., Ma, L., Plump, A., Yuan, W., Ornitz, D.M., Tamada, A., Murakami, F., Goodman, C.S., Tessier-Lavigne, M., 2004. Conserved roles for Slit and Robo proteins in midline commissural axon guidance. Neuron 42, 213–223. https://doi.org/10.1016/s0896-6273(04)00179-5

Lowery, L.A., Van Vactor, D., 2009. The trip of the tip: understanding the growth cone machinery. Nat Rev Mol Cell Biol 10, 332–343. https://doi.org/10.1038/nrm2679

Lyuksyutova, A.I., Lu, C.-C., Milanesio, N., King, L.A., Guo, N., Wang, Y., Nathans, J., Tessier-Lavigne, M., Zou, Y., 2003. Anterior-posterior guidance of commissural axons by Wnt-frizzled signaling. Science 302, 1984–1988. https://doi.org/10.1126/science.1089610

Ma, Y., Li, J., Chiu, I., Wang, Y., Sloane, J.A., Lü, J., Kosaras, B., Sidman, R.L., Volpe, J.J., Vartanian, T., 2006. Toll-like receptor 8 functions as a negative regulator of neurite outgrowth and inducer of neuronal apoptosis. J Cell Biol 175, 209–215. https://doi.org/10.1083/jcb.200606016

MacNeil, L.T., Hardy, W.R., Pawson, T., Wrana, J.L., Culotti, J.G., 2009. UNC-129 regulates the balance between UNC-40 dependent and independent UNC-5 signaling pathways. Nat Neurosci 12, 150–155. https://doi.org/10.1038/nn.2256

Mandai, K., Guo, T., St Hillaire, C., Meabon, J.S., Kanning, K.C., Bothwell, M., Ginty, D.D., 2009. LIG family receptor tyrosine kinase-associated proteins modulate growth factor signals during neural development. Neuron 63, 614–627. https://doi.org/10.1016/j.neuron.2009.07.031

Mandai, K., Reimert, D.V., Ginty, D.D., 2014. Linx mediates interaxonal interactions and formation of the internal capsule. Neuron 83, 93–103. https://doi.org/10.1016/j.neuron.2014.05.020

Marler, K.J.M., Becker-Barroso, E., Martínez, A., Llovera, M., Wentzel, C., Poopalasundaram, S., Hindges, R., Soriano, E., Comella, J., Drescher, U., 2008. A TrkB/EphrinA interaction controls retinal axon branching and synaptogenesis. J Neurosci 28, 12700–12712. https://doi.org/10.1523/JNEUROSCI.1915-08.2008

Maro, G.S., Klassen, M.P., Shen, K., 2009. A beta-catenin-dependent Wnt pathway mediates anteroposterior axon guidance in C. elegans motor neurons. PLoS One 4, e4690. https://doi.org/10.1371/journal.pone.0004690

Matsumoto, Y., Irie, F., Inatani, M., Tessier-Lavigne, M., Yamaguchi, Y., 2007. Netrin-1/DCC signaling in commissural axon guidance requires cell-autonomous expression of heparan sulfate. J Neurosci 27, 4342–4350. https://doi.org/10.1523/JNEUROSCI.0700-07.2007

Mi, S., Lee, X., Shao, Z., Thill, G., Ji, B., Relton, J., Levesque, M., Allaire, N., Perrin, S., Sands, B., Crowell, T., Cate, R.L., McCoy, J.M., Pepinsky, R.B., 2004. LINGO-1 is a component of the Nogo-66 receptor/p75 signaling complex. Nat Neurosci 7, 221–228. https://doi.org/10.1038/nn1188

Mi, S., Miller, R.H., Lee, X., Scott, M.L., Shulag-Morskaya, S., Shao, Z., Chang, J., Thill, G., Levesque, M., Zhang, M., Hession, C., Sah, D., Trapp, B., He, Z., Jung, V., McCoy, J.M., Pepinsky, R.B., 2005. LINGO-1 negatively regulates myelination by oligodendrocytes. Nat Neurosci 8, 745–751. https://doi.org/10.1038/nn1460

Moffat, L.L., Robinson, R.E., Bakoulis, A., Clark, S.G., 2014. The conserved transmembrane RING finger protein PLR-1 downregulates Wnt signaling by reducing Frizzled, Ror and Ryk cell-surface levels in C. elegans. Development 141, 617–628. https://doi.org/10.1242/dev.101600

Mohamed, A.M., Chin-Sang, I.D., 2006. Characterization of loss-of-function and gain-of-function Eph receptor tyrosine kinase signaling in C. elegans axon targeting and cell migration. Dev Biol 290, 164–176. https://doi.org/10.1016/j.ydbio.2005.11.019

Najarro, E.H., Wong, L., Zhen, M., Carpio, E.P., Goncharov, A., Garriga, G., Lundquist, E.A., Jin, Y., Ackley, B.D., 2012. Caenorhabditis elegans flamingo cadherin fmi-1 regulates GABAergic neuronal development. J Neurosci 32, 4196–4211. https://doi.org/10.1523/JNEUROSCI.3094-11.2012

Nam, J., Mah, W., Kim, E., 2011. The SALM/Lrfn family of leucine-rich repeat-containing cell adhesion molecules. Seminars in Cell & Developmental Biology, Prions and Amyloids & Synapse and Brain 22, 492–498. https://doi.org/10.1016/j.semcdb.2011.06.005

Nürnberger, T., Brunner, F., Kemmerling, B., Piater, L., 2004. Innate immunity in plants and animals: striking similarities and obvious differences. Immunol Rev 198, 249–266. https://doi.org/10.1111/j.0105-2896.2004.0119.x

O'Donnell, M., Chance, R.K., Bashaw, G.J., 2009. Axon growth and guidance: receptor regulation and signal transduction. Annu Rev Neurosci 32, 383–412. https://doi.org/10.1146/annurev.neuro.051508.135614

Oinuma, I., Katoh, H., Negishi, M., 2004. Molecular dissection of the semaphorin 4D receptor plexin-B1-stimulated R-Ras GTPase-activating protein activity and neurite remodeling in hippocampal neurons. J Neurosci 24, 11473–11480. https://doi.org/10.1523/JNEUROSCI.3257-04.2004

Okabe, S., Hirokawa, N., 1991. Actin dynamics in growth cones. J Neurosci 11, 1918–1929.

Packer, J.S., Zhu, Q., Huynh, C., Sivaramakrishnan, P., Preston, E., Dueck, H., Stefanik, D., Tan, K., Trapnell, C., Kim, J., Waterston, R.H., Murray, J.I., 2019. A lineage-resolved molecular atlas of C. elegans embryogenesis at single-cell resolution. Science 365. https://doi.org/10.1126/science.aax1971

Pakkenberg, B., Pelvig, D., Marner, L., Bundgaard, M.J., Gundersen, H.J.G., Nyengaard, J.R., Regeur, L., 2003. Aging and the human neocortex. Exp Gerontol 38, 95–99. https://doi.org/10.1016/s0531-5565(02)00151-1

Pan, C.-L., Howell, J.E., Clark, S.G., Hilliard, M., Cordes, S., Bargmann, C.I., Garriga, G., 2006. Multiple Wnts and frizzled receptors regulate anteriorly directed cell and growth cone migrations in Caenorhabditis elegans. Dev Cell 10, 367–377. https://doi.org/10.1016/j.devcel.2006.02.010

Panza, P., Sitko, A.A., Maischein, H.-M., Koch, I., Flötenmeyer, M., Wright, G.J., Mandai, K., Mason, C.A., Söllner, C., 2015. The LRR receptor Islr2 is required for retinal axon routing at the vertebrate optic chiasm. Neural Dev 10, 23. https://doi.org/10.1186/s13064-015-0050-x

Patel, S.D., Chen, C.P., Bahna, F., Honig, B., Shapiro, L., 2003. Cadherin-mediated cell-cell adhesion: sticking together as a family. Curr Opin Struct Biol 13, 690–698. https://doi.org/10.1016/j.sbi.2003.10.007

Patel, T.D., Jackman, A., Rice, F.L., Kucera, J., Snider, W.D., 2000. Development of sensory neurons in the absence of NGF/TrkA signaling in vivo. Neuron 25, 345–357. https://doi.org/10.1016/s0896-6273(00)80899-5

Patel, T.D., Kramer, I., Kucera, J., Niederkofler, V., Jessell, T.M., Arber, S., Snider, W.D., 2003. Peripheral NT3 signaling is required for ETS protein expression and central patterning of proprioceptive sensory afferents. Neuron 38, 403–416. https://doi.org/10.1016/s0896-6273(03)00261-7

Peltola, M.A., Kuja-Panula, J., Lauri, S.E., Taira, T., Rauvala, H., 2011. AMIGO is an auxiliary subunit of the Kv2.1 potassium channel. EMBO Rep 12, 1293–1299. https://doi.org/10.1038/embor.2011.204

Perez-Pinera, P., García-Suarez, O., Germanà, A., Díaz-Esnal, B., de Carlos, F., Silos-Santiago, I., del Valle, M.E., Cobo, J., Vega, J.A., 2008. Characterization of sensory deficits in TrkB knockout mice. Neurosci Lett 433, 43–47. https://doi.org/10.1016/j.neulet.2007.12.035

Petrinovic, M.M., Duncan, C.S., Bourikas, D., Weinman, O., Montani, L., Schroeter, A., Maerki, D., Sommer, L., Stoeckli, E.T., Schwab, M.E., 2010. Neuronal Nogo-A regulates neurite fasciculation, branching and extension in the developing nervous system. Development 137, 2539–2550. https://doi.org/10.1242/dev.048371

Pettitt, J., 2005. The cadherin superfamily. WormBook 1–9. https://doi.org/10.1895/wormbook.1.50.1

Pocock, R., Hobert, O., 2008. Oxygen levels affect axon guidance and neuronal migration in Caenorhabditis elegans. Nat Neurosci 11, 894–900. https://doi.org/10.1038/nn.2152

Poliak, S., Morales, D., Croteau, L.-P., Krawchuk, D., Palmesino, E., Morton, S., Cloutier, J.-F., Charron, F., Dalva, M.B., Ackerman, S.L., Kao, T.-J., Kania, A., 2015. Synergistic integration of Netrin and ephrin axon guidance signals by spinal motor neurons. Elife 4. https://doi.org/10.7554/eLife.10841

Prasad, B.C., Clark, S.G., 2006. Wnt signaling establishes anteroposterior neuronal polarity and requires retromer in C. elegans. Development 133, 1757–1766. https://doi.org/10.1242/dev.02357

Rafidi, H., Mercado, F., Astudillo, M., Fry, W.H.D., Saldana, M., Carraway, K.L., Sweeney, C., 2013. Leucine-rich Repeat and Immunoglobulin Domain-containing Protein-1 (Lrig1) Negative Regulatory Action toward ErbB Receptor Tyrosine Kinases Is Opposed by Leucine-rich Repeat and Immunoglobulin Domain-containing Protein 3 (Lrig3)*. Journal of Biological Chemistry 288, 21593–21605. https://doi.org/10.1074/jbc.M113.486050

Rajasekharan, S., Kennedy, T.E., 2009. The netrin protein family. Genome Biol 10, 239. https://doi.org/10.1186/gb-2009-10-9-239

Ranscht, B., 1994. Cadherins and catenins: interactions and functions in embryonic development. Curr Opin Cell Biol 6, 740–746. https://doi.org/10.1016/0955-0674(94)90102-3

Reissner, C., Runkel, F., Missler, M., 2013. Neurexins. Genome Biology 14, 213. https://doi.org/10.1186/gb-2013-14-9-213

Rhiner, C., Gysi, S., Fröhli, E., Hengartner, M.O., Hajnal, A., 2005. Syndecan regulates cell migration and axon guidance in C. elegans. Development 132, 4621–4633. https://doi.org/10.1242/dev.02042

Riehl, R., Johnson, K., Bradley, R., Grunwald, G.B., Cornel, E., Lilienbaum, A., Holt, C.E., 1996. Cadherin function is required for axon outgrowth in retinal ganglion cells in vivo. Neuron 17, 837–848. https://doi.org/10.1016/s0896-6273(00)80216-0

Rose, D., Zhu, X., Kose, H., Hoang, B., Cho, J., Chiba, A., 1997. Toll, a muscle cell surface molecule, locally inhibits synaptic initiation of the RP3 motoneuron growth cone in Drosophila. Development 124, 1561–1571.

Rothberg, J.M., Hartley, D.A., Walther, Z., Artavanis-Tsakonas, S., 1988. slit: an EGF-homologous locus of D. melanogaster involved in the development of the embryonic central nervous system. Cell 55, 1047–1059. https://doi.org/10.1016/0092-8674(88)90249-8

Rothberg, J.M., Jacobs, J.R., Goodman, C.S., Artavanis-Tsakonas, S., 1990. slit: an extracellular protein necessary for development of midline glia and commissural axon pathways contains both EGF and LRR domains. Genes Dev 4, 2169–2187. https://doi.org/10.1101/gad.4.12a.2169

Salzberg, Y., Ramirez-Suarez, N.J., Bülow, H.E., 2014. The proprotein convertase KPC-1/furin controls branching and self-avoidance of sensory dendrites in Caenorhabditis elegans. PLoS Genet 10, e1004657. https://doi.org/10.1371/journal.pgen.1004657

Sawa, H., Korswagen, H.C., 2013. Wnt signaling in C. elegans. WormBook 1–30. https://doi.org/10.1895/wormbook.1.7.2

Schmitz, C., Wacker, I., Hutter, H., 2008. The Fat-like cadherin CDH-4 controls axon fasciculation, cell migration and hypodermis and pharynx development in Caenorhabditis elegans. Dev Biol 316, 249–259. https://doi.org/10.1016/j.ydbio.2008.01.024

Schwab, M.E., 2010. Functions of Nogo proteins and their receptors in the nervous system. Nat Rev Neurosci 11, 799–811. https://doi.org/10.1038/nrn2936

Schwarz, V., Pan, J., Voltmer-Irsch, S., Hutter, H., 2009. IgCAMs redundantly control axon navigation in Caenorhabditis elegans. Neural Dev 4, 13. https://doi.org/10.1186/1749-8104-4-13

Schwieterman, A.A., Steves, A.N., Yee, V., Donelson, C.J., Bentley, M.R., Santorella, E.M., Mehlenbacher, T.V., Pital, A., Howard, A.M., Wilson, M.R., Ereddia, D.E., Effrein, K.S., McMurry, J.L., Ackley, B.D., Chisholm, A.D., Hudson, M.L., 2016. The Caenorhabditis elegans Ephrin EFN-4 Functions Non-cell Autonomously with Heparan Sulfate Proteoglycans to Promote Axon Outgrowth and Branching. Genetics 202, 639–660. https://doi.org/10.1534/genetics.115.185298

Scott, P.G., Dodd, C.M., Bergmann, E.M., Sheehan, J.K., Bishop, P.N., 2006. Crystal structure of the biglycan dimer and evidence that dimerization is essential for folding and stability of class I small leucine-rich repeat proteoglycans. J Biol Chem 281, 13324–13332. https://doi.org/10.1074/jbc.M513470200

Scott, P.G., McEwan, P.A., Dodd, C.M., Bergmann, E.M., Bishop, P.N., Bella, J., 2004. Crystal structure of the dimeric protein core of decorin, the archetypal small leucine-rich repeat proteoglycan. Proc Natl Acad Sci U S A 101, 15633–15638. https://doi.org/10.1073/pnas.0402976101

Segal, R.A., 2003. Selectivity in neurotrophin signaling: theme and variations. Annu Rev Neurosci 26, 299–330. https://doi.org/10.1146/annurev.neuro.26.041002.131421

Shekarabi, M., Moore, S.W., Tritsch, N.X., Morris, S.J., Bouchard, J.-F., Kennedy, T.E., 2005. Deleted in colorectal cancer binding netrin-1 mediates cell substrate adhesion and recruits Cdc42, Rac1, Pak1, and N-WASP into an intracellular signaling complex that promotes growth cone expansion. J Neurosci 25, 3132–3141. https://doi.org/10.1523/JNEUROSCI.1920-04.2005

Shinza-Kameda, M., Takasu, E., Sakurai, K., Hayashi, S., Nose, A., 2006. Regulation of layer-specific targeting by reciprocal expression of a cell adhesion molecule, capricious. Neuron 49, 205–213. https://doi.org/10.1016/j.neuron.2005.11.013

Shmelkov, S.V., Hormigo, A., Jing, D., Proenca, C.C., Bath, K.G., Milde, T., Shmelkov, E., Kushner, J.S., Baljevic, M., Dincheva, I., Murphy, A.J., Valenzuela, D.M., Gale, N.W., Yancopoulos, G.D., Ninan, I., Lee, F.S., Rafii, S., 2010. Slitrk5 deficiency impairs corticostriatal circuitry and leads to obsessive-compulsive-like behaviors in mice. Nat Med 16, 598–602, 1p following 602. https://doi.org/10.1038/nm.2125

Small, J.V., 1995. Getting the actin filaments straight: nucleation-release or treadmilling? Trends Cell Biol 5, 52–55. https://doi.org/10.1016/s0962-8924(00)88939-4

Soler-Llavina, G.J., Arstikaitis, P., Morishita, W., Ahmad, M., Südhof, T.C., Malenka, R.C., 2013. Leucine-rich repeat transmembrane proteins are essential for maintenance of long-term potentiation. Neuron 79, 439–446. https://doi.org/10.1016/j.neuron.2013.06.007

Söllner, C., Wright, G.J., 2009. A cell surface interaction network of neural leucine-rich repeat receptors. Genome Biol 10, R99. https://doi.org/10.1186/gb-2009-10-9-r99

Song, S., Zhang, B., Sun, H., Li, X., Xiang, Y., Liu, Z., Huang, X., Ding, M., 2010. A Wnt-Frz/Ror-Dsh pathway regulates neurite outgrowth in Caenorhabditis elegans. PLoS Genet 6. https://doi.org/10.1371/journal.pgen.1001056

Soto, F., Watkins, K.L., Johnson, R.E., Schottler, F., Kerschensteiner, D., 2013. NGL-2 regulates pathway-specific neurite growth and lamination, synapse formation, and signal transmission in the retina. J Neurosci 33, 11949–11959. https://doi.org/10.1523/JNEUROSCI.1521-13.2013

Speicher, S., García-Alonso, L., Carmena, A., Martín-Bermudo, M.D., de la Escalera, S., Jiménez, F., 1998. Neurotactin functions in concert with other identified CAMs in growth cone guidance in Drosophila. Neuron 20, 221–233. https://doi.org/10.1016/s0896-6273(00)80451-1

Steigemann, P., Molitor, A., Fellert, S., Jäckle, H., Vorbrüggen, G., 2004. Heparan sulfate proteoglycan syndecan promotes axonal and myotube guidance by slit/robo signaling. Curr Biol 14, 225–230. https://doi.org/10.1016/j.cub.2004.01.006

Steimel, A., Wong, L., Najarro, E.H., Ackley, B.D., Garriga, G., Hutter, H., 2010. The Flamingo ortholog FMI-1 controls pioneer-dependent navigation of follower axons in C. elegans. Development 137, 3663–3673. https://doi.org/10.1242/dev.054320

Stepniak, E., Radice, G.L., Vasioukhin, V., 2009. Adhesive and signaling functions of cadherins and catenins in vertebrate development. Cold Spring Harb Perspect Biol 1, a002949. https://doi.org/10.1101/cshperspect.a002949

Stoeckli, E.T., 2018. Understanding axon guidance: are we nearly there yet? Development 145. https://doi.org/10.1242/dev.151415

Suter, D.M., Forscher, P., 2000. Substrate-cytoskeletal coupling as a mechanism for the regulation of growth cone motility and guidance. J Neurobiol 44, 97–113.

Sutphin, G.L., Backer, G., Sheehan, S., Bean, S., Corban, C., Liu, T., Peters, M.J., van Meurs, J.B.J., Murabito, J.M., Johnson, A.D., Korstanje, R., Cohorts for Heart and Aging Research in Genomic Epidemiology (CHARGE) Consortium Gene Expression Working Group, 2017. Caenorhabditis elegans orthologs of human genes differentially expressed with age are enriched for determinants of longevity. Aging Cell 16, 672–682. https://doi.org/10.1111/acel.12595

Svensk, E., Devkota, R., Ståhlman, M., Ranji, P., Rauthan, M., Magnusson, F., Hammarsten, S., Johansson, M., Borén, J., Pilon, M., 2016. Caenorhabditis elegans PAQR-2 and IGLR-2 Protect against Glucose Toxicity by Modulating Membrane Lipid Composition. PLoS Genet 12, e1005982. https://doi.org/10.1371/journal.pgen.1005982

Takahashi, N., Takahashi, Y., Putnam, F.W., 1985. Periodicity of leucine and tandem repetition of a 24-amino acid segment in the primary structure of leucine-rich alpha 2-glycoprotein of human serum. Proc Natl Acad Sci U S A 82, 1906–1910. https://doi.org/10.1073/pnas.82.7.1906

Takeichi, M., 1995. Morphogenetic roles of classic cadherins. Curr Opin Cell Biol 7, 619–627. https://doi.org/10.1016/0955-0674(95)80102-2

Tang, L.T., Diaz-Balzac, C.A., Rahman, M., Ramirez-Suarez, N.J., Salzberg, Y., Lázaro-Peña, M.I., Bülow, H.E., 2019. TIAM-1/GEF can shape somatosensory dendrites independently of its GEF activity by regulating F-actin localization. Elife 8. https://doi.org/10.7554/eLife.38949

Tang, Y., Nyengaard, J.R., De Groot, D.M., Gundersen, H.J., 2001. Total regional and global number of synapses in the human brain neocortex. Synapse 41, 258–273. https://doi.org/10.1002/syn.1083

Tanoue, T., Takeichi, M., 2005. New insights into Fat cadherins. J Cell Sci 118, 2347–2353. https://doi.org/10.1242/jcs.02398

Teichmann, S.A., Chothia, C., 2000. Immunoglobulin superfamily proteins in Caenorhabditis elegans. J Mol Biol 296, 1367–1383. https://doi.org/10.1006/jmbi.1999.3497

Tojima, T., Hines, J.H., Henley, J.R., Kamiguchi, H., 2011. Second messengers and membrane trafficking direct and organize growth cone steering. Nat Rev Neurosci 12, 191–203. https://doi.org/10.1038/nrn2996

Ulian-Benitez, S., Bishop, S., Foldi, I., Wentzell, J., Okenwa, C., Forero, M.G., Zhu, B., Moreira, M., Phizacklea, M., McIlroy, G., Li, G., Gay, N.J., Hidalgo, A., 2017. Kek-6: A truncated-Trk-like receptor for Drosophila neurotrophin 2 regulates structural synaptic plasticity. PLOS Genetics 13, e1006968. https://doi.org/10.1371/journal.pgen.1006968

Ultsch, M.H., Wiesmann, C., Simmons, L.C., Henrich, J., Yang, M., Reilly, D., Bass, S.H., de Vos, A.M., 1999. Crystal structures of the neurotrophin-binding domain of TrkA, TrkB and TrkC. J Mol Biol 290, 149–159. https://doi.org/10.1006/jmbi.1999.2816

Usui, T., Shima, Y., Shimada, Y., Hirano, S., Burgess, R.W., Schwarz, T.L., Takeichi, M., Uemura, T., 1999. Flamingo, a seven-pass transmembrane cadherin, regulates planar cell polarity under the control of Frizzled. Cell 98, 585–595. https://doi.org/10.1016/s0092-8674(00)80046-x

Van Loy, T., Vandersmissen, H.P., Van Hiel, M.B., Poels, J., Verlinden, H., Badisco, L., Vassart, G., Vanden Broeck, J., 2008. Comparative genomics of leucine-rich repeats containing G protein-coupled receptors and their ligands. General and Comparative Endocrinology 155, 14–21. https://doi.org/10.1016/j.ygcen.2007.06.022

Varadarajan, S.G., Kong, J.H., Phan, K.D., Kao, T.-J., Panaitof, S.C., Cardin, J., Eltzschig, H., Kania, A., Novitch, B.G., Butler, S.J., 2017. Netrin1 Produced by Neural Progenitors, Not Floor Plate Cells, Is Required for Axon Guidance in the Spinal Cord. Neuron 94, 790-799.e3. https://doi.org/10.1016/j.neuron.2017.03.007

Vitriol, E.A., Zheng, J.Q., 2012. Growth cone travel in space and time: the cellular ensemble of cytoskeleton, adhesion, and membrane. Neuron 73, 1068–1081. https://doi.org/10.1016/j.neuron.2012.03.005

Wadachi, R., Hargreaves, K.M., 2006. Trigeminal nociceptors express TLR-4 and CD14: a mechanism for pain due to infection. J Dent Res 85, 49–53. https://doi.org/10.1177/154405910608500108

Wadsworth, W.G., Bhatt, H., Hedgecock, E.M., 1996. Neuroglia and pioneer neurons express UNC-6 to provide global and local netrin cues for guiding migrations in C. elegans. Neuron 16, 35–46. https://doi.org/10.1016/s0896-6273(00)80021-5

Wang, J., Chan, C.-K., Taylor, J.S.H., Chan, S.-O., 2008. The growth-inhibitory protein Nogo is involved in midline routing of axons in the mouse optic chiasm. J Neurosci Res 86, 2581–2590. https://doi.org/10.1002/jnr.21717

Wang, X., Roy, P.J., Holland, S.J., Zhang, L.W., Culotti, J.G., Pawson, T., 1999. Multiple ephrins control cell organization in C. elegans using kinase-dependent and -independent functions of the VAB-1 Eph receptor. Mol Cell 4, 903–913. https://doi.org/10.1016/s1097-2765(00)80220-8

Wang, X., Zhang, W., Cheever, T., Schwarz, V., Opperman, K., Hutter, H., Koepp, D., Chen, L., 2008. The C. elegans L1CAM homologue LAD-2 functions as a coreceptor in MAB-20/Sema2 mediated axon guidance. J Cell Biol 180, 233–246. https://doi.org/10.1083/jcb.200704178

White, J.G., Southgate, E., Thomson, J.N., Brenner, S., 1986. The structure of the nervous system of the nematode Caenorhabditis elegans. Philos Trans R Soc Lond B Biol Sci 314, 1–340. https://doi.org/10.1098/rstb.1986.0056

Williams, A.F., Barclay, A.N., 1988. The immunoglobulin superfamily--domains for cell surface recognition. Annu Rev Immunol 6, 381–405. https://doi.org/10.1146/annurev.iy.06.040188.002121

Windisch, J.M., Auer, B., Marksteiner, R., Lang, M.E., Schneider, R., 1995. Specific neurotrophin binding to leucine-rich motif peptides of TrkA and TrkB. FEBS Lett 374, 125–129. https://doi.org/10.1016/0014-5793(95)01047-i

Yam, P.T., Charron, F., 2013. Signaling mechanisms of non-conventional axon guidance cues: the Shh, BMP and Wnt morphogens. Curr Opin Neurobiol 23, 965–973. https://doi.org/10.1016/j.conb.2013.09.002

Yamagata, A., Goto-Ito, S., Sato, Y., Shiroshima, T., Maeda, A., Watanabe, M., Saitoh, T., Maenaka, K., Terada, T., Yoshida, T., Uemura, T., Fukai, S., 2018. Structural insights into modulation and selectivity of transsynaptic neurexin-LRRTM interaction. Nat Commun 9, 3964. https://doi.org/10.1038/s41467-018-06333-8

Yamagishi, S., Hampel, F., Hata, K., Del Toro, D., Schwark, M., Kvachnina, E., Bastmeyer, M., Yamashita, T., Tarabykin, V., Klein, R., Egea, J., 2011. FLRT2 and FLRT3 act as repulsive guidance cues for Unc5-positive neurons. EMBO J 30, 2920–2933. https://doi.org/10.1038/emboj.2011.189

Yamashita, T., Fujitani, M., Yamagishi, S., Hata, K., Mimura, F., 2005. Multiple signals regulate axon regeneration through the Nogo receptor complex. Mol Neurobiol 32, 105–111. https://doi.org/10.1385/MN:32:2:105

Yim, Y.S., Kwon, Y., Nam, J., Yoon, H.I., Lee, K., Kim, D.G., Kim, E., Kim, C.H., Ko, J., 2013. Slitrks control excitatory and inhibitory synapse formation with LAR receptor protein tyrosine phosphatases. Proc Natl Acad Sci U S A 110, 4057–4062. https://doi.org/10.1073/pnas.1209881110

Yoshikawa, S., McKinnon, R.D., Kokel, M., Thomas, J.B., 2003. Wnt-mediated axon guidance via the Drosophila Derailed receptor. Nature 422, 583–588. https://doi.org/10.1038/nature01522

Yu, C., Sun, X., Li, J., Chan, S.-O., Wang, L., 2020. Analysis of axon divergence at the optic chiasm in nogo-a knockout mice. Neurosci Lett 731, 135109. https://doi.org/10.1016/j.neulet.2020.135109

Yu, T.W., Hao, J.C., Lim, W., Tessier-Lavigne, M., Bargmann, C.I., 2002. Shared receptors in axon guidance: SAX-3/Robo signals via UNC-34/Enabled and a Netrin-independent UNC-40/DCC function. Nat Neurosci 5, 1147–1154. https://doi.org/10.1038/nn956

Zallen, J.A., Kirch, S.A., Bargmann, C.I., 1999. Genes required for axon pathfinding and extension in the C. elegans nerve ring. Development 126, 3679–3692.

Zallen, J.A., Yi, B.A., Bargmann, C.I., 1998. The conserved immunoglobulin superfamily member SAX-3/Robo directs multiple aspects of axon guidance in C. elegans. Cell 92, 217–227. https://doi.org/10.1016/s0092-8674(00)80916-2

Zhang, K., Zhang, Y., Gu, L., Lan, M., Liu, Chuncheng, Wang, M., Su, Y., Ge, M., Wang, T., Yu, Y., Liu, Chang, Li, L., Li, Q., Zhao, Y., Yu, Z., Wang, F., Li, N., Meng, Q., 2018. Islr regulates canonical Wnt signaling-mediated skeletal muscle regeneration by stabilizing Dishevelled-2 and preventing autophagy. Nature Communications 9, 5129. https://doi.org/10.1038/s41467-018-07638-4

Zhang, P., Lu, H., Peixoto, R.T., Pines, M.K., Ge, Y., Oku, S., Siddiqui, T.J., Xie, Y., Wu, W., Archer-Hartmann, S., Yoshida, K., Tanaka, K.F., Aricescu, A.R., Azadi, P., Gordon, M.D., Sabatini, B.L., Wong, R.O.L., Craig, A.M., 2018. Heparan Sulfate Organizes Neuronal Synapses through Neurexin Partnerships. Cell 174, 1450-1464.e23. https://doi.org/10.1016/j.cell.2018.07.002

Zhang, Q., Wang, J., Fan, S., Wang, L., Cao, L., Tang, K., Peng, C., Li, Z., Li, W., Gan, K., Liu, Z., Li, X., Shen, S., Li, G., 2005. Expression and functional characterization of LRRC4, a novel brain-specific member of the LRR superfamily. FEBS Letters 579, 3674–3682. https://doi.org/10.1016/j.febslet.2005.05.058

Zhao, X., Kuja-Panula, J., Sundvik, M., Chen, Y.-C., Aho, V., Peltola, M.A., Porkka-Heiskanen, T., Panula, P., Rauvala, H., 2014. Amigo Adhesion Protein Regulates Development of Neural Circuits in Zebrafish Brain*. Journal of Biological Chemistry 289, 19958–19975. https://doi.org/10.1074/jbc.M113.545582

Zou, W., Dong, X., Broederdorf, T.R., Shen, A., Kramer, D.A., Shi, R., Liang, X., Miller, D.M., Xiang, Y.K., Yasuda, R., Chen, B., Shen, K., 2018. A Dendritic Guidance Receptor Complex Brings Together Distinct Actin Regulators to Drive Efficient F-Actin Assembly and Branching. Dev Cell 45, 362-375.e3. https://doi.org/10.1016/j.devcel.2018.04.008

# Appendix A.

# IGLR-2 neurite outgrowth defects

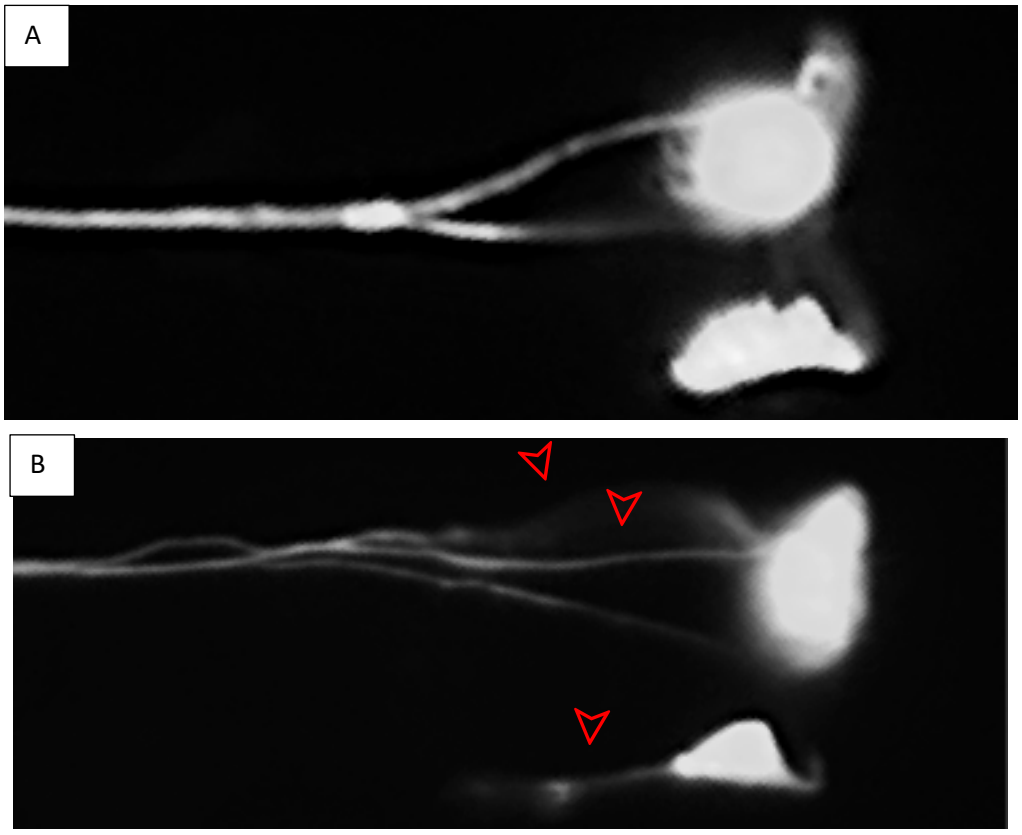


**Figure A1 *iglr-2*(*et34*) PVQ defects**
**a)** Wildtype PVQ neurons sending their axons into the VNC. **b)** This *iglr-2*(*et34*) worm has what appears to be two axons extending from PVQL (two upper red arrows). PVQR also has an extra neurite extending out of its anterior surface (lower red arrow). Marker used: *hdIs26[odr-2::CFP & sra-6::DsRed2] III*.

# Appendix B.

# Data for *Iron* genes without significant axon guidance defects

**Table B1 *Iron-1*(*gk5081*) pan-neuronal VNC axon guidance defects**

| Ventral Nerve Cord | Marker Strain^ N = 787 | *Iron-1*(*gk5081*) N = 102 |
|---|---|---|
| **Wildtype** | 95% | 96% |
| **Anterior Crossovers** | 2% | 1% |
| **Posterior Crossovers** | 3% | 2% |
| **Late Separation** | 0% | 1% |

^The marker used was *evIs111[rgef-1::GFP]*.

**Table B2 *Iron-1*(*gk5081*) PVPR axon guidance defects**

| PVPR | Marker Strain^ N = 294 | *Iron-1*(*gk5081*) N = 100 |
|---|---|---|
| **Wildtype** | 94% | 96% |
| **Crossover** | 6% | 2% |
| **Late Separation** | 1% | 2% |

^The marker used was *hdIs26[odr-2::CFP, sra-6::DsRed2]*.

**Table B3 *Iron-4*(*gk5099*) pan-neuronal VNC axon guidance defects**

| Ventral Nerve Cord | Marker Strain^ N = 787 | *Iron-4*(*gk5099*) N = 96 |
|---|---|---|
| **Wildtype** | 95% | 99% |
| **Anterior Crossovers** | 2% | 0% |
| **Posterior Crossovers** | 3% | 1% |
| **Late Separation** | 0% | 0% |

^The marker used was *evIs111[rgef-1::GFP]*.

**Table B4 *Iron-4*(*gk5099*) PVPR axon guidance defects**

| PVPR | Marker Strain^ N = 294 | Iron-4(gk5099) N = 105 |
|---|---|---|
| **Wildtype** | 94% | 93% |
| **Crossover** | 6% | 6% |
| **Late Separation** | 1% | 1% |

^The marker used was *hdIs26[odr-2::CFP, sra-6::DsRed2]*.

**Table B5 *Iron-6*(*gk736335*) pan-neuronal VNC axon guidance defects**

| Ventral Nerve Cord | Marker Strain^ N = 787 | *Iron-6*(*gk736335*) N = 99 |
|---|---|---|
| **Wildtype** | 95% | 97% |
| **Anterior Crossover** | 2% | 0% |
| **Posterior Crossover** | 3% | 2% |
| **Late Separation** | 0% | 1% |

^The marker used was *evIs111[rgef-1::GFP]*.

**Table B6 *Iron-6*(*gk736335*) DNC axon guidance defects**

| Dorsal Nerve Cord | Marker Strain^ N = 245 | *Iron-6*(*gk736335*) N = 103 |
|---|---|---|
| **Wildtype** | 99% | 97% |
| **Defasciculation** | 1% | 3% |

^The marker used was *evIs111[rgef-1::GFP]*.

**Table B7 *Iron-6*(*gk736335*) PVPR axon guidance defects**

| PVPR | Marker Strain^ N = 159 | *Iron-6*(*gk736335*) N = 100 |
|---|---|---|
| **Wildtype** | 93% | 97% |
| **Crossover** | 6% | 3% |
| **Late Separation** | 1% | 0% |

^The marker used was *hdIs29[odr-2::CFP, sra-6::DsRed2]*.

**Table B8 *Iron-7*(*gk5353*) pan-neuronal VNC axon guidance defects**

| Ventral Nerve Cord | Marker Strain^ N = 787 | *Iron-7*(*gk5353*) N = 99 |
|---|---|---|
| **Wildtype** | 95% | 92% |
| **Anterior Crossovers** | 2% | 0% |
| **Posterior Crossovers** | 3% | 7% |
| **Late Separation** | 0% | 1% |

^The marker used was *evIs111[rgef-1::GFP]*.

**Table B9 *Iron-7*(*gk5353*) DNC axon guidance defects**

| Dorsal Nerve Cord | Marker Strain^ N = 245 | *Iron-7*(*gk5353*) N = 100 |
|---|---|---|
| **Wildtype** | 99% | 100% |
| **Defasciculation** | 1% | 0% |

^The marker used was *evIs111[rgef-1::GFP]*.

**Table B10 *Iron-7*(*gk5353*) PVPR axon guidance defects**

| PVPR | Marker Strain^ N = 163 | *Iron-7*(*gk5353*) N = 109 |
|---|---|---|
| **Wildtype** | 90% | 91% |
| **Crossover** | 10% | 8% |
| **Late Separation** | 0% | 1% |

^The marker used was *hdIs28[odr-2::CFP, sra-6::DsRed2]*.

**Table B11 *Iron-10*(*gk5064*) pan-neuronal VNC axon guidance defects**

| Ventral Nerve Cord | Marker Strain^ N = 787 | *Iron-10*(*gk5064*) N = 100 |
|---|---|---|
| **Wildtype** | 95% | 94% |
| **Anterior Crossovers** | 2% | 1% |
| **Posterior Crossovers** | 3% | 3% |
| **Late Separation** | 0% | 2% |

^The marker used was *evIs111[rgef-1::GFP]*.

**Table B12 *Iron-10*(*gk5064*) DNC axon guidance defects**

| Dorsal Nerve Cord | Marker Strain^ N = 245 | *Iron-10*(*gk5064*) N = 108 |
|---|---|---|
| **Wildtype** | 99% | 99% |
| **Defasciculation** | 1% | 1% |

^The marker used was *evIs111[rgef-1::GFP]*.

**Table B13 *Iron-10*(*gk5064*) PVPR axon guidance defects**

| PVPR | Marker Strain^ N = 159 | *Iron-10*(*gk5064*) N = 102 |
|---|---|---|
| **Wildtype** | 93% | 91% |
| **Crossover** | 6% | 8% |
| **Late Separation** | 1% | 0% |
| **Leave** | 0% | 1% |

^The marker used was *hdIs29[odr-2::CFP, sra-6::DsRed2]*.

**Table B14 *Iron-12*(*gk187625*) pan-neuronal VNC axon guidance defects**

| Ventral Nerve Cord | Marker Strain^ N = 787 | *Iron-12* (*gk187625*) N = 102 |
|---|---|---|
| **No Defect** | 95% | 90% |
| **Anterior Crossover** | 2% | 0% |
| **Posterior Crossover** | 3% | 8%* |
| **Late Separation** | 0% | 2% |

***p<0.001; **p<0.01; *p<0.05 ($\chi 2$ test). ^The marker used was *evIs111[rgef-1::GFP]*.

**Table B15 *Iron-12*(*gk187625*) DNC axon guidance defects**

| Dorsal Nerve Cord | Marker Strain^ N = 245 | *Iron-12* (*gk187625*) N = 51 |
|---|---|---|
| **Wildtype** | 99% | 100% |
| **Defasciculation** | 1% | 0% |

^The marker used was *evIs111[rgef-1::GFP]*.

**Table B16 *Iron-12*(*gk187625*) PVPR axon guidance defects**

| PVPR | Marker Strain^ N = 159 | *Iron-12* (*gk187625*) N = 93 |
|---|---|---|
| **No Defect** | 93% | 96% |
| **Crossover** | 6% | 3% |
| **Late Separation** | 1% | 1% |

^The marker used was *hdIs29[odr-2::CFP, sra-6::DsRed2]*.

**Table B17 *Iron-13*(*gkDf31*) pan-neuronal VNC axon guidance defects**

| Ventral Nerve Cord | Marker Strain^ N = 787 | *Iron-13*(*gkDf31*) N = 98 |
|---|---|---|
| **Wildtype** | 95% | 93% |
| **Anterior Crossover** | 2% | 0% |
| **Posterior Crossover** | 3% | 5% |
| **Late Separation** | 0% | 2% |

^The marker used was *evIs111[rgef-1::GFP]*.

**Table B18 *Iron-13*(*gkDf31*) DNC axon guidance defects**

| Dorsal Nerve Cord | Marker Strain^ N = 245 | *Iron-13*(*gkDf31*) N = 61 |
|---|---|---|
| **Wildtype** | 99% | 100% |
| **Defasciculation** | 1% | 0% |

^The marker used was *evIs111[rgef-1::GFP]*.

**Table B19 *Iron-13*(*gkDf31*) PVPR axon guidance defects**

| PVPR | Marker Strain^ N = 159 | *Iron-13*(*gkDf31*) N = 108 |
|---|---|---|
| **Wildtype** | 93% | 93% |
| **Crossover** | 6% | 6% |
| **Late Separation** | 1% | 1% |

^The marker used was *hdIs29[odr-2::CFP, sra-6::DsRed2]*.

**Table B20 *Iron-15*(*gk918201*) pan-neuronal VNC axon guidance defects**

| Ventral Nerve Cord | Marker Strain^ N = 787 | *Iron-15*(*gk918201*) N = 102 |
|---|---|---|
| **Wildtype** | 95% | 93% |
| **Anterior Crossovers** | 2% | 3% |
| **Posterior Crossovers** | 3% | 4% |
| **Late Separation** | 0% | 0% |

^The marker used was *evIs111[rgef-1::GFP]*.

**Table B21 *Iron-15*(*gk918201*) DNC axon guidance defects**

| Dorsal Nerve Cord | Marker Strain^ N = 245 | *Iron-15*(*gk918201*) N = 51 |
|---|---|---|
| **Wildtype** | 99% | 100% |
| **Defasciculation** | 1% | 0% |

^The marker used was *evIs111[rgef-1::GFP]*.

**Table B22 *Iron-15*(*gk918201*) PVPR axon guidance defects**

| PVPR | Marker Strain^ N = 294 | *Iron-15*(*gk918201*) N = 101 |
|---|---|---|
| **Wildtype** | 94% | 95% |
| **Crossover** | 6% | 4% |
| **Late Separation** | 1% | 0% |
| **PVPR premature stop** | 0% | 1% |

^The marker used was *hdIs26[odr-2::CFP, sra-6::DsRed2]*.

**Table B23 *dma-1*(*wy686*) pan-neuronal VNC axon guidance defects**

| Ventral Nerve Cord | Marker Strain^ N = 787 | *dma-1*(*wy686*) N = 101 |
|---|---|---|
| **Wildtype** | 95% | 95% |
| **Anterior Crossover** | 2% | 2% |
| **Posterior Crossover** | 3% | 2% |
| **Late Separation** | 0% | 1% |

^The marker used was *evIs111[rgef-1::GFP]*.

**Table B24 *dma-1*(*wy686*) DNC axon guidance defects**

| Dorsal Nerve Cord | Marker Strain^ N = 245 | *dma-1*(*wy686*) N = 100 |
|---|---|---|
| **Wildtype** | 99% | 100% |
| **Defasciculation** | 1% | 0% |

^The marker used was *evIs111[rgef-1::GFP]*.

**Table B25 *dma-1*(*wy686*) PVPR axon guidance defects**

| PVPR | Marker Strain^ N = 294 | *dma-1*(*wy686*) N = 75 |
|---|---|---|
| **Wildtype** | 94% | 97% |
| **Crossover** | 6% | 3% |
| **Late Separation** | 1% | 0% |

^The marker used was *hdIs26[odr-2::CFP, sra-6::DsRed2]*.

**Table B26 *lron-11*(*ok2333*) PVQL following PVPR data**

| PVQL | *lron-11*(*ok2333*) N = 110 |
|---|---|
| **PVQL always followed PVPR** | 98% |
| **PVQL didn't follow PVPR** | 1% |

PVQL was deemed to have not followed PVPR if it crossed into the right tract without PVPR, or if PVPR crossed into the right tract and PVQL didn't follow.

# Appendix C.

# The primers used to genotype *C. elegans* populations

**Table C1 Primer pairs used in PCRs to genotype *C. elegans* populations**

| Gene (allele) | Primer A (Sequence 5' to 3') | Primer B (Sequence 5' to 3') | Wildtype Band Size (bp) | Mutant Band Size (bp) | Potential Problems |
|---|---|---|---|---|---|
| ***lron-1*** **(*gk5081*)** | lron-1_gk5081_ex1 (TTTCTGGGACTTGACATACC) | lron-1_gk5081_P2 (TGGTGTATTGCTGATGGTTA) | 655 | 0 | |
| ***lron-1*** **(*gk5081*)** | lron-1_gk5081_insertionF (TACGTAGAGCTCGGTACCTC) | lron-1_gk5081_insertion R (GGTCGATTATCACTTTAGCA) | 0 | 185 | |
| ***lron-3*** **(*ok2614*)** | lron-3_ok2614_ex1 (CCCACATTTCTCATTCACTC) | lron-3_ok2614_ex2 (ATATTAAACCAAGACCCAACC) | 2267 | 507 | |
| ***lron-3*** **(*ok2614*)** | lron-3_ok2614_ex2 (ATATTAAACCAAGACCCAACC) | lron-3_ok2614_P1 (TAGGACAGGTGGATTTAGAAC) | 1500 | 0 | |
| ***lron-3*** **(*gk5319*)** | lron-3_ok2614_ex1 (CCCACATTTCTCATTCACTC) | lron-3_ok2614_P2 (GTGAAAGGTGGTAGATCAAAG) | 1413 | 0 | |
| ***lron-3*** **(*gk5319*)** | lron-3_ok2614_ex2 (ATATTAAACCAAGACCCAACC) | lron-3_ok2614_P1 (TAGGACAGGTGGATTTAGAAC) | 1500 | 0 | |
| ***lron-4*** **(*gk5099*)** | lron-4_gk5099_P1 (AGTTGGTATGAACCTTGGTG) | lron-4_gk5099_P2 (GGCTTACACATCAAACCAGT) | 192 | 0 | |
| ***lron-4*** **(*gk5099*)** | lron-4_gk5099_insertionF (TACGTAGAGCTCGGTACCTC) | lron-4_gk5099_insertion R (GGTCGATTATCACTTTAGCA) | 185 | 0 | |
| ***lron-5*** **(*gk959442*)** | lron-5_gk959442_geno1 (GAGGTTAGTCGGGAAGAACT) | lron-5_gk959442_geno2 (TCGATCCGCATACTTTCTAT) | 509 | 509 (point mutation) | |
| ***lron-6*** **(*gk736335*)** | lron-6_gk736335l6geno1 (GAAGATAAAGAAGAACGAAGACG) | lron-6_gk736335l6geno2 (AGTGATGGCTATGTTGAGTG) | 900 | 900 (point mutation) | |

| Gene (allele) | Primer A (Sequence 5' to 3') | Primer B (Sequence 5' to 3') | Wildtype Band Size (bp) | Mutant Band Size (bp) | Potential Problems |
|---|---|---|---|---|---|
| ***lron-7*** **(*gk5353*)** | lron-7_gk5353_ex3 (TTTGTGTGTCGTTTGTGTCT) | lron-7_gk5353_in4 (CACTTTAGCGATTACCAACC) | 0 | 1598 | The mutant band showed up inconsistently and non-specific bands were observed |
| ***lron-10*** **(*gk5064*)** | lron-10_gk5064_ex1 (CCACTCTTTGGGTCTCTGT) | lron-10_gk5064_P2 (GCGTCGACATAACTTCGT) | 0 | 116 | The mutant band is faint |
| ***lron-10*** **(*gk5064*)** | lron-10_gk5064_ex1 (CCACTCTTTGGGTCTCTGT) | lron-10_gk5064_ex2 (AGAGAGTTTCGGCTTCAAGA) | 349 | 0 | The Wildtype band is faint |
| ***lron-11*** **(*ok2333*)** | lron-11_ok2333_ex7 (TGACAGCGTACATCTTGG) | lron-11_ok2333_ex8 (TGACGGGAAAGAGGAAAGG) | 1650 | 500 | |
| ***lron-11*** **(*ok2333*)** | lron-11_ok2333_p5 (GTGCTCTTCATCCTTCTCCTG) | lron-11_ok2333_ex8 (TGACGGGAAAGAGGAAAGG) | 450 | 0 | |
| ***lron-11*** **(*gk5321*)** | lron-11_ok2333_ex7 (TGACAGCGTACATCTTGG) | lron-11_ok2333_ex8 (TGACGGGAAAGAGGAAAGG) | 1650 | 0 | |
| ***lron-11*** **(*gk5321*)** | lron-11_gk5321-in1 (TTCGGGGTGTAAAGTTCAGC) | lron-11_ok2333_ex8 (TGACGGGAAAGAGGAAAGG) | 0 | 615 | |
| ***lron-12*** **(*gk187625*)** | lron-12_gk187625ex3 (CATCTAAAGAATTGGGCCTG) | lron-12_gk187625ex4 (AAAGAAGAGATTGATGGAAGATG) | 1872 | 1872 (point mutation) | |
| ***lron-13*** **(*gkDf31*)** | lron-13_gkdf31_ex2 (CGGAGCGAAACTAGCAAT) | lron-13_gkdf31_P1 (GGAACAGTAAGTAAACGGTACG) | 498 | 0 | |
| ***lron-13*** **(*gkDf31*)** | lron-13_gkDf31_ex4 (TGACTTCCAGAAAATGCTTC) | lron-13_gkDf31_Ex5 (CAACAAAAACGACATTTCGAC) | 1400 | 600 | This deletion is larger than predicted at Wormbase.org |
| ***lron-14*** **(*gk401715*)** | lron-14_gk401715_geno1 (TCCTGAAAACCTGACCGACT) | lron-14_gk401715_geno2 (TGAGCTAACGTGAGCAGCAT) | 576 | 576 (point mutation) | |
| ***lron-15*** **(*gk441339*)** | lron-15_gk441339_geno1 (GAAACAACAAAGTTCGAAGG) | lron-15_gk441339_geno2 (TTTCGGAAGATCAGCTAGAG) | 836 | 836 (point mutation) | |

| Gene (allele) | Primer A (Sequence 5' to 3') | Primer B (Sequence 5' to 3') | Wildtype Band Size (bp) | Mutant Band Size (bp) | Potential Problems |
|---|---|---|---|---|---|
| ***dma-1*** **(*wy686*)** | dma-1_wy686_ex1 (TCTATTTCCCACCCAACTGC) | dma-1_wy686_ex2 (ACACCGATCCGTCATTTTTC) | 7000 | 3500 | The mutant band showed up inconsistently |
| ***dma-1*** **(*wy686*)** | dma-1_wy686_p1 (TCCTTTTTGCCGCACTACTT) | dma-1_wy686_ex2 (ACACCGATCCGTCATTTTTC) | 985 | 0 | Sometimes a non-specific 200-300 band was observed for mutants |
| ***iglr-1*** **(*gk687851*)** | iglr-1_gk687851_Ex1 (CTGGAAACGTTAGACCTGAG) | iglr-1_gk687851_Ex2 (ACTCGTCACGCAGTTTTATT) | 1340 | 1340 (point mutation) | |
| ***iglr-2*****(*et34*)** | iglr-2_Ex1 (AAGTAATTGTGCCGGTAAGA) | iglr-2_Ex2 (ATATCGAGCAGAGAACctga) | 2290 | 2290 (point mutation) | |

The sequencing primers used to identify point mutations are in the Table C2.

**Table C2 Sequencing primers used to idenitfy point mutations**

| Gene (allele) | Sequencing Primer (Sequence 5' to 3') | Wildtype Flanking sequence (5' to 3') | Mutant Flanking Sequence (5' to 3') | Point Mutation |
|---|---|---|---|---|
| ***lron-5* (*gk959442*)** | lron-5_gk959442_seq1 (GAGGTATTAGTGGGAC ACGA) | TTTACGAGTTGATC AAAATCCTCTCCGA TGTGATTGTTCCCT GTATGACAT | TTTACGAGTTGAT CAAAATCCTCTCT GATGTGATTGTTC CCTGTATGACAT | C to T |
| ***lron-6* (*gk736335*)** | lron-6_gk736335l6sequ2 (CAACTTCTCCACTCAA CAATG) | GGAGCAATATGACT GGATGTTGGAACAA ATGGAAGTTTATAG AGAATTAGA | GGAGCAATATGAC TGGATGTTGGAAT AAATGGAAGTTTAT AGAGAATTAGA | C to T |
| ***lron-12* (*gk187625*)** | lron-12_gk187625seq3 (GAAATACAATCGGAGA CTTGG) | GATGAAATGGATGA CTAGTGTTGAGGTA AGGATTTTATATGA TTAAAAACC | GATGAAATGGATG ACTAGTGTTGAGA TAAGGATTTTATAT GATTAAAAACC | G to A |
| ***lron-14* (*gk401715*)** | lron-14_gk401715_seq1 (GCAGAAGAATCCATTA ACCA) | TGAAGTCATCA AGTTTTGCTGG TTCCAAATTTCA AGTCAAATTGTT TTTATCCGAGAA TCCACTAC | TGAAGTCATCA AGTTTTGCTGG TTCCAAATTTT AAGTCAAATTG TTTTTATCCGA GAATCCACTAC | C to T |
| ***lron-15* (*gk918201*)** | lron-15_gk441339_seq3 | AACACCAGAAGCTT TAAGAGATTTGCGA AATTTGACACATTT GAATCTAAA | AACACCAGAAGCT TTAAGAGATTTGT GAAATTTGACACA TTTGAATCTAAA | C to T |
| ***iglr-1* (*gk687851*)** | iglr-1_gk687851_seq (CTCGGGGTTCAAACGA ATAC) | TTGTTCGTGTACAT CTCGTGATATGCAG GATTACGGCGCAAT AACTATTGT | TTGTTCGTGTACAT CTCGTGATATGTA GGATTACGGCGCA ATAACTATTGT | C to T |
| ***iglr-2* (*et34*)** | iglr-2_seq1 (CGATTTACCTCGGAGA ATTA) | ATTCAACGTTTGGA ACTTCACAATTGGC AACATGATCAGCTT AATTTCGAT | ATTCAACGTTTGG AACTTCACAATTAG CAACATGATCAGC TTAATTTCGAT | G to A |